

# For Reference

---

**NOT TO BE TAKEN FROM THIS ROOM**

# For Reference

NOT TO BE TAKEN FROM THIS ROOM

Ex LIBRIS  
UNIVERSITATIS  
ALBERTAENSIS













THE UNIVERSITY OF ALBERTA

ELECTRON TUNNELING INTO SUPERCONDUCTING LEAD  
SUBJECTED TO HYDROSTATIC PRESSURE

by

W. J. Keeler



A THESIS

SUBMITTED TO THE FACULTY OF GRADUATE STUDIES  
IN PARTIAL FULFILLMENT OF THE REQUIREMENTS FOR THE  
DEGREE OF DOCTOR OF PHILOSOPHY

DEPARTMENT OF PHYSICS

EDMONTON, ALBERTA

MAY, 1968



## UNIVERSITY OF ALBERTA

## FACULTY OF GRADUATE STUDIES

The undersigned certify that they have read, and recommend to the Faculty of Graduate Studies for acceptance, a thesis entitled ELECTRON TUNNELING INTO SUPERCONDUCTING LEAD SUBJECTED TO HYDROSTATIC PRESSURE, submitted by W. J. Keeler, in partial fulfillment of the requirements for the degree of Doctor of Philosophy.



## ACKNOWLEDGEMENTS

It gives me great pleasure to thank Dr. J. P. Franck, my research supervisor, for his generous and instructive help throughout this project.

Special thanks are due Dr. J. S. Rogers for his helpful discussions concerning the electronics, and for the use of his conductance bridge.

I wish to thank the Low Temperature technical staff, and in particular, Mr. H. McClung, for supplying the necessary liquid helium, as well as for assisting in the construction and maintenance of the cryostat.

The financial support of the Physics Department and the National Research Council is gratefully acknowledged.

Finally, I would like to thank my wife for her constant encouragement throughout this work, and for her help in typing the thesis.





## ABSTRACT

Studies of superconductors as a function of pressure have, until now, been concerned mainly with the bulk properties of the metals. A study of the shift of some of the microscopic properties of strong-coupling Pb with pressure has been undertaken and this thesis reports the results of this pressure study. The method of investigation used was the electron tunneling technique, where the pressure production was achieved by suspending the samples in a solid helium bath. The energy gap and phonon spectrum of Pb as reflected in the junction conductance curves were studied as a function of pressure for the first time.

The average value of  $dT_c/dP$  from many different junctions is in agreement with published results for bulk Pb. Shifts in the predominant transverse and longitudinal phonon groups were observed. These shifts occur in the dispersive region of the two main phonon branches. Gruneisen  $\gamma$ 's of  $\gamma(\bar{\omega}_t) = 2.52$  and  $\gamma(\bar{\omega}_\ell) = 3.32$  were obtained for the phonon peak regions, and these can be favourable compared with results from thermal expansion work.

The "recombination effect" was studied and found to be smaller than predicted, and perhaps absent altogether.



The reduced relation  $(\Delta_o(T)/kT_c)/(\Delta_o(T)/kT_c)_{\text{BCS}}$  was studied as a function of reduced temperature, and pressure. The results indicate that  $2\Delta_o(0)/kT_c$  is pressure dependent, in contrast to accepted speculations. Also, the reduced energy gap  $\Delta_o(T)/\Delta_o(0)$  as a function of reduced temperature  $t$ , follows the BCS relation to within a few percent; even under pressure.

The frequency dependence of  $\lambda$ , as defined by McMillan (1968), was found to be  $\propto 1/\langle\omega^2\rangle$  in agreement with theory.

The electron-phonon coupling constant ( $\alpha^2(\omega)$ ) was found to decrease under increased pressure. This reduction in  $\alpha^2(\omega)$  results in a shift in the properties of strong-coupling superconducting Pb toward the predictions of the BCS weak-coupling theory.



## TABLE OF CONTENTS

CHAPTER	PAGE
I INTRODUCTION	1
1 Experiments Leading up to a Microscopic Theory	2
II THEORY OF SUPERCONDUCTIVITY	
1 The Electron-Phonon Interaction	7
2 The Bardeen, Cooper, Schrieffer Theory	10
3 The BCS Theory at Finite Temperature	16
4 Tunneling and the Superconducting Density of States	17
5 Introduction to Strong-Coupling Superconductivity	22
6 Zero-Temperature Strong-Coupling Theory	24
7 Application to the Tunneling Process	28
8 Phonon Emission Processes and the Density of States	29
9 Strong-Coupling Theory at Finite Temperature	34
10 Calculation of Thermodynamic Quantities	36
III THE CRYOSTAT AND PRESSURE SYSTEM	
1 The Cryostat	38
2 The High Pressure Bomb	42
3 Pressure Production	46
4 High Pressure Electrical Lead Seal	47
5 Precautionary Measures	48
6 Thermometry	49



IV	THE ELECTRONIC DETECTION SYSTEM	
1	Introduction	51
2	Circuit Operation	54
3	Bridge Circuit Analysis	57
4	Conductance Calibration	60
V	EXPERIMENTAL METHOD	
1	Specimen Preparation and Mounting Procedure	63
2	Description of a Typical Run	65
3	Low Temperature Pressure Production	66
4	Pressure Dependence of the Barrier	67
VI	RESULTS AND DISCUSSIONS	
1	The Pressure Dependence of the Transition Temperature	73
2	Phonon Shifts in Pb Under Pressure	76
3	The Pressure Dependence of the Energy Gap	91
4	Changes in the Thermodynamic Properties with Pressure	106
5	Other Shifts in Pb Under Pressure	111
6	The Recombination Effect	119
VII	CONCLUSION	124
	APPENDICES	
A	Pressure Shifts in $F(\omega)$	127
B	A Recent Article on Strong-Coupling Theory	130
C	Reprints	
	BIBLIOGRAPHY	135







## LIST OF FIGURES

1.	Two final states for a given initially occupied state in the tunneling process between a normal and a superconducting metal.	21
2.	The normalized conductance $\sigma$ , and $d\sigma/dV$ for a Pb-Al tunnel junction. Also shown is $\alpha^2(\omega)F(\omega)$ calculated by McMillan and Rowell (1965).	30
3.	A plot of $\Delta_1(\omega)$ and $\Delta_2(\omega)$ for reduced temperatures of $t = 0$ and $t = 0.98$ .	32
4.	A cross-section of the cryostat used.	39
5.	The $\text{He}^4$ melting curve.	41
6.	$\text{He}^4$ isochores.	43
7.	The high pressure bomb.	44
8.	A block diagram of the detection system.	55
9.	The bridge circuit.	56
10.	The simplified bridge circuit.	58
11.	Tunnel resistance vs pressure for junctions 1345B and 1345.	69
12.	Tunnel resistance vs pressure for junctions 1345D and 1345E.	70
13.	Semi-logarithmic plot of tunnel resistance vs pressure.	71



14. The normalized conductance  $\sigma$  for junction 1345C at  $P = 0$  bar and  $P = 3172.0$  bar. The gap-edge energies are set to coincide. 77
  
15. Normalized conductance  $\sigma$  and second derivative  $d^2i/dv^2$  (in arbitrary units) for junction 1345C at  $T = 1.4^\circ\text{K}$ . The energy range near the longitudinal phonon peak is shown. Solid lines are at  $P = 0$ , broken lines are at  $P = 3445$  bar. 78
  
16. Normalized conductance  $\sigma$  and second derivative  $d^2i/dv^2$  (in arbitrary units) for junction 1345C at  $T = 1.4^\circ\text{K}$ . The energy range near the transverse phonon peak is shown. Solid lines are at  $P = 0$ , broken lines are at  $P = 3445$  bar. 79
  
17. Energy gap (at the gap edge) of Pb as a function of temperature. Order of runs: black dot ( $P = 0$ ); open circles ( $P = 2730$  bar); black squares ( $P = 0$ ). 92
  
18. Squared reduced energy gap (at the gap edge) of Pb as a function of reduced temperature. Black dots and squares ( $P = 0$ ); open circles ( $P = 2730$  bar). 94
  
19. Plot of  $(\Delta/kT_c)/(\Delta/kT_c)_{\text{BCS}}$  vs reduced temperature; black dots and squares,  $P = 0$ ; open circles,  $P = 2730$  bar. 95
  
20. The gap region conductance at  $2^\circ\text{K}$  for junction 1345C. Pressures are,  $P = 0$  and  $P = 2730$  bar. 97



21. The gap region conductance at  $2^{\circ}\text{K}$  for junction 13450<sup>1</sup>. Pressures are,  $P = 0$  and  $P = 3445$  bar. 98
22. Normalized conductance  $\sigma$  for junctions 1345 and 1345A (full lines); the parameter gives the reduced temperature. The dashed lines are calculated normalized conductance for  $t = 0.92$  and  $0.95$ . The arrows indicate the energies  $\omega_t - \Delta_o(T)$  and  $\omega_t + \Delta_o(T)$ . 121
23. Normalized conductance  $\sigma$  for junction 1345A at reduced temperature  $t = 0.92$  and  $t = 0.95$ ; and for pressures  $P = 0$  bar and  $P = 2393.0$  bar. 123



## CHAPTER I

## INTRODUCTION

In 1911 Onnes discovered superconductivity while measuring the electrical resistance of mercury wires at low temperature. Since then the state has been found in many other metals and alloys, and is reversible in the sense of a true thermodynamic phase state.

Experiments by Meissner and Ochsenfeld (1933) established that a superconductor expels all magnetic flux from its interior. (We limit ourselves to a discussion of Type 1 superconductors.) It was found that by applying a magnetic field greater than some critical value,  $H_c$ , the normal resistive state could be restored. The critical field was temperature dependent below the superconducting transition temperature,  $T_c$ , the dependence being approximately of the form

$$H_c = H_0(1 - (T/T_c)^2).$$

An abrupt jump in the specific heat at the transition temperature in zero magnetic field, also indicated that the transition was a phase change of second order.

Phenomenological theories were proposed first by Gorter and Casimir (1934) and later by F. and H. London





(1934, 1935). These were based on a two-fluid model concept. One fluid, the normal component, consisted of ordinary electrons, while the second fluid consisted of the super-electrons. In the London theory, the normal fluid was treated using classical electrodynamics, while the concept of infinite conductivity and perfect diamagnetism were incorporated in dealing with the superfluid component.

### I.1 Experiments Leading up to a Microscopic Theory

In 1950 Fröhlich theoretically predicted that the critical temperature should depend on the isotopic mass of a superconductor according to the relation  $T_c M^{\frac{1}{2}} = \text{const.}$  This was experimentally found to be the case independently by Maxwell (1950) and by Reynolds et al (1951). This result established the fact that the lattice must be involved in the mechanism for superconductivity.

Between 1950 and 1957, many different experiments were suggesting simultaneously that the superconducting state exhibits an energy gap  $2\Delta$  in the single particle density of states function near the Fermi surface. These experiments included specific heat measurements, infrared transmission experiments, electromagnetic radiation absorption measurements, and ultrasonic attenuation experiments.



These results, coupled with the earlier known result that most superconductors obey the same laws of corresponding states to a good degree, formed the starting point for a microscopic theory.

Fröhlich (1950) proposed a theory of superconductivity based on an attractive electron-electron interaction mediated by virtual phonon exchange. The electrons were not necessarily from states of opposite momenta, a refinement later proposed by Cooper (1956). In detail Fröhlich established the criterion for superconductivity, namely that if the attractive electron-electron interaction dominates the repulsive Coulomb interaction between the electrons, a metal becomes a superconductor. However, due to his perturbation approach, which could not be carried out with sufficient accuracy, the quantitative features of the theory failed.

Cooper (1956) showed that a pair of electrons of opposite momentum and spin, interacting via a momentum dependent potential above a filled Fermi sea of non-interacting electrons, would form a bound pair. The potential must be attractive in the region of the Fermi surface although it could be arbitrarily weak. Finally, Bardeen, Cooper, and Schrieffer (1957), henceforth (BCS), succeeded in producing a successful theory which involved macroscopic occupation of such pair states.



Simultaneously, Bogolyubov (1958) in Russia formulated an independent theory based on a somewhat different mathematical approach.

More recently, a sophisticated description of the behaviour of superconductors has become possible through the use of field theoretic Green's functions techniques. These calculations make use of information regarding electron-phonon coupling strengths and explicit phonon distributions.

Because of the dependence of superconductivity on the lattice, studies of superconductors subjected to pressure have been carried on for some time. The literature has been reviewed by Brandt and Ginzburg (1965), by Levy and Olsen (1965), by Olsen and Rohrer (1960), and by Swenson (1960) in his "High Pressure Physics" survey.

The greater part of the work done to date on studying the influence of pressure on superconductors has been in determining the sign and magnitude of  $\partial T_c / \partial P$  and  $\partial H_c / \partial P$ . Characteristically, most superconductors decrease in both  $T_c$  and  $H_c$  with increasing pressure. This is the case in Pb. Bismuth is interesting in that it is not a superconductor unless a pressure of from 20,000 - 40,000 atmospheres is applied to it. Thus it is felt that only one phase of Bi, the one not normally





found at room temperature, will superconduct at low temperature.

An increase in the critical temperature is observed in zirconium, titanium, and a small number of binary alloys. Thallium shows an increase in  $T_c$  to about 2000 bars and then it begins to decrease.

There seems to be very little experimental information on the shift in microscopic parameters of superconductors under pressure. The only published data are from experiments by Hodder and Briscoe (1966) and by Zavaritskii (1967), both groups worked with Pb. Hodder and Briscoe have subjected Pb-Pb tunnel junctions to mechanical bending. They observe a shift in the gap-parameter  $\Delta_0$  which they try to relate to a volume dependence. However, their method is very inaccurate because of shear strains set up in the specimen. More recently, Zavaritskii has investigated the strain dependence of the phonon spectrum in Pb. He deposits the Pb strips of a tunnel junction at low temperature and in this way achieves maximum lattice distortion. By annealing the junctions to successively higher temperatures and measuring the accompanying phonon distributions, he obtains some information about the behaviour of a superconductor with varying amounts of strain in the lattice.





It was decided that experiments on tunnel junctions subjected to hydrostatic pressure, would be attempted. Provided the technique was feasible, this would be the best way to measure the pressure dependence of the energy gap parameter  $\Delta_0$ . Tunnel junctions made from Al-Al-oxide-Pb were chosen with the object of studying superconducting Pb. Pb is highly compressible, has a large  $T_c$  and gap value, and exhibits strong phonon structure in its density of states which could serve as a means of measuring phonon shifts under pressure.

The next Chapters briefly review existing superconductivity theory and its application to strong-coupling Pb. A discussion of the cryostat and electronic apparatus is given, followed by the laboratory procedure. Results are presented and discussed in Chapter VI.



## CHAPTER II

## THEORY OF SUPERCONDUCTIVITY

II.1 The Electron-Phonon Interaction

The electron-phonon interaction plays an essential role in determining the physical properties of a metal. In calculating effects due to interaction between the electron and phonon systems, the many body Hamiltonian for the system is first set down in terms of "bare" particles consisting of single electrons occupying Bloch states, and quantized vibrations of the ionic lattice. Next, coupling between these particles leads to a set of "dressed" particles in terms of which, properties of the physical system can be derived. The nature and strength of the electron-phonon coupling has important consequences for the properties of metals.

Included in the zero order Hamiltonian  $H_0$  is a term representing the interaction of the electrons with the ions in their equilibrium positions. The difference between this potential and the full electron-ion potential remains as a perturbation which is eventually related to an electron-phonon coupling parameter.

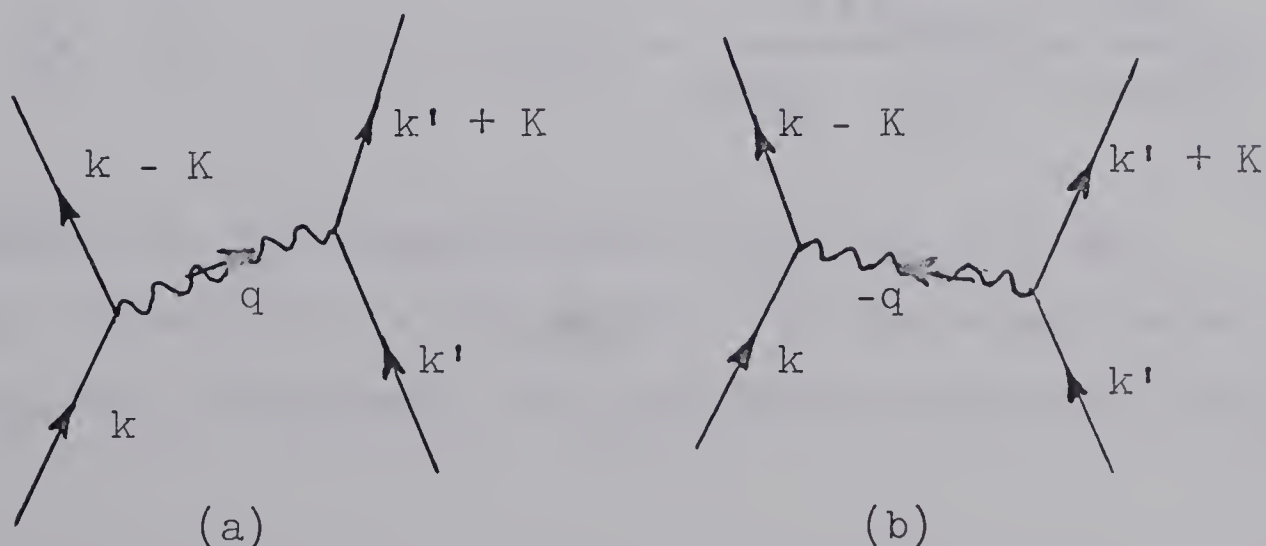
In the case of weak coupling between the electron



and phonon systems, the electron excitations are long lived and their energies well defined. This seems to be the case whether the interaction is retarded or not.

On the other hand, when the interaction is strong, the retardation of the electron-phonon interaction leads to damping mechanisms and hence particle lifetime effects when considering the excitations of the electron distribution. (These lifetime effects are not present if an instantaneous interaction is allowed.) The form of the phonon spectrum as well as the electron distribution (Fermi surface shape) play significant roles in determining the predictions of a specific theoretical calculation.

It is generally assumed that the electron-phonon interaction is essential in bringing about superconductivity in most (if not all) superconductors. The electron-phonon interaction can lead to electron-electron coupling in the following processes:





either (a) an electron in state  $\vec{k}$  emits a phonon and is scattered to  $\vec{k} - \vec{K}$  while electron  $\vec{k}'$  absorbs it and is scattered to  $\vec{k}' + \vec{K}$ , or (b) a phonon with wave vector  $-\vec{q}$  is emitted by  $\vec{k}'$ . By second order perturbation theory, the matrix elements for the transitions are

$$\langle \vec{k} - \vec{K}, \vec{k}' + \vec{K} | V | \vec{k}, \vec{k}' \rangle = \frac{M_{\vec{k}, \vec{k}-\vec{K}} M_{\vec{k}', \vec{k}'+\vec{K}}^*}{\epsilon_{\vec{k}} - [\epsilon_{\vec{k}-\vec{K}} + \hbar\omega_{\vec{q}}]} \quad \text{II-1}$$

and

$$\langle \vec{k} - \vec{K}, \vec{k}' + \vec{K} | V | \vec{k}, \vec{k}' \rangle = \frac{M_{\vec{k}, \vec{k}-\vec{K}} M_{\vec{k}', \vec{k}'+\vec{K}}^*}{\epsilon_{\vec{k}} - [\epsilon_{\vec{k}-\vec{K}} - \hbar\omega_{\vec{q}}]} \quad \text{II-2}$$

where the electron energy  $\epsilon_{\vec{k}}$  is measured relative to the Fermi surface,  $\hbar\omega_{\vec{q}}$  is the energy of the exchanged phonon and  $\vec{K}$  is its wave-vector ( $\vec{K} = \vec{q}$  for normal processes).  $M$  is the matrix element for the electron-phonon interaction. Combining these under the assumption that the electron-phonon matrix elements  $M$  and  $M^*$  are the same in the energy range of interest gives:

$$\langle \vec{k} - \vec{K}, \vec{k}' + \vec{K} | V | \vec{k}, \vec{k}' \rangle = \frac{2 |M_{\vec{k}, \vec{k}-\vec{K}}|^2 \hbar\omega_{\vec{q}}}{[\epsilon_{\vec{k}} - \epsilon_{\vec{k}-\vec{K}}]^2 - (\hbar\omega_{\vec{q}})^2} \quad \text{II-3}$$

Clearly for the energy region  $|\epsilon_{\vec{k}} - \epsilon_{\vec{k}-\vec{K}}| < \hbar\omega_{\vec{q}}$  this interaction is attractive. In the normal-superconducting transition, only processes within an energy







$kT_c$  of the Fermi surface are important, where  $T_c$  is the transition temperature. Since generally  $kT_c \ll \hbar\omega_q$  for  $\omega_q$  of the order of the Debye frequency,

$$V(K) \sim \frac{-2 |M_{k,k-K}|^2}{\hbar\omega_q} . \quad \text{II-4}$$

A second possible interaction between electrons is the Coulomb repulsion, which can be written in terms of a screening parameter  $\lambda$  as

$$V_{\text{Coul}}(K) = \frac{4\pi e^2}{\lambda^2 + K^2} . \quad \text{II-5}$$

The total interaction will be therefore given by

$$V(K) = \frac{-2 |M_{k,k-K}|^2}{\hbar\omega_q} + \frac{4\pi e^2}{\lambda^2 + K^2} . \quad \text{II-6}$$

If  $V(K)$  is negative, an attractive force is felt between the electrons.

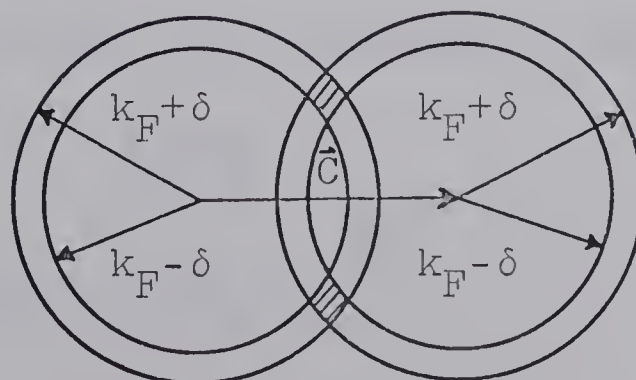
## II.2 The Bardeen, Cooper, Schrieffer Theory

In 1957, BCS formulated the first successful theory of superconductivity. Cooper (1956) had found earlier, that when two electrons interact with an arbitrarily small attractive interaction  $V$  above a



filled sea of non-interacting electrons, binding results between the pair. Such a bound pair is called a Cooper pair.

The BCS theory considers a system in which a large number of electrons interact via the potential  $V$  in pairs. The matrix elements which take a pair of electrons from any two initial states to any other two states satisfying momentum conservation, alternate in sign because of Fermi-Dirac statistics. If these configurations occurred in the ground state with roughly equal weight, the net interaction would be small. BCS showed that a coherent low energy state can be produced by choosing a subset of configurations between which the matrix elements are negative. This subset consists of states composed completely of paired states, all having the same momentum  $\vec{k} + \vec{k}' = \vec{C}$ . The greatest lowering in energy occurs when the greatest amount of pairing is produced. For ground state pairing, this occurs when  $\vec{C} = 0$ , as can be seen from the following diagram by Cooper.





The possible values of  $\vec{k}$  and  $\vec{k}'$  lie in the narrow shell straddling  $\vec{k}_F$ . Also those values satisfying  $\vec{k} + \vec{k}' = \vec{C}$  lie in the two shaded regions. This shows that the maximum amount of pairing is obtained when  $\vec{C} = 0$ .

Further study shows that exchange energy considerations require that pair electrons are of opposite spin, since the interaction is reduced for parallel spins.

Thus BCS consider a reduced problem in which only configurations where states are occupied in pairs  $\vec{k}\uparrow$  and  $-\vec{k}\downarrow$  are important. They introduce a reduced Hamiltonian which includes only the interactions between zero momentum pairs, and this presumably accounts for most of the condensation energy. A Hartree-type trial wave function  $\Psi(u_k, v_k)$  is introduced, which satisfies the pairing condition. Here  $v_k^2$  is the probability that the  $k^{\text{th}}$  pair is occupied and  $u_k^2$  is the probability that it is unoccupied.

The energy corresponding to the reduced Hamiltonian is calculated treating  $v_k$  and  $u_k$  as variational parameters. A minimum value in the condensation energy  $W_c$  is obtained when these parameters are given by:

$$v_k^2 = \frac{1}{2}(1 - \epsilon_k/E_k) \quad \text{II-7}$$

and

$$u_k^2 = \frac{1}{2}(1 + \epsilon_k/E_k). \quad \text{II-8}$$





The energies  $E_k$  are given by the dispersion relation

$$E_k = \sqrt{\epsilon_k^2 + \Delta_k^2} \quad \text{II-9}$$

where  $\epsilon_k$  is the ordinary Bloch energy measured from the Fermi surface, and  $\Delta_k$  is defined by

$$\Delta_k = \sum_{k'} V_{kk'} u_k v_{k'} \quad \text{II-10}$$

Substituting for  $u_{k'}$  and  $v_{k'}$  produces a self-consistency condition given by,

$$\Delta_k = \sum_{k'} \frac{V_{kk'} \Delta_{k'}}{2E_{k'}} \quad \text{II-11}$$

This is referred to as the gap equation. The energies  $E_k$  turn out to be the single particle-like excitation energies of the system. BCS neglect anisotropic effects and assume that  $V_{kk'}$ , or  $V(K)$  can be replaced by a constant average matrix element such that

$$V = \langle V(K) \rangle_{Av} \quad \text{for } |\epsilon| \leq \hbar\omega_q$$

$$= 0 \quad \text{elsewhere.}$$

Here  $\omega_q$  is an average phonon frequency chosen equal to the Debye frequency  $\omega_D$ . BCS also assume that the density of Bloch states is constant and equal to the value at the Fermi level ( $N(0)$ ) in the range  $|\epsilon| \leq \hbar\omega_q$ .





The assumption that  $V = \text{constant}$  leads to  $\Delta_k = \text{constant}$ , and

$$\Delta_0 = \frac{\hbar\omega_q}{\sinh(1/N(0)V)} . \quad \text{II-12}$$

$\Delta_0$  is called the gap parameter. Under these same assumptions the condensation energy becomes,

$$W_s - W_n = W_c = \frac{-2N(0)(\hbar\omega_q)^2}{\exp[2/N(0)V] - 1} . \quad \text{II-13}$$

Empirically,  $W_c$  is of the order of  $N(0)(kT_c)^2$  and in general  $kT_c$  is much less than  $\hbar\omega_q$ . According to II-13 this will occur if  $N(0)V \ll 1$ , which is termed the weak-coupling limit. Then we have the simplified expressions:

$$W_c = -2N(0)(\hbar\omega_q)^2 \exp\left[\frac{-2}{N(0)V}\right] \quad \text{II-14}$$

$$\Delta_0 = 2\hbar\omega_q \exp\left[\frac{-1}{N(0)V}\right] \quad \text{II-15}$$

Excitations above the ground state occur when one or more of the ground state pairs is broken up, or when pairs are excited. It was shown by BCS that the excitation energy for creating one unpaired quasi-particle in state  $k$  is given by  $E_k = (\epsilon_k^2 + \Delta_0^2)^{\frac{1}{2}}$ . However, such excitations can only be created in pairs; the minimum excitation energy is therefore  $2\Delta_0$ . It was also shown



that excited pairs can be formally treated as a pair of excited quasi-particles. The excitations behave like independent fermions. We have, therefore, a one-to-one correspondence between excited states and the Bloch-type excitations in the normal metal.

One can use this fact to calculate the density of excited states in a superconductor. We have from this one-to-one relationship:

$$N_n(\epsilon_k) d\epsilon_k = N_s(E_k) dE_k \quad \text{II-16}$$

or

$$N_s(E_k) = N_n(\epsilon_k) \frac{d\epsilon_k}{dE_k}. \quad \text{II-17}$$

Differentiating the dispersion relation gives:

$$N_s(E_k) = \frac{N_n(\epsilon_k) E_k}{\epsilon_k + \Delta \frac{d\Delta}{d\epsilon_k}}. \quad \text{II-18}$$

For a constant gap parameter, the normalized superconducting density of states becomes:

$$n_s(E_k) = \frac{N_s(E_k)}{N_n(E_k)} = \text{Re} \frac{E}{(E^2 - \Delta^2)^{\frac{1}{2}}} \quad \text{II-19}$$

and  $n_s$  is sharply peaked at energies given by  $E = \pm \Delta$ .



### II.3 The BCS Theory at Finite Temperature

The behaviour of the superconductor for  $T > 0^\circ\text{K}$  is obtained by BCS by minimizing its free energy. They obtain expressions very similar to the ground-state calculations. In particular, the quasi-particle energies are given by:

$$E_k = (\epsilon_k^2 + \Delta_0(T)^2)^{\frac{1}{2}} \quad \text{II-20}$$

where  $\Delta_0(T)$  is now the temperature-dependent energy-gap. The density of states, equation II-19, is therefore temperature-dependent.  $\Delta_0(T)$  is found to go to zero at some finite temperature,  $T_c$ , and this is recognized as the transition temperature. In the weak-coupling limit,  $N(0)V \ll 1$ , the following relations hold:

$$kT_c = 1.14\hbar\omega \exp(-1/N(0)V) \quad \text{II-21}$$

$$2\Delta_0(0) = 3.528 kT_c. \quad \text{II-22}$$

The reduced energy gap  $\Delta_0(T)/\Delta_0(0)$  is a universal function of reduced temperature  $t = T/T_c$ . In particular, near  $T_c$ , the following expressions hold:

$$\Delta_0(T) = 3.069 kT_c (1 - T/T_c)^{\frac{1}{2}} \quad \text{II-23}$$

or

$$\Delta_0(T)/\Delta_0(0) = 1.74 (1 - T/T_c)^{\frac{1}{2}}. \quad \text{II-24}$$

A complete tabulation of  $\Delta_0$  and other parameters of the BCS superconductor has been given by Muhlischlegel (1959).



It is well known from a thermodynamical treatment, that the transition at  $T = T_c$  is of second order, exhibiting a finite discontinuity in specific heat. The BCS theory predicts for this:

$$\frac{C_{es} - C_{en}}{C_{en}} = \frac{3}{2\pi^2} \frac{d(\Delta/kT_c)^2}{dt} \quad \text{II-25}$$

which gives the universal number:

$$\frac{C_{es} - C_{en}}{C_{en}} = 1.43 \quad \text{II-26}$$

#### II.4 Tunneling and the Superconducting Density of States

A detailed one-to-one correspondence between tunnel junction conductance and the superconducting density of states has been established by Bardeen (1961) and by Cohen, Falicov, and Phillips (1962). A simplified version of this will be outlined briefly in the present section.

A tunnel junction consists of a metal-insulator-metal sandwich formed by first depositing a metal layer onto a suitable backing, allowing its surface to oxidize forming the insulator, and then cross-depositing a second metal layer. Provided the barrier oxide layer is sufficiently thin, electrons can penetrate through it by quantum mechanical tunneling.







A simple model for the tunnel current exists for a normal-superconducting (n-s) junction (Shapiro et al, 1962), that is, a junction in which one metal is in the normal state and the other is in the superconducting state. Assuming a tunneling probability  $|M|^2$  for barrier penetration which is to be taken independent of temperature and energy for a bias of up to  $\sim 30$  millivolts, the transition probability per unit time for an electron in an occupied state  $k_1$  tunneling to an unoccupied state  $k_2$  on the other side of the barrier is:

$$P = 2\pi |M|^2 f_i (1 - f_f) N_f \quad \text{II-27}$$

$N_f$  is the density of final states and  $f_i$  and  $f_f$  are Fermi functions for the initial and final states. If a voltage  $V$  is now impressed across the junction, the net tunneling current will be the sum of the two one-way currents. Thus, (gathering all the constant factors into one)

$$i(V) = \text{const} \int_{-\infty}^{\infty} \{ N_1(E) f(E) N_2(E + eV) [1 - f(E + eV)] - [N_1(E) f(E + eV) N_2(E + eV) (1 - f(E))] \} dE \quad \text{II-28}$$

where  $E$  is the energy measured from the Fermi level.

Collecting

$$i(V) = \text{const} \int_{-\infty}^{\infty} N_1(E) N_2(E + eV) [f(E) - f(E + eV)] dE. \quad \text{II-29}$$



Recalling equation II-19, the density of states for a superconductor, with energy measured from the Fermi level, is given by the form

$$N_T(\omega) = N(0) \operatorname{Re} \left( \frac{\omega}{(\omega^2 - \Delta^2)^{\frac{1}{2}}} \right) \quad \text{II-30}$$

and for  $\omega = eV < \Delta$ ,  $N_T(\omega) = 0$ . Integrating II-29 from  $E_F$  (choice of  $\omega = 0$ ) to  $\omega = eV$  for a n-s junction, and forgetting factors of two, for  $T = 0$

$$i_{ns}(V) = \text{const } e N_1(0) N_2(0) [(eV)^2 - \Delta^2]^{\frac{1}{2}}. \quad \text{II-31}$$

Therefore the junction conductance, assuming the normal density of states is constant, is

$$\frac{di(V)}{dv} = \text{const } e N_1(0) N_2(0) \frac{eV}{((eV)^2 - \Delta^2)^{\frac{1}{2}}} \quad \text{II-32}$$

and the normalized conductance is

$$\sigma = \frac{(di/dV)_{ns}}{(di/dV)_{nn}} = \frac{\operatorname{Re} |eV|}{((eV)^2 - \Delta^2)^{\frac{1}{2}}} = \frac{N_T(\omega)}{N(0)}. \quad \text{II-33}$$

Thus the normalized conductance gives a direct measure of the normalized density of states in a superconductor.

Coherence effects associated with the interdependence of an electron in state  $\vec{k}\uparrow$  with an electron in state  $-\vec{k}\downarrow$  often arise when considering single particle processes in a superconductor. These effects do not occur, however,



when the one-particle tunneling process between a normal and superconducting metal is considered. Consider the illustrations in figure 1, due to Schrieffer. An electron in  $\vec{k}'$  beneath the Fermi surface in the normal metal tunnels through the oxide to state  $\vec{k}''$  above the Fermi surface in the superconductor. In the process a hole is left behind giving an excitation energy  $\epsilon_\alpha = |\epsilon_{\vec{k}'}|$  for this metal. In addition, a quasi-particle is placed in  $\vec{k}''$  giving an excitation energy  $\epsilon_\beta = (\epsilon_{\vec{k}'}^2 + \Delta_{\vec{k}'}^2)^{\frac{1}{2}}$  for the superconductor. This process can go on only if the pair state  $(\vec{k}'', -\vec{k}'')$  is initially empty; this occurs with the probability  $u_{\vec{k}'}^2$ . Energy is conserved if  $|\epsilon_{\vec{k}'}| + E_{\vec{k}'} = V$ . Another energy conserving process is shown in figure 1(b), where tunneling into  $\vec{k}''$  beneath the Fermi surface now occurs with probability  $u_{\vec{k}''}^2$ . However,  $\epsilon_{\vec{k}'} = -\epsilon_{\vec{k}''}$  so that from equations II-7 and II-8,  $u_{\vec{k}''}^2 = v_{\vec{k}'}^2$ , so that the total probability for the tunneling process is  $u_{\vec{k}'}^2 + v_{\vec{k}'}^2 = 1$  as far as Pauli principle restrictions are concerned. The tunneling current is then given by summing only over states above (or below) the Fermi surface in the superconductor and replacing the coherence factor by unity.

The BCS theory has been reviewed in detail by several authors. See, for example, books by J. R. Schrieffer (1964) and G. Rickayzen (1965).

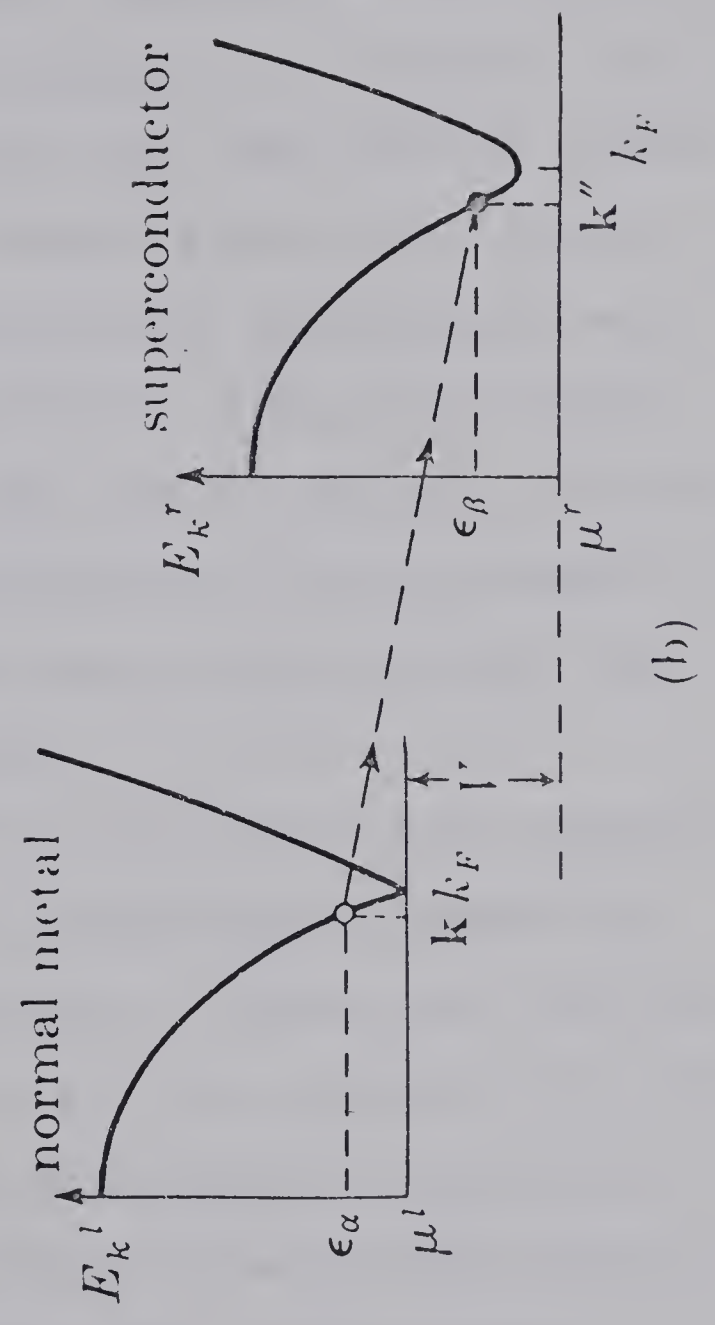
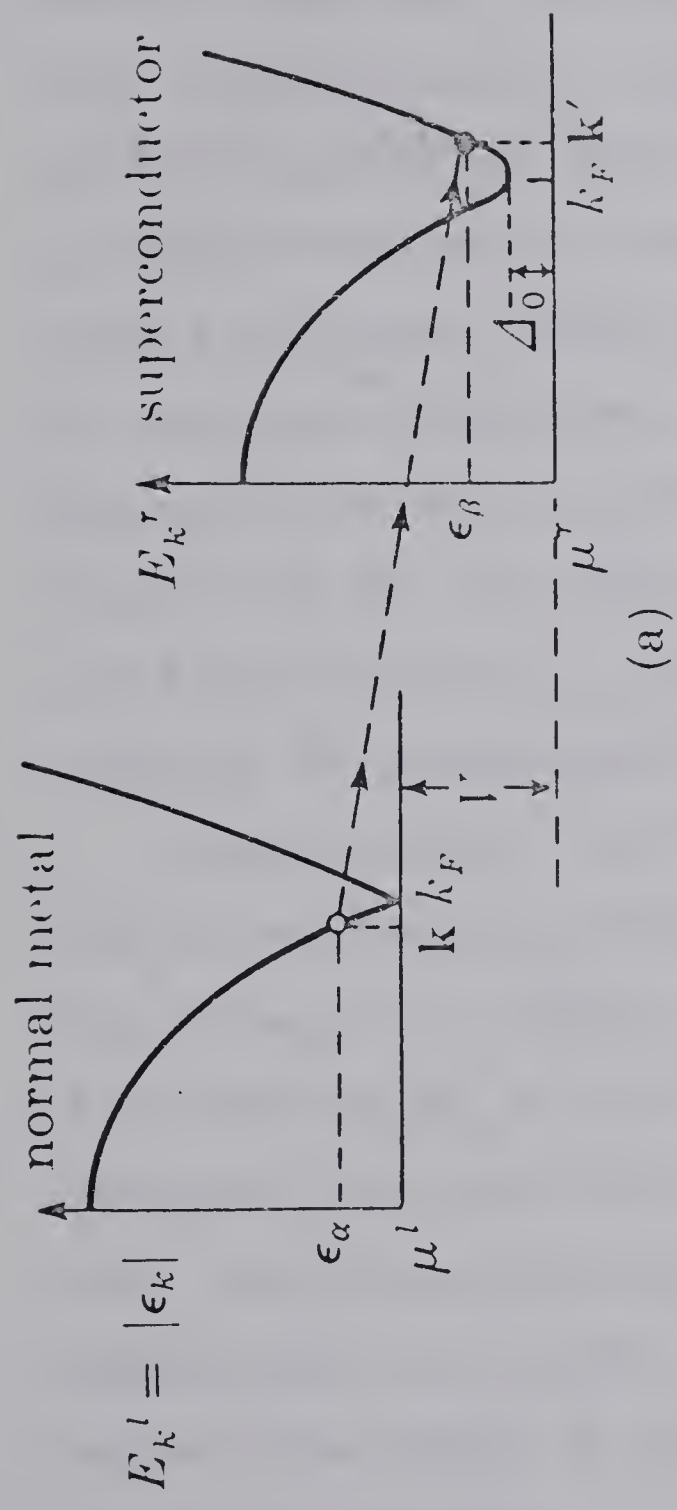


Figure 1

Two final states for a given initially occupied state in the tunneling process between a normal and a superconducting metal. (Taken from Schrieffer — "Theory of Superconductivity" (1964) p 83.)









## II.5 Introduction to Strong-Coupling Superconductivity

The BCS theory contained no explicit assumptions about the electron-phonon interaction. In fact, any interaction which could produce the effect of  $V$  would do equally well for their theory. This is the only adjustable parameter in the theory and is to be obtained from measured quantities such as  $T_c$ , etc. The laws of corresponding states which arise naturally from this type of single parameter theory are satisfied surprisingly well by most superconductors, so that the form of the interaction is not critical for many superconductors. However, for Pb and Hg, two superconductors with low  $\Theta_D$  values and high values of  $T_c$ , significant deviations from the simplest BCS predictions occur.

The fact that these deviations occur is not surprising if one considers that the weak coupling assumption  $kT_c \ll \hbar\omega_q$  is no longer satisfied. Stating the condition as a ratio  $\Theta_D/T_c$  we find that for Al, a typical BCS superconductor, the ratio is  $\sim 350$  while for Pb, the ratio is  $\sim 14$ . Both Pb and Hg are referred to as strong-coupling superconductors and the ratio  $\Theta_D/T_c$  is often used to measure the amount of strong-coupling character a given superconductor has.

One can illustrate the deviations from BCS behaviour for strong-coupling Pb by listing the following experi-



mental results.

(1) The condensation energy at  $T = 0^\circ\text{K}$  is given by  $H_0^2/8\pi$ . For Pb this equals  $24,900 \pm \text{erg/cm}^3$ . The BCS expression for the condensation energy is given as  $\frac{1}{2}N(0)\Delta_0^2 = 31,000 \pm 2,000 \text{ erg/cm}^3$  (Swihart et al 1965). Thus the BCS prediction is too high.

(2) The BCS energy-gap transition temperature relation was  $2\Delta_0(0) = 3.528kT_c$ . In Pb the experimentally obtained value is  $2\Delta_0(0) = 4.45kT_c$  and in Hg it is  $2\Delta_0(0) = 4.6kT_c$ . The value of the gap- $T_c$  ratio shows in general a strong correlation with the  $\Theta_D/T_c$  ratio, and consequently it can also be used to measure the degree of strong-coupling in a superconductor. Weak-coupling superconductors generally show good agreement with the BCS value of  $2\Delta_0(0) = 3.53 kT_c$ .

(3) The BCS theory predicts an electronic specific heat jump

$$\Delta C_{el} = 1.43 \gamma T_c.$$

This gives  $\sim 30.8 \text{ mJ} \cdot \text{mole}^{-1} \cdot ^\circ\text{K}^{-1}$  using the measured value of the transition temperature of Pb. Directly measured calorimetric results for the specific heat jump vary from  $\sim 52.9 - 58.1 \text{ mJ} \cdot \text{mole}^{-1} \cdot ^\circ\text{K}^{-1}$  (Clement et al 1952, Decker et al 1958, and Shiffman et al 1963).

(4) The critical field  $H_c$  shows a positive deviation from the simple relation  $H_c = H_0(1 - t^2)$  where  $t = T/T_c$





is the reduced temperature. The BCS theory predicts a small negative deviation, which is found in all superconductors so far investigated with the exception of Pb and Hg.

(5) The density of states as obtained from electron-tunneling experiments shows large resonance type deviations from the BCS expression (eqn. II-19).

## II.6 Zero-Temperature Strong-Coupling Theory

The BCS theory itself can be worked out in the strong-coupling limit (i.e.  $N(0)V \sim 1$ ). See, for example, Thouless (1960). It is found that no drastic deviations from the weak-coupling limit occur. The gap ratio  $2\Delta_0(0)/kT_c$  goes to a limit of 4.00 in the unphysical limit  $N(0)V = \infty$ . In Pb,  $N(0)V \sim 0.4$  and for this the ratio still remains close to 3.53.

Calculations were also carried out (Swihart 1962) assuming different forms for the interaction  $V$ , representing more closely the actual electron-phonon interaction. These calculations were only partially successful. It was, for example, not possible to reproduce in detail the observed structure in the electron tunneling data of Pb. All these calculations use an instantaneous electron-electron interaction, and also neglect lifetime effects. The phonon mediated electron-electron interaction is,





however, a retarded interaction. In the case of strong-coupling, this has to be taken into account. This leads to qualitatively different results than those of an instantaneous interaction theory. One must treat the system using a Hamiltonian which contains explicitly the electron-phonon interaction (the so-called "Frohlich Hamiltonian" (Frohlich 1950)) rather than representing the interaction by an effective instantaneous electron-electron interaction.

Eliashberg (1960) showed how the ground state spectrum could be obtained for this Hamiltonian. These calculations were extended, with particular emphasis on the electron-tunneling for Pb, by Scalapino, Schrieffer, and Wilkins (1963, 1966), by Schrieffer (1964), and by Scalapino and Anderson (1964). All of these approaches use the field theoretic Green's functions technique. The results can be expressed in terms of two complex functions of energy  $Z(\omega)$  and  $\varphi(\omega)$  (where the energy  $\omega$  is measured relative to the Fermi energy). A further function  $\Delta(\omega) = \varphi(\omega)/Z(\omega)$  is introduced. In the weak-coupling limit where this theory goes over into the weak-coupling BCS theory,  $\Delta(\omega)$  goes over into the energy gap  $\Delta_0$ . In the normal state  $\Delta(\omega)$  vanishes.  $\Delta(\omega)$  is therefore the analogue of the energy gap in the BCS theory. There is still, as in the weak-coupling theory, a certain minimum energy for creation



of a quasi-particle, this gap is denoted by  $\Delta_0$ . For energies below the gap edge energy,  $\Delta(\omega)$  is constant and therefore, in the strong-coupling theory, the gap is usually referred to as the "gap at the gap-edge", and is denoted by  $\Delta(\Delta) = \Delta_0$ . Since  $\Delta(\omega)$  is generally complex, it is often expressed as  $\Delta(\omega) = \Delta_1(\omega) + i\Delta_2(\omega)$ .

The functions  $\varphi(\omega)$  and  $Z(\omega)$  are given by the following expressions:

$$\varphi(\omega) = \int_0^{\omega_c} d\omega' \operatorname{Re} \left( \frac{\Delta'}{(\omega'^2 - \Delta'^2)^{\frac{1}{2}}} \right) (K_+(\omega, \omega') - N(0)U_c) \quad \text{II-34}$$

$$\omega[1 - Z(\omega)] = \int_0^{\omega_c} d\omega' \operatorname{Re} \left( \frac{\omega'}{(\omega'^2 - \Delta'^2)^{\frac{1}{2}}} \right) K_-(\omega', \omega). \quad \text{II-35}$$

Also,

$$\Delta(\omega) = \frac{1}{Z(\omega)} \int_0^{\omega_c} d\omega' \operatorname{Re} \left( \frac{\Delta'}{(\omega'^2 - \Delta'^2)^{\frac{1}{2}}} \right) (K_+(\omega, \omega') - N(0)U_c). \quad \text{II-36}$$

The kernels  $K_+$  and  $K_-$  are given by:

$$K_{\pm} = \sum_{\lambda} \int_0^{\infty} dv \alpha_{\lambda}^2(v) F_{\lambda}(v) [(\omega' + \omega + v + i0^+)^{-1} \pm (\omega' - \omega + v - i0^+)^{-1}]. \quad \text{II-37}$$

Here  $F_{\lambda}(v)$  is the normalized phonon spectrum, the polarization being denoted by  $\lambda$ ,  $\alpha_{\lambda}^2(v)$  is an average electron-phonon coupling constant,  $\omega_c$  is a cut-off energy taken at approximately  $\omega_c = 10 \omega_D$ , and  $U_c$  is the Coulomb pseudo-



potential characterizing the short-range, instantaneous Coulomb interaction. The explicit appearance of the phonon spectrum and electron-phonon coupling constant makes the results of the theory strongly dependent on the specific properties of the system. Scalapino et al (1965) have calculated the s-wave average of the electron-phonon coupling  $\alpha_{\lambda}^2(\omega)$ . They obtain,

$$\alpha_{\lambda}^2(\omega) = \frac{q_D^3}{6\pi^2} \left[ \sum_K \int \frac{d\Omega_q}{4\pi} \frac{|v_{q+K_{\lambda}}|^2}{2\omega_{q\lambda}} \frac{m}{2p_F |q+K|} \theta(2p_F - |q+K|) \right].$$

II-38

Here  $q_D$  is the Debye wave vector,  $p_F$  the Fermi wave vector, and  $m$  is the mass due to the band structure with Coulomb corrections but without corrections for the electron-phonon interaction.  $\theta$  is a unit step function vanishing when its argument is less than zero and equal to 1 otherwise. A discussion of the results of the theory, must therefore be based on specific assumptions regarding the system under consideration.

The strong-coupling theory has also been developed for finite temperatures using thermodynamical Greens functions techniques. Some of the results will be given in the next sections.





## II.7 Application to the Tunneling Process

Scalapino, Schrieffer, and Wilkins (1966) and Schrieffer, Scalapino, and Wilkins (1963) used strong-coupling theory to calculate the tunnel current in a superconductor-normal metal tunnel junction. They found that equation II-33 still holds but now the gap-parameter is replaced by the energy dependent gap  $\Delta(\omega)$  such that

$$\frac{N_T(\omega)}{N(0)} = \text{Re} \left( \frac{\omega}{(\omega^2 - \Delta(\omega)^2)^{\frac{1}{2}}} \right) . \quad \text{II-39}$$

Thus strong-coupling theory replaces the constant BCS energy gap by the function  $\Delta(\omega)$  and the normalized tunneling density of states becomes  $N_T(\omega)/N(0)$ . This is in 1:1 correspondence with the experimentally measured junction conductance as before. The normalized density of states can be calculated by solving simultaneously the coupled equations for  $\Delta(\omega)$  for a particular choice of phonon spectrum and coupling constant  $\alpha^2(\omega)$ , and then using the energy dependent value of  $\Delta(\omega)$  in equation II-39. Calculations along these lines have been performed by Rowell and Kopf (1965), by Scalapino and Anderson (1964), and by others. In general these calculations showed excellent agreement with experimentally obtained curves.

McMillan and Rowell (1965) took the further step of actually inverting this process. They guess at  $\alpha^2(\omega)F(\omega)$





and solve the gap equations choosing  $U_c$  to give the experimental value of  $\Delta_o$ . They then calculate the electronic density of states. Linear feedback techniques are then used to correct  $\alpha^2(\omega)F(\omega)$  for the "error"  $N_s^{\text{exp}}(\omega) - N_s^{\text{calc}}(\omega)$ . In this way they can obtain the actual form of  $\alpha^2(\omega)F(\omega)$  from experimental data on the density of states. Their result is shown in figure 2 along with plots of the normalized conductance  $\sigma$  (i.e. the density of states) and  $d\sigma/dV$ .

## II.8 Phonon Emission Processes and the Density of States

The structure in the normalized conductance curve (as well as in  $d\sigma/dV$ ) centered around 4.4 meV and 8.5 meV is associated with phonon emission processes. Physically these processes occur in the following way. Quasi-particles at the longitudinal and transverse energies  $\omega_\ell$  and  $\omega_t$ , have a relatively high chance of losing energy by emission of phonons. They then drop to the peaked density of states region near the gap edge. Energetically this occurs when

$$V = \Delta_o + \omega_\lambda \quad \text{II-40}$$

and to a lesser extent at harmonic frequencies.

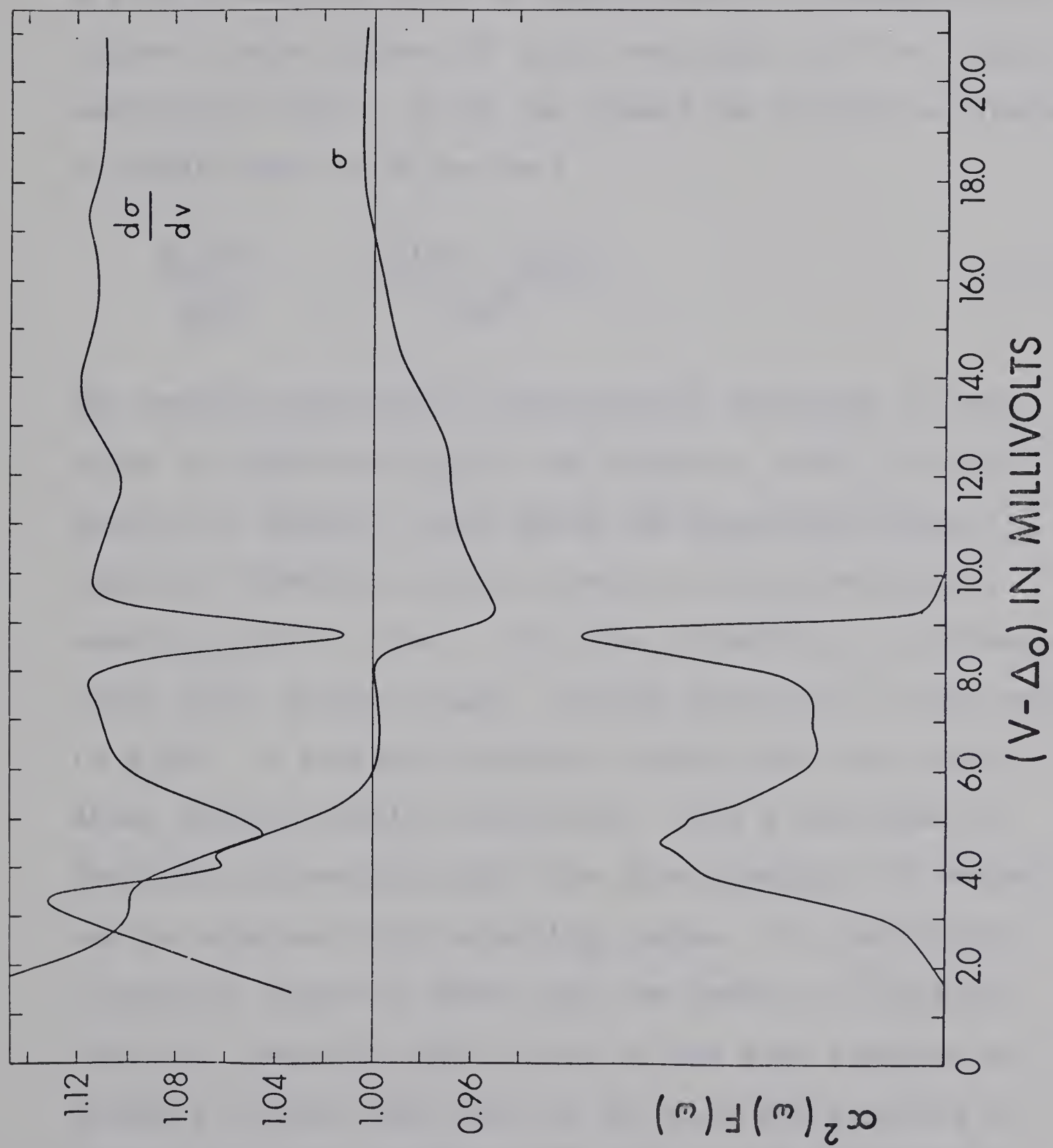
The resonance structure is reproduced in model calculations for the density of states. This can be seen



Figure 2

The normalized conductance  $\sigma$ , and  $d\sigma/dV$  for a Pb-Al tunnel junction. Also shown is  $\alpha^2(\omega)F(\omega)$  calculated by McMillan and Rowell (1965).







most easily by expressing  $\Delta(\omega)$  as

$$\Delta(\omega) = \Delta_1(\omega) + i\Delta_2(\omega) \quad \text{II-41}$$

where  $\Delta_1(\omega)$  and  $\Delta_2(\omega)$  are real functions. These functions are then calculated for a model chosen to represent Pb.

Figure 3 shows curves of  $\Delta_1(\omega)$  and  $\Delta_2(\omega)$  for  $T = 0$  and a particular model. If we now expand the density of states to first order in  $\Delta^2$  we have

$$\frac{N_T(\omega)}{N(0)} = 1 + \frac{\Delta_1^2(\omega) - \Delta_2^2(\omega)}{2\omega^2} + \dots \quad \text{II-42}$$

The emission process is reflected as structure in the plots of  $\Delta_1(\omega)$  and  $\Delta_2(\omega)$ , and from eqn. II-42, in the density of states. Just below the transverse phonon emission threshold  $\Delta_1(\omega)$  increases with increasing  $\omega$ , causing  $N_T(\omega)$  to rise. After the threshold,  $\Delta_1$  decreases while  $\Delta_2(\omega)$  becomes large, thereby producing a sharp drop in  $N_T(\omega)$ . A similar situation occurs near the longitudinal phonon emission threshold. Thus a good deal of detailed information about the phonon density of states can be obtained from tunneling curves. In particular, a study of figure 2 shows that the peaks in  $\alpha^2(\omega)F(\omega)$  (that is, peaks in  $F(\omega)$ ) occur at the same energies as minima in  $d\sigma/dV$ , and occur at the mid-height points of the structure drop-offs in  $\sigma$ . One should therefore be





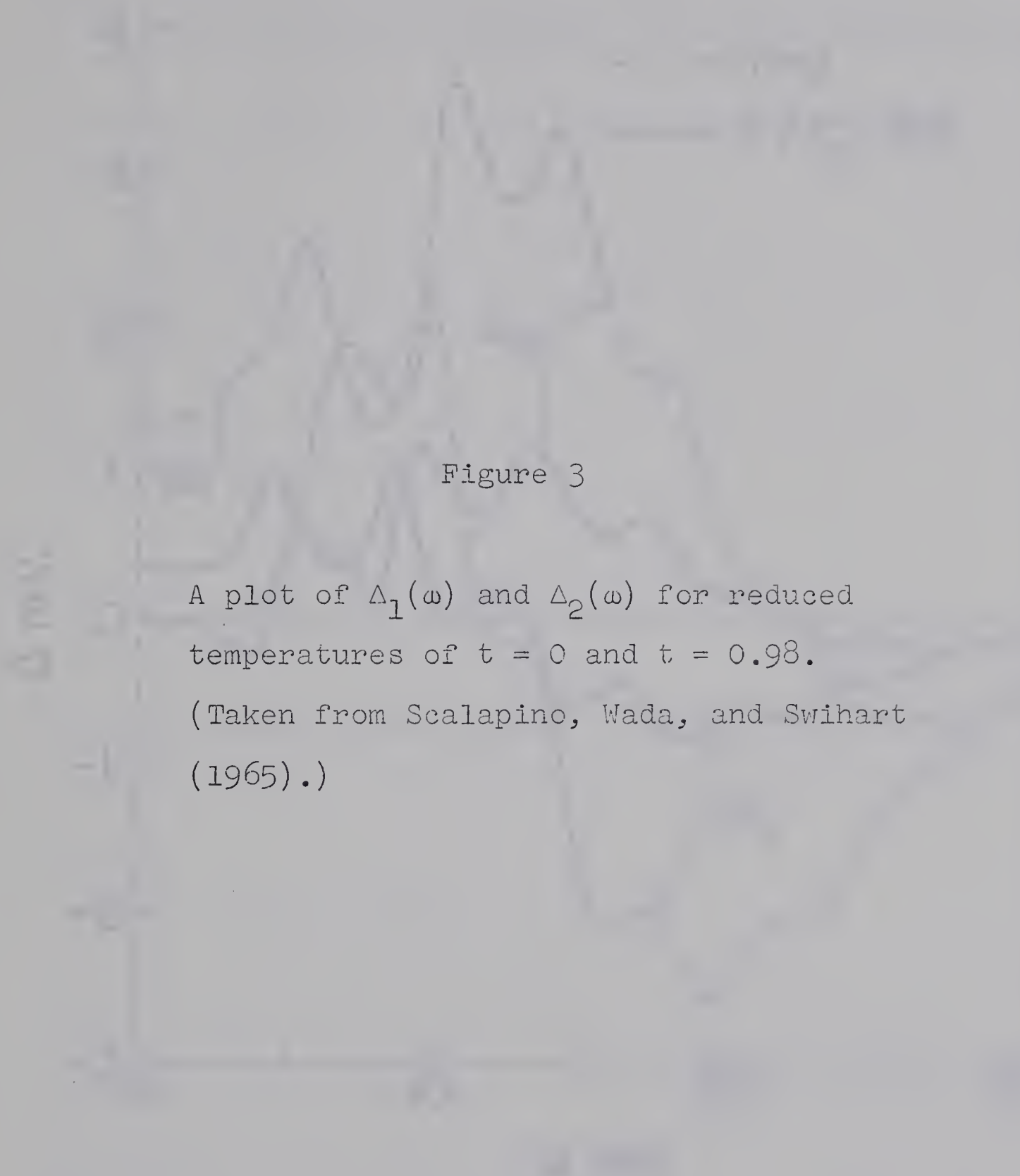
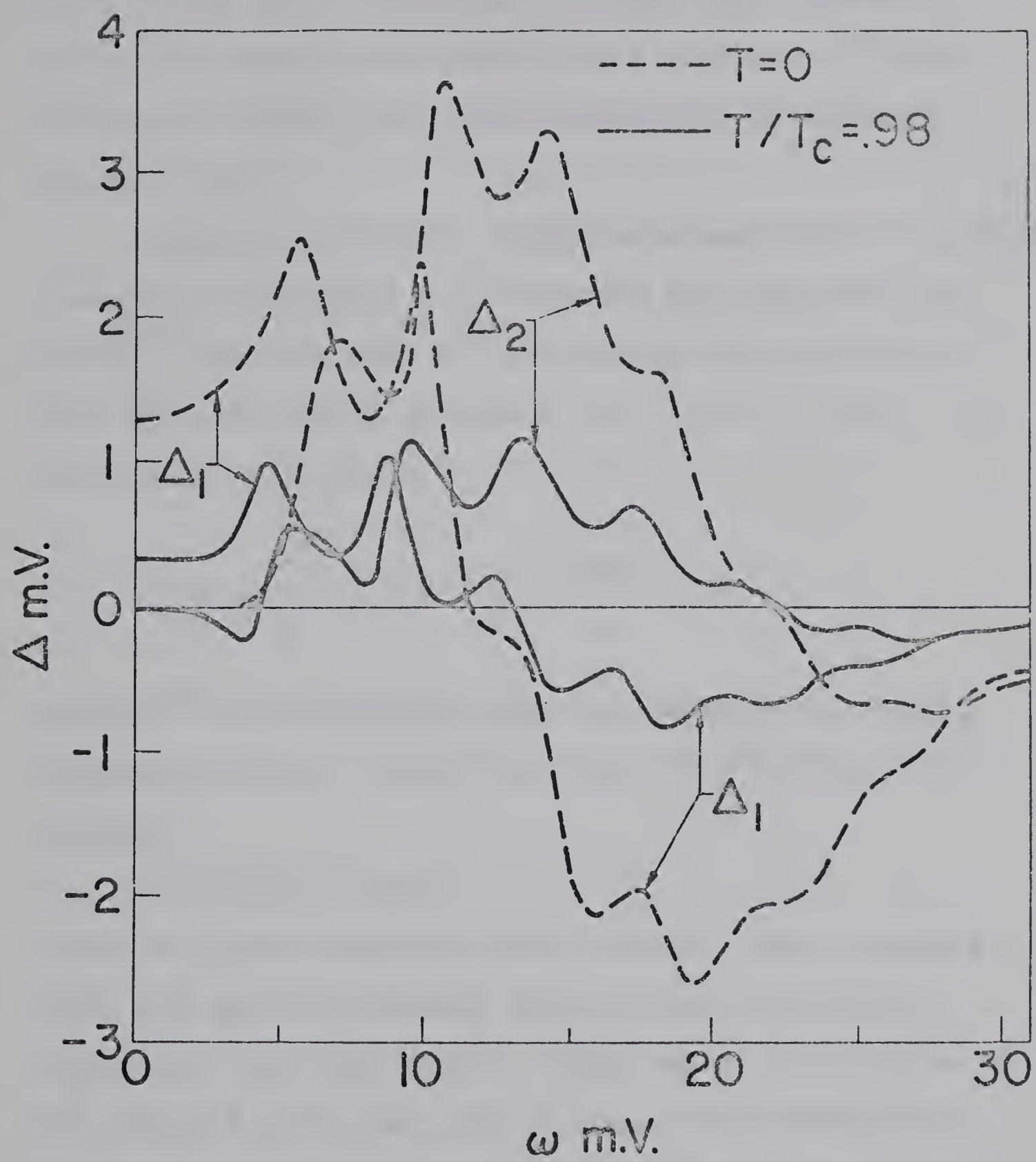


Figure 3

A plot of  $\Delta_1(\omega)$  and  $\Delta_2(\omega)$  for reduced temperatures of  $t = 0$  and  $t = 0.98$ .

(Taken from Scalapino, Wada, and Swihart (1965).)







able to use the conductance structure and  $d\sigma/dV$  for measuring phonon peak shifts under pressure. This is discussed further when such results are presented in section VI.2.

McMillan and Rowell (1965) have used their calculated results of  $\alpha^2(\omega)F(\omega)$  in estimating the effective mass of Pb. This was done by calculating the real part of the renormalization parameter  $Z(\omega)$  for  $\omega = 0$  and  $T = 0$ . They then have (since  $\Delta = 0$  as well),

$$Z_n(0) = \frac{m^*}{m} = 1 + 2 \int_0^\infty \frac{\alpha^2(\omega)F(\omega)}{\omega} d\omega$$

where  $m^*$  is the apparent mass due to electron-phonon renormalization. Using their plot of  $\alpha^2(\omega)F(\omega)$  they obtain

$$m^* = 2.33 \pm 0.02 m$$

where  $m$  is the ordinary electron mass. This compares with 2.2 and 2.4 obtained theoretically by Swihart, Scalapino, and Wada (1965), using model calculations of  $\alpha^2(\omega)F(\omega)$  for Pb, and with a value of 2.1 obtained by specific heat measurements (Keesom et al, 1963). The value of the effective mass (which can in large measure be accounted for by the electron-phonon interaction) demonstrates, in yet one more way, the importance of the strong interaction on the properties of Pb.



## II.9 Strong-Coupling Theory at Finite Temperature

Scalapino, Wada, and Swihart (1965) and Swihart, Scalapino, and Wada (1965) have extended the gap calculations to finite temperature using strong-coupling theory. They have published curves of  $\Delta_1(\omega, T)$  and  $\Delta_2(\omega, T)$  for  $t = T/T_c = 0.98$  and  $t = 0.95$  and a model chosen to represent Pb. In these calculations they chose for Pb a lattice spectrum consisting of two Lorentzians centered at  $\omega_t = 4.4$  meV and  $\omega = 8.5$  meV. The electron-phonon coupling constants  $\alpha_\ell^2$  and  $\alpha_t^2$  were chosen to obtain agreement with the experimentally determined zero temperature gap at the gap-edge. Calculations were made for  $\alpha_\ell^2/\alpha_t^2 = 1$  (case 1) and  $\alpha_\ell^2/\alpha_t^2 = 2$  (case 2). The  $t = 0.98$  results are included in figure 3. Their results can be summarized as follows:

- (1) The resonance peaks connected with phonon emission are sharpened at non-zero temperatures, and are shifted down in energy in accordance with a reduction in the energy gap with increase in temperature.
- (2) Near  $\omega = 0$ ,  $\Delta_1(\omega)$  is flatter as a function of energy.
- (3) New resonance structure occurs near the frequencies  $\omega_\lambda - \Delta_o(T)$  which is most evident near  $\omega_t - \Delta_o(T)$ , where  $\Delta_2(\omega, T)$  goes through a negative resonance peak.





The new resonances are thought to be associated with recombination processes between injected electrons (as from tunneling) and thermally excited quasi-particles in the high density of states region near the gap edge  $\Delta_o(T)$ . The combined particles emit a phonon, and form a ground state pair. The rate of the process is a maximum when the total energy  $V$  of the injected electron and excited quasi-particle at  $\Delta_o(T)$  is equal to a frequency corresponding to a peak in the phonon density of states (i.e.  $V + \Delta_o(T) = \omega_\lambda$ ). This additional structure in  $\Delta(\omega)$  should appear in the tunneling density of states. They have published theoretically expected tunnel junction conductance curves for  $t = 0.95$  and  $t = 0.92$ . An investigation of this effect is discussed in section VI.6.

(4) The calculation of  $T_c$  from the gap relation leads to  $2\Delta_o(0) = 4.40 kT_c$  in case 1 and  $2\Delta_o(0) = 4.33 kT_c$  in case 2.

(5) The reduced gap at the gap-edge energy  $\Delta_o(T)/\Delta_o(0)$  as a function of reduced temperature  $t$  is "within a couple of percent" of the BCS expression.

An additional comment on the gap- $T_c$  relation is in order. Using the measured gap value for Pb ( $\Delta_o(0) = 1.34$  meV), the transition temperature would have to be  $\sim 11.3^\circ\text{K}$  for the BCS ratio  $2\Delta_o(0)/kT_c = 3.53$  to hold. Wada (1964A)



associates the observed value of  $\sim 4.4$  with the strong-coupling resonant processes which give rise to quasi-particle damping. Since the damping rate is greater at higher temperatures where more excited quasi-particles are produced, the transition temperature is reduced much more than the zero temperature energy gap, thereby increasing the ratio  $2\Delta_0(0)/kT_c$ .

## II.10 Calculation of Thermodynamic Quantities

Wada (1964B) has undertaken a calculation of some of the thermodynamic quantities in Pb using strong-coupling theory. In particular, he attempts to reconcile the discrepancies in  $\Delta C_{el}$  and the condensation energy relation mentioned earlier. He has shown that in general

$$\frac{H_0^2}{8\pi} = \frac{N(0)}{4\alpha - 1} I(T) \quad \text{II-43}$$

where  $H_0$  is the zero-temperature critical field, and  $I(T)$  is a functional of the electron-phonon renormalization functions  $Z_n$  and  $Z_s$  and of the complex gap. The exponent  $\alpha$  appears in the isotope effect as

$$H_0 \propto M^{-\alpha} \quad \text{II-44}$$

and  $\alpha = \frac{1}{2}$  for Pb. Therefore,  $4\alpha - 1$  reduces to 1 so that

$$\frac{H_0^2}{8\pi} = N(0)I(T). \quad \text{II-45}$$



In the weak coupling limit,  $I$  goes properly over into  $I = \frac{1}{2}\Delta_0^2$  to yield the BCS result. One can therefore introduce the ratio  $I/\frac{1}{2}\Delta_0^2$  and use this as an approximate measure of the coupling strength. For Pb,  $I/\frac{1}{2}\Delta_0^2 = 0.83$  so the condensation energy is smaller than the BCS prediction.

Wada has also derived an expression for the jump in electronic specific heat:

$$\Delta C_{el} = - N(0) \frac{d^2 I(T)}{dt^2} \quad \text{II-46}$$

Carrying out the derivative of the function  $I$  he obtains,

$$\Delta C_{el} = - kN(0)\beta_c^3 \left[ \frac{1}{2} \int_0^\infty \frac{d\omega \partial \Delta^2 / \partial \beta_c}{\cosh^2(\beta_c \omega / 2)} - \int_0^\infty \frac{d\omega}{2\omega^2} \frac{\partial}{\partial \omega} \left( \frac{\partial \Delta^2}{\partial \beta_c} \right)^2 \tanh \frac{\beta_c \omega}{2} \right] \quad \text{II-47}$$

where  $\beta = 1/kT$ ,  $\Delta = \Delta(\omega)$ , and  $k$  is Boltzmann's constant.

Thus knowing the proper energy dependence of  $\partial \Delta^2 / \partial \beta_c$  one can in principle calculate  $\Delta C_{el}$ . Wada remarks, "we may conclude that the present theory is likely to predict a larger jump in specific heat and give better agreement with the experimental results for the strong coupling superconductors than the BCS results."





## CHAPTER III

## THE CRYOSTAT AND PRESSURE SYSTEM

III.1 The Cryostat

The cryostat was suspended inside a two-dewar coolant system. The outer dewar contained liquid nitrogen and the inner dewar contained liquid helium four ( $\text{He}^4$ ). Figure 4 shows a cross-section of the cryostat.

Since a working temperature range of  $\sim 1.4^\circ\text{K}$  to  $\sim 40^\circ\text{K}$  was required, a  $\text{He}^4$  reservoir was soldered to the specimen bomb. By admitting liquid helium from the inner dewar through the needle valve control and then reducing pressure on the enclosed liquid vapor with a vacuum pump, a low temperature limit of approximately  $1.25^\circ\text{K}$  could be reached. Installation of heater resistors enabled the higher temperatures to be reached quickly when necessary.

The cryostat vacuum pump tubes consisted of  $3/4$  inch diameter thin-wall stainless steel tubing. This was chosen because of its strength and low thermal conductivity. The high pressure capillary tube entered the cryostat vacuum jacket ten inches above the top of



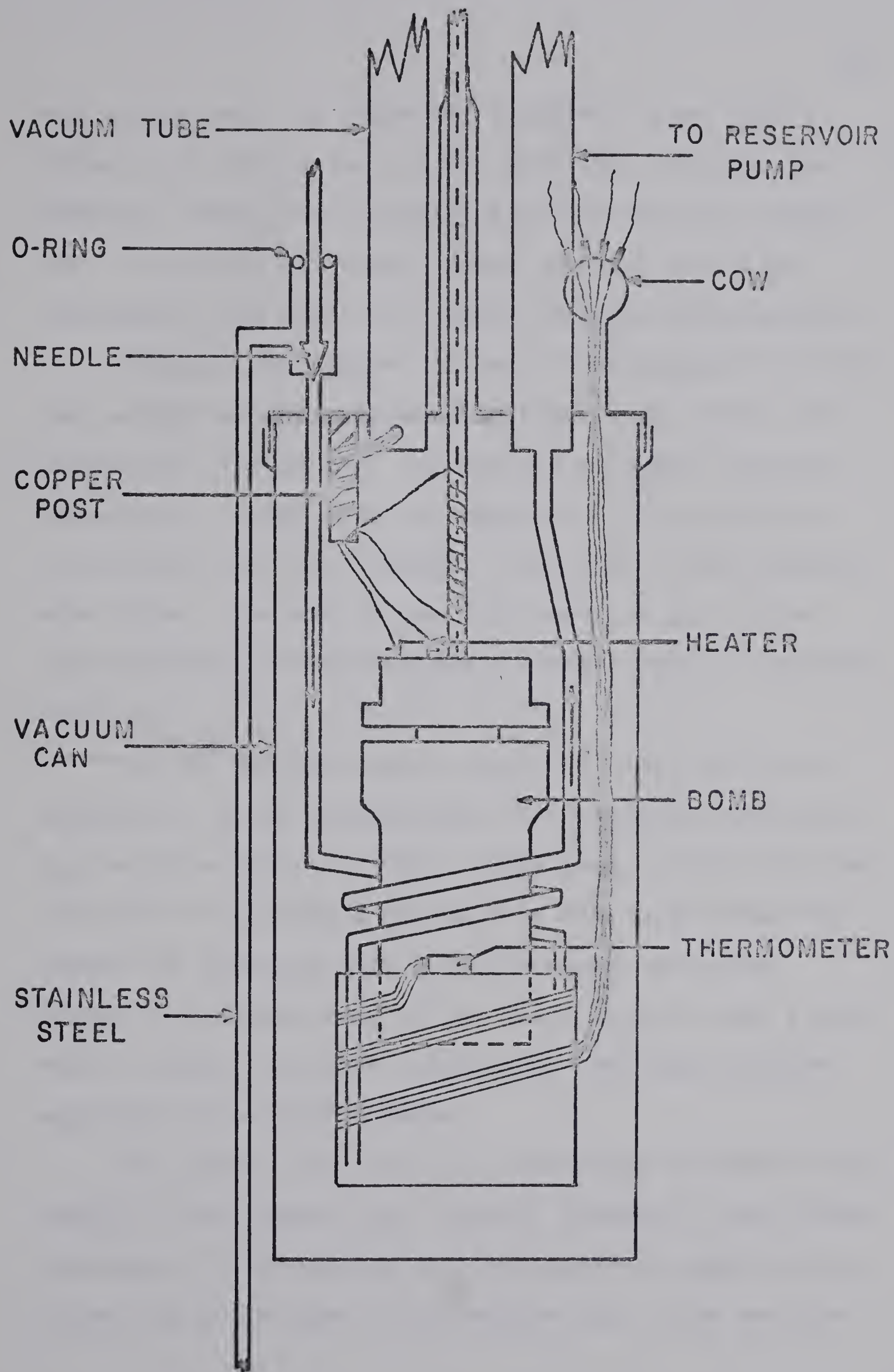




Figure 4

A cross-section of the cryostat used.







the vacuum can. By inserting stainless steel tubing between the vacuum can and the capillary contact, the pressure tubing was thermally isolated from the vacuum can. This step was taken to help prevent capillary blockage at the point of contact during pressurization.

Manganin resistance wire was wound spirally around the outside of the pressure capillary both inside and outside the vacuum can. By passing a current through these wires, extra heat was supplied to the capillary to help prevent its blockage. Even after these measures were taken, freezing of the high pressure gas at the capillary inlet to the vacuum can still posed a definite problem.

The  $\text{He}^4$  melting curve (figure 5) shows that at a pressure of 5,000 atmospheres, the freezing temperature  $T_m$ , is quite high at  $\sim 40^\circ\text{K}$ . After pressurizing the bomb, about 600 cc of liquid helium from the inner dewar was needed for freezing this gas at constant pressure. During the earlier runs it was found that if this liquid was in contact with the vacuum can, the high pressure capillary invariably blocked.

The problem was solved by connecting stainless steel tubing to the needle valve control leading to the helium reservoir. By extending this tubing about eight to ten inches below the base of the vacuum can, which was now

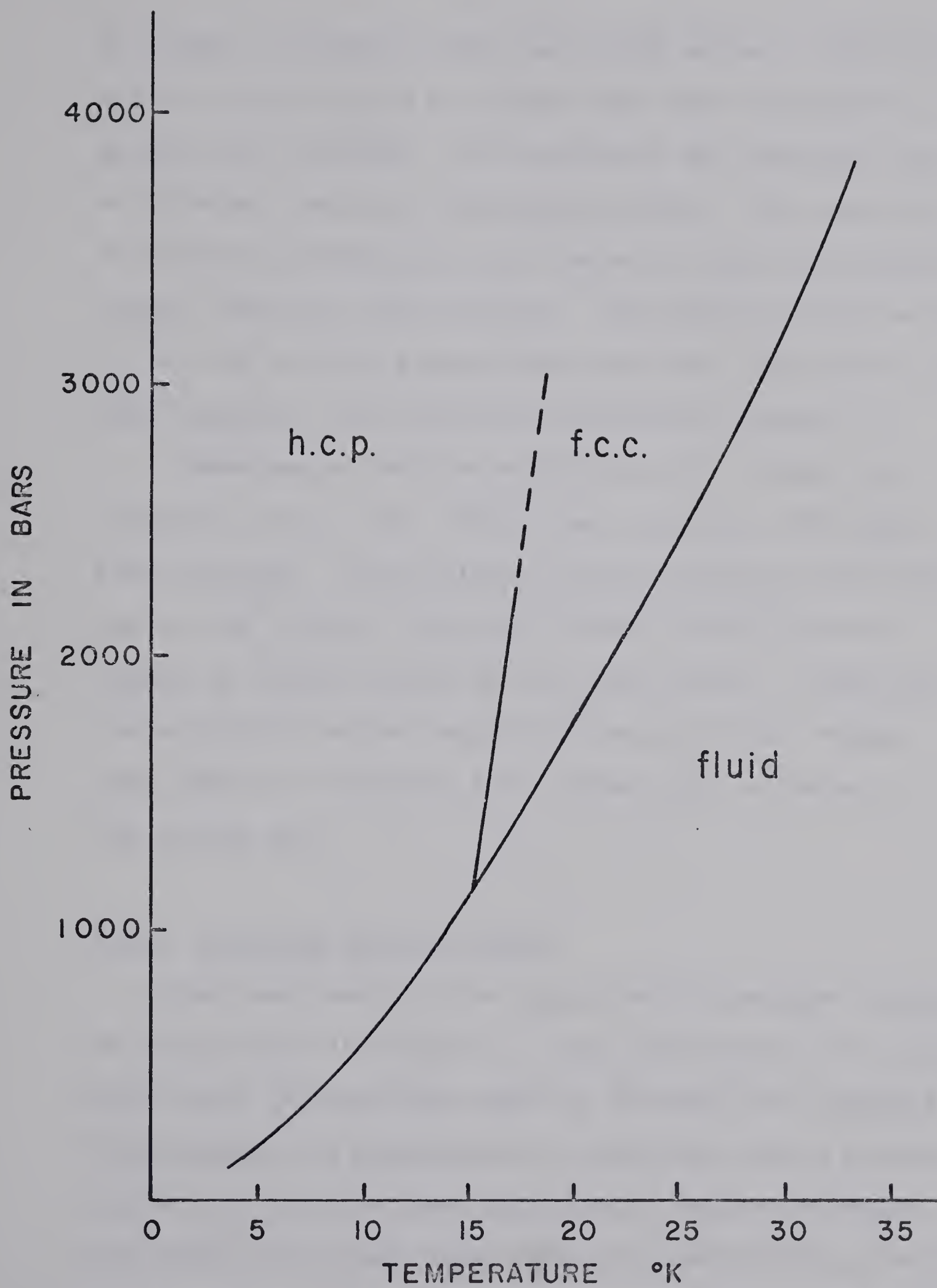


Figure 5

The  $\text{He}^4$  melting curve. (Due to Mills and Grilly (1955) and Dugdale (1965).)









no longer in contact with the liquid helium, sufficient helium coolant could be sucked into the reservoir to produce the freezing. The capillary now remained open so constant pressure freezing occurred. This resulted in frozen-in pressures about twice as large as constant volume freezing could produce. The pressure drop between  $T_m$  and the working temperature was about 10% which is in good agreement with published isochores (figure 6).

Thermometer leads were fed into the vacuum can through a glass "cow" vacuum seal provided with kovar feed-throughs. This method insured adequate lead anchoring at 4.2°K since the leads passed through several inches of liquid helium in the inner dewar. Leads for the capillary heater were fed down one of the vacuum pump tubes and anchored to a copper post soldered to the vacuum can.

### III.2 The High Pressure Bomb

The bomb used for the experimental pressure chamber is illustrated in figure 7. The bomb material is copper with about 2% beryllium added to increase its hardness. This material is preferable to stainless steel because, while both have the same approximate rupture strength, the Cu-Be has a much higher thermal conductivity, and does not become brittle at low temperature. The Cu-Be was



Figure 6

$\text{He}^4$  isochores. (Taken from Dugdale  
and Simon (1953).)



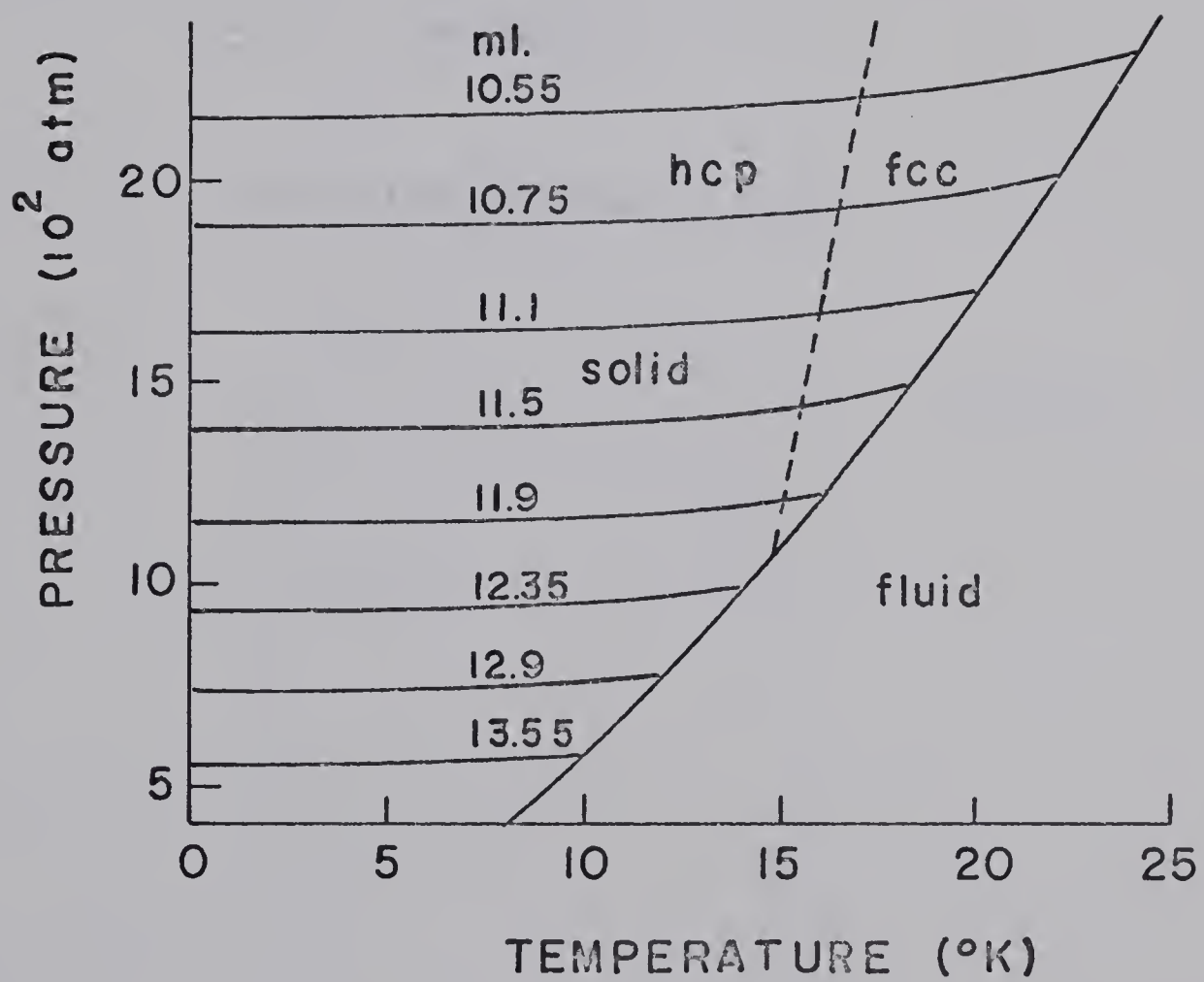


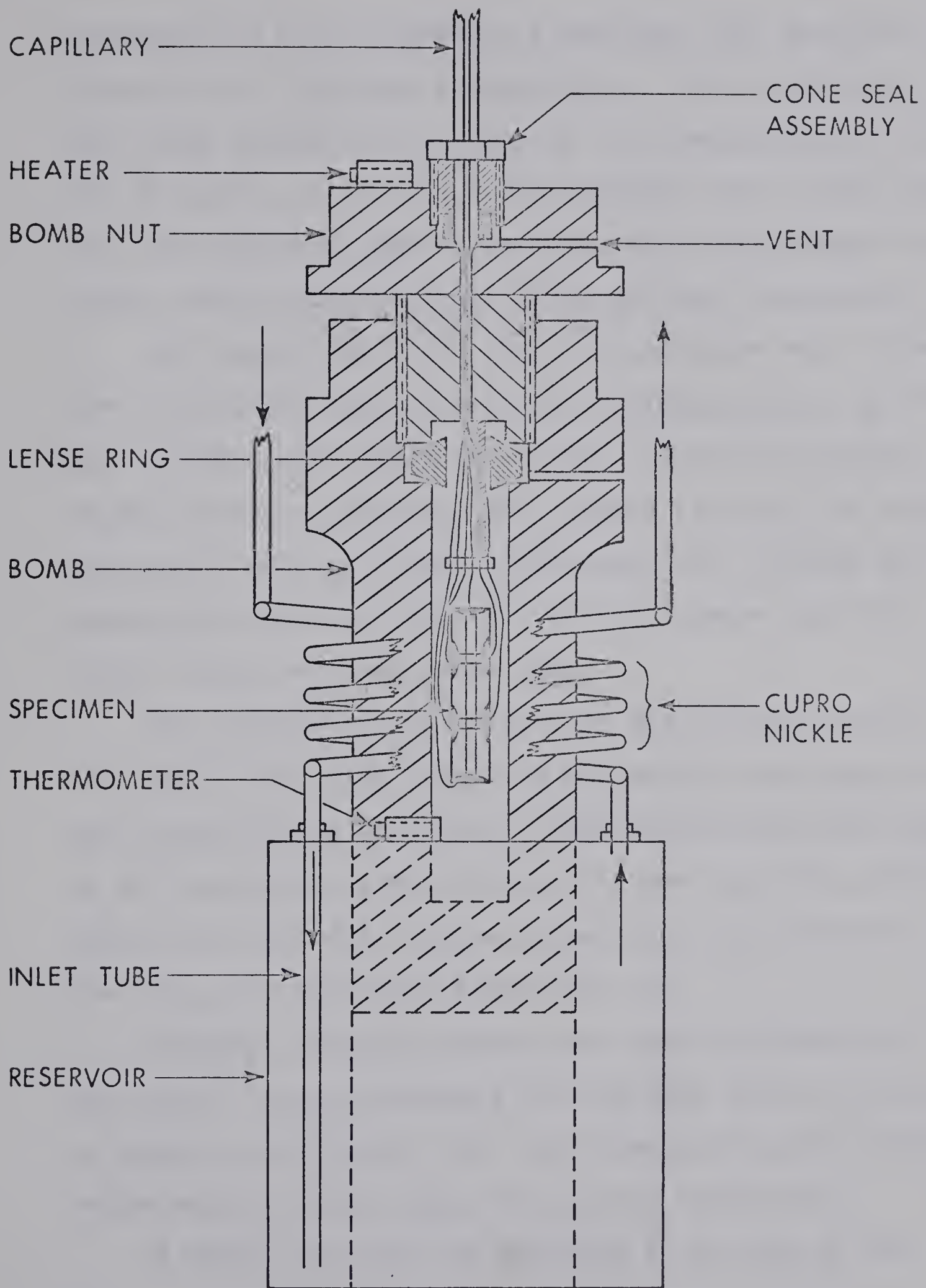




Figure 7

The high pressure bomb.







purchased as a half hardened alloy from "The Beryllium Corporation", Reading, Pennsylvania. After machining, it was fully hardened by heating it to a temperature of  $600^{\circ}\text{K}$  for  $1\frac{1}{2}$  hours. A diamond press hardness test of the full and half hardened samples verified that the hardness was indeed about twice as great after the heat treatment.

The lense ring which forms the pressure seal between the nut and the bomb was made of stainless steel, ground and polished with edges cut at  $37^{\circ}$ . Hence an increase in gas pressure increases the outward force on the ring so that it acts as a self tightening seal. Notice the relief hole drilled into the bomb to release gas that might escape past the lense ring.

The cylindrical  $\text{He}^4$  reservoir was soldered around the bomb. The inlet tube from the needle valve goes to the bottom of the reservoir. Thus during the first stages of  $\text{He}^4$  admission, the bottom of the bomb was the coldest. Therefore, the solid helium formed from the bottom of the bomb, and then grew toward the top.

Thermal isolation between the pumping chamber and the vacuum can was achieved by inserting about 10 inches of spiral cupro-nickel into the lines joining the needle valve and the vacuum pump tube to the reservoir.

A heater resistor was attached to the top of the



bomb nut and a calibrated germanium thermometer was mounted on the reservoir. Thermometer lead anchoring to the specimen bomb was achieved by wrapping the leads around the reservoir several times and then cementing them to it with General Electric baking varnish type GE9825. The lowest temperature attainable in the cryostat was about  $1.25^{\circ}\text{K}$ .

The specimen leads were introduced into the bomb through the high pressure gas capillary. The leads were terminated on a teflon strip as shown. Specimen mounting involved soldering the specimen leads to the appropriate terminals.

### III.3 Pressure Production

The gas pressure system was purchased from Harwood Engineering, Walpole, Massachusetts. It consists of three pumping stages. The first stage and the second stage occur at either ends of a double acting piston which is oil driven and reversed for consecutive strokes by electrical micro-switches which control an oil diverting mechanism. Stage 1 exhausts into stage 2. An inlet pressure of 800 psi at stage 1 is increased to a maximum of 12,000 psi at the output of stage 2. This stage exhausts into an intensifier chamber which can be isolated from the stage 2 pump by manually operating a





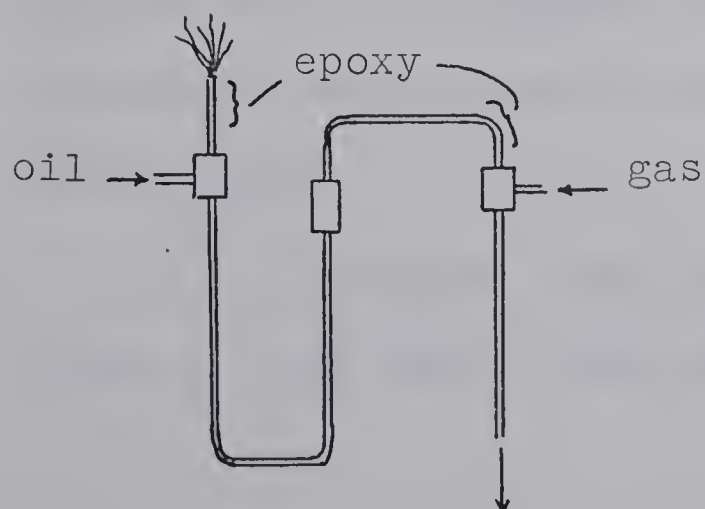


needle valve. The third or intensifier stage is an oil driven piston stage (area multiplication of 14). The oil pressure is provided by an air diaphragm pump for this stage. A motor driven pump provides oil pressure to stages one and two. The intensifier is connected through another needle valve to the specimen bomb.

The bomb pressure (and intensifier pressure if the connecting needle valve is open) is measured by using the resistance of a manganin wire as the sensing device. The resistance is measured with a Wheatstone bridge circuit and the imbalance is calibrated in units of psi. The instrument accuracy is better than 1%.

#### III.4 High Pressure Electrical Lead Seal

Six electrical leads to the inside of the high pressure bomb were needed. This allows four terminal measurements to be made on two junctions mounted on the same substrate. The high pressure lead seal described by Goree, McDowell, and Scott (1965) was used. This method involves a room temperature high pressure seal.



Size 34 gauge insulated copper wires were fed through about 12 feet of high pressure capillary and couplings as illustrated.



Eccobond 104 epoxy purchased from Emerson and Cumming Inc. was squeezed into the high pressure tube at the two places shown. Before pressurizing, oil is admitted and frozen in the U-tube with liquid  $N_2$ . We have found that in this way pressure up to 60,000 psi could be contained quite adequately. However, after two or three months of standing at room temperature and zero pressure, the epoxy seals had a tendency to soften and fail under subsequent pressurizing. We ascribe this to the presence of the oil. For pressures near 100,000 psi, it would probably be necessary to make a new seal before every run. For pressures around 50,000 psi, a plug of frozen oil would hold the pressure even if the gas leaked past the epoxy seals.

### III.5 Precautionary Measures

The production of high gas pressure coupled with low temperature requires some safety precautions since a vacuum failure can result in a rapid warming up of the system with a consequent large pressure build-up. In assembling the pressure system the following precautions were taken;

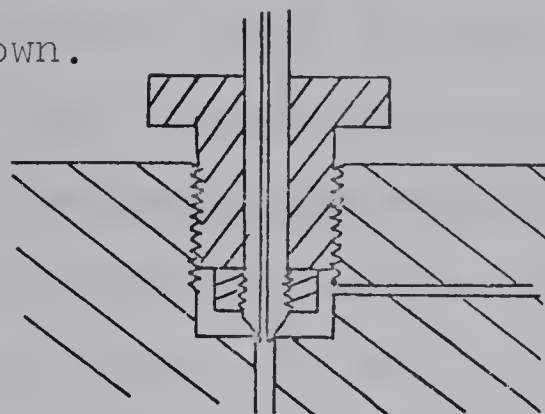
- (1) Pressure lines were either shielded by angle iron or tied down to prevent possible whip-lashing if



one of the joints broke.

(2) All joints were positioned so that they pointed away from potential working areas.

(3) All capillary connection joints were conical jam seals as shown.



A vent between the seal and thread was always present to prevent pressure build-up in the event of a leak at the cone seal. Absence of this vent could have resulted in ejection of the tube if a leak at the seal developed.

(4) The whole cryostat was mounted inside a 1/4 inch plate steel closet lined inside and out with 3/4 inch plywood. This completed the shielding of all of the high pressure volume.

### III.6 Thermometry

Temperature measurements were obtained using a germanium thermometer\*. This was calibrated to 0.1%

---

\*I wish to thank Dr. Franck for the use of his calibrated thermometer throughout this work.



accuracy against  $\text{He}^3$  and  $\text{He}^4$  vapor pressures from  $0.65^\circ\text{K}$  to  $4.2^\circ\text{K}$ . For temperatures from  $4.2^\circ\text{K}$  to  $\sim 7.5^\circ\text{K}$  the thermometer was calibrated against a second germanium thermometer, which in turn had been calibrated against a gas thermometer to an accuracy of 0.1%. During the calibration of the second germanium thermometer, a re-determination of the transition temperature of unstrained pure bulk Pb gave  $7.196 \pm 0.005^\circ\text{K}$ , in good agreement with the value of  $7.193 \pm 0.005^\circ\text{K}$  reported by Franck and Martin (1961). The estimated temperature uncertainty is  $\pm 0.1\%$  for all temperatures below  $7.5^\circ\text{K}$ .







## CHAPTER IV

## THE ELECTRONIC DETECTION SYSTEM

IV.1 Introduction

The investigation of characteristic microscopic metal properties at low temperature calls for especially low level probe signals. Ideally, thermal smearing,  $kT$ , should be the limitation where  $k$  is Boltzmann's constant. Since  $kT$  is approximately  $86 \mu\text{eV}$  at  $1^\circ\text{K}$ , our boundary condition is clearly defined.

Noise arises from such statistical fluctuation phenomena as Johnson noise in resistors and shot noise in vacuum tubes and semiconductors; these both produce a white noise spectrum in which the noise power per unit bandwidth is the same at all frequencies. Another source is the gain modulation or flicker effect noise associated with both vacuum tubes and amplifying circuits. This noise frequency spectrum varies as  $1/f$  so that a large contribution to the total noise occurs near dc. Interference phenomena which are not really noise, but produce the same effect in obscuring the signal, include power line pick-up and radio-frequency interference.

With respect to white noise, little can be gained by moving the signal frequency to a different value.



However, the contribution of the white noise to the output voltage of the detection system is directly proportional to the square root of the bandwidth, and can be reduced to an arbitrarily small value by reducing the bandwidth. For  $1/f$  noise and interference, an operating frequency different from dc and from interfering frequencies can be selected. Considerable effort was made to shield against pick-up. The residual level was about 1 to 2 microvolts, and consisted of 60 cycle and 1 megacycle contributions. The latter contribution was the smaller and came from the computer stationed four floors away.

The tunnel junction normalized conductance  $\sigma$  is related to the superconducting density of states by the relation  $\sigma = (di/dv)_{ns}/(di/dv)_{nn} = N_T(\omega)/N(0)$ . Both  $\sigma$  and its derivative  $d\sigma/dv$  can be obtained by applying an ac signal and using harmonic detection techniques.

If the voltage modulation amplitude is kept constant, the current  $i$ , passing through the junction may be written in terms of a Taylor series:

$$i(v) = i(v_0) + (di/dv)_{v_0} m \cos \omega t + \frac{1}{4} (d^2 i / dv^2)_{v_0} m^2 (1 + \cos 2\omega t) + \dots, \quad \text{IV-1}$$

where  $m$  is the constant voltage modulation amplitude, and  $v_0$  is the dc junction bias voltage. Therefore, the component of voltage across the junction at angular fre-



quency  $\omega$  is proportional to  $di/dv$  and the component at  $2\omega$  is proportional to  $d^2i/dv^2$ .

The respective informations at frequencies  $\omega$  and  $2\omega$  were obtained using a bridge system (to be described) and a lock-in amplifier as the signal detector.

A lock-in amplifier is essentially a narrow band detector in which a signal is beat with a reference signal of the same frequency giving a dc output; the upper side-band is stopped by a low pass filter. The low pass filter determines the bandwidth of the lock-in output. The main advantages of the lock-in device over a tuned amplifier circuit are:

- (1) it is easily tunable since the reference frequency determines the center frequency of the pass band

- (2) no matter how narrow the bandwidth of the detection system, the center of the pass band is always locked to the signal frequency when the signal is available for use as the reference.

Thus by moving the signal frequency to about 1700 cycles per second, and using the lock-in amplifier as a detector with an input frequency pass band of about 100 cps, the thermal noise voltage is almost completely removed from the signal input voltage. Only the thermal noise associated with the pass band frequencies contributes to the noise background.





## IV.2 Circuit Operation

A block diagram of the detection system is shown in figure 8. For the conductance measurements, signal at frequency  $\omega$  is required. In the case of  $d\sigma/dv$ , the second harmonic component,  $2\omega$ , generated across the non-linear tunnel resistance  $R_t$ , must be measured. The latter is accomplished by setting the reference frequency to  $2\omega$  in a frequency doubler circuit connected to the oscillator. At the same time, the lock-in input frequency is set to  $2\omega$ .

The bridge circuit which produces the required constant voltage condition is shown in figure 9.\* The junction resistance and capacitance are balanced by  $C_d$  and  $R_d$ . The latter consists of two 10 turn potentiometers in series. As the dc bias is swept with a motor drive, changes in the tunnel characteristic results in a voltage difference being fed to the input of the operational amplifier. This amplifier has a gain of approximately 50,000. The voltage difference is amplified and current feedback through the 10k feedback resistor to the junction. The feedback current is such that the signals across  $R_d$  and  $R_t$  are equalized to a good approximation.

---

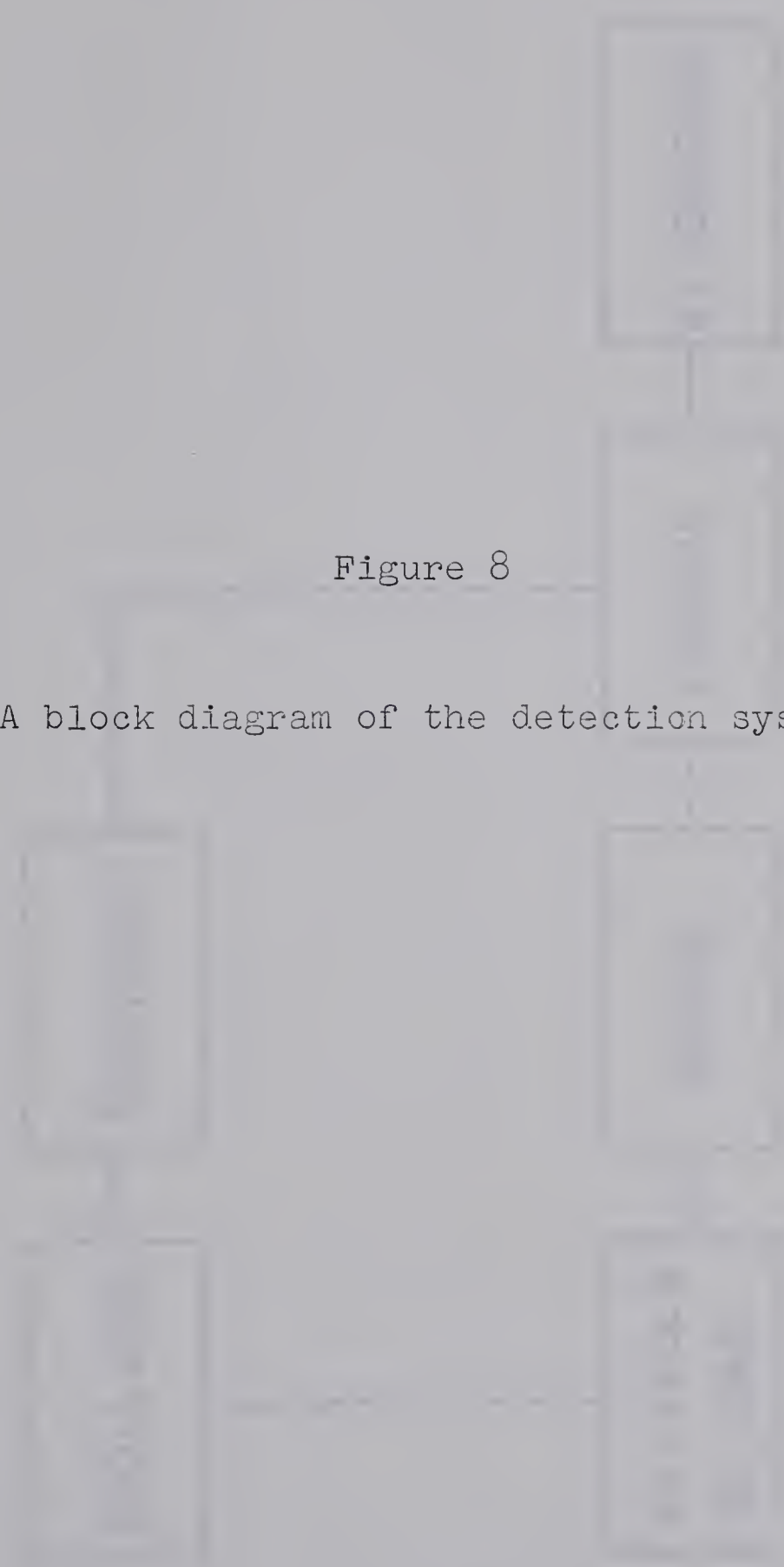
\*It is a pleasure to thank Dr.J.S. Rogers for his suggestions regarding the electronics, and particularly for his construction of this bridge circuit.





Figure 8

A block diagram of the detection system.





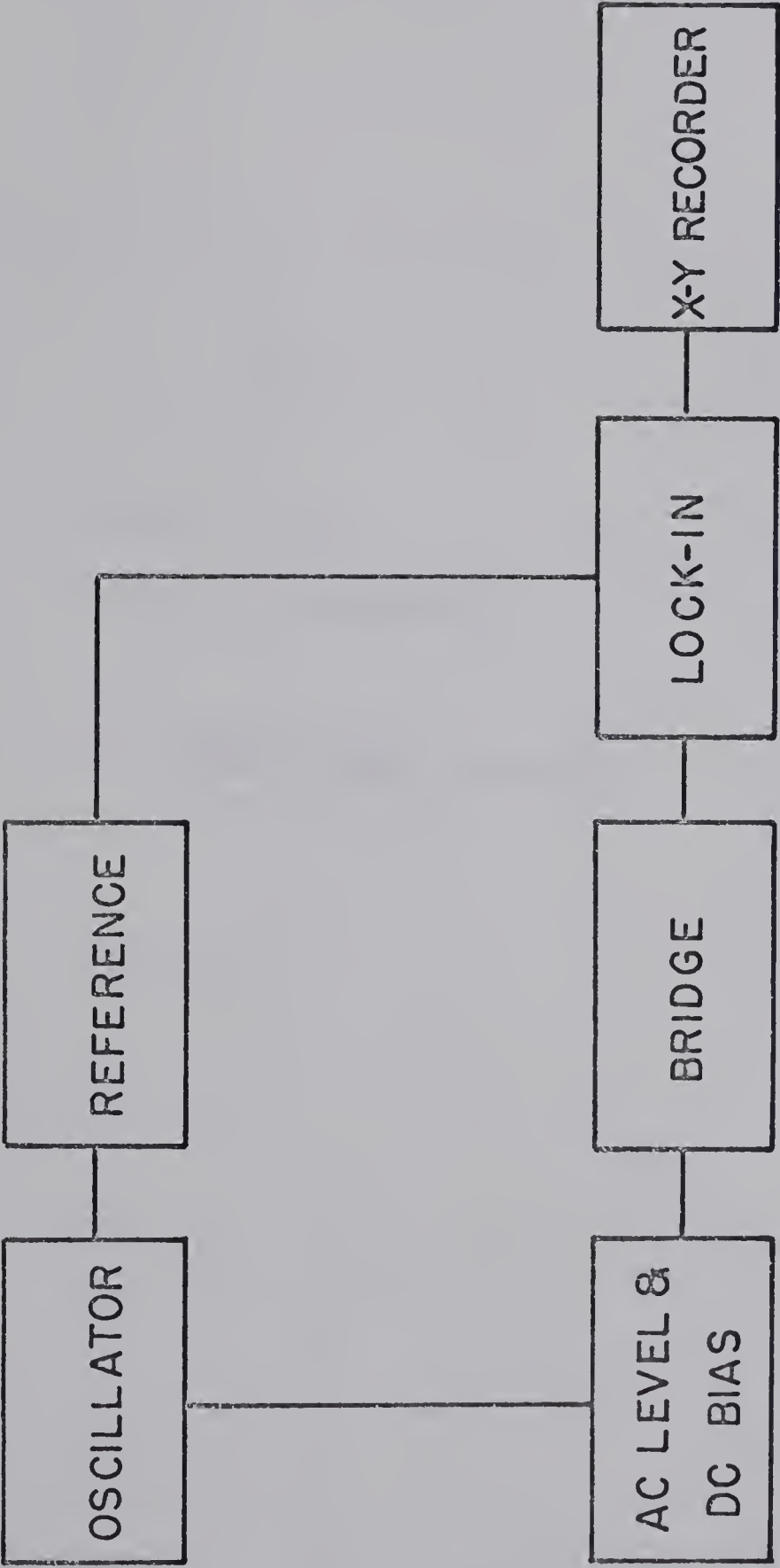


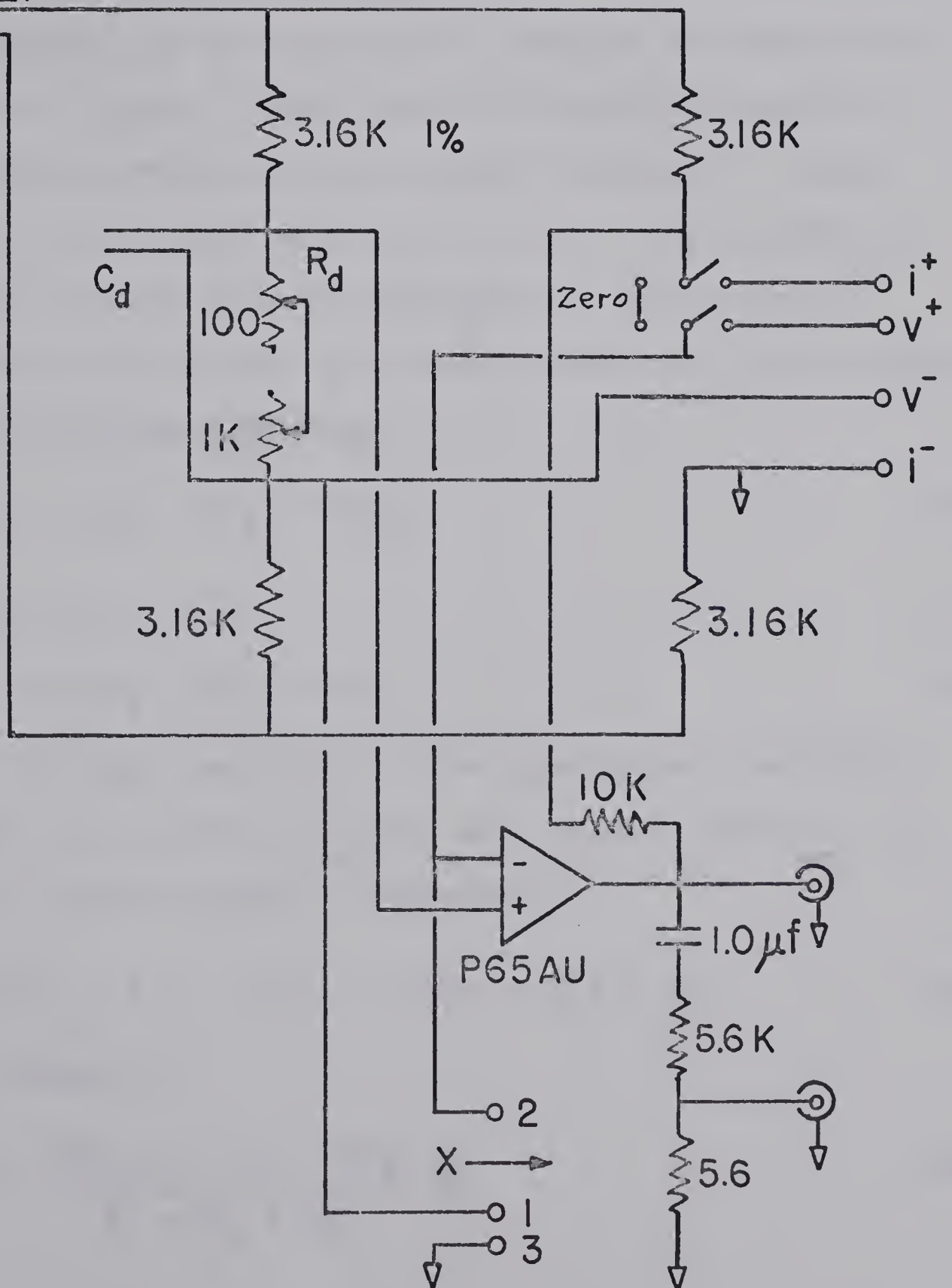


Figure 9

The bridge circuit.



SUPPLY







The feedback current required for equalization is a direct measure of  $di/dv$ , as shown below. This is therefore converted into a voltage and fed to the input of the lock-in amplifier.

### IV.3 Bridge Circuit Analysis

Consider for the purpose of analysis the simplified circuit of figure 10 (the deleted resistors simply act as isolation resistors and current limiters). Assume that  $C_d = C_t$  so the reactance is zero. ( $C_t \sim 0.025 \mu f$  and thus dominates stray inductance.) The current  $i$  consists of dc as well as ac contributions, and the operational amplifier input is

$$e_o = A(iR_d - iR_t - \delta iR_t). \quad \text{IV-2}$$

Also

$$e_o = A(e_+ - e_-) \quad \text{IV-3}$$

$$= \delta i(R_f + R_t) + iR_t. \quad \text{IV-4}$$

Since the input impedance of the operational amplifier is  $\sim 100 \text{ k}\Omega$ , and is therefore much greater than  $R_t$ , no circuit loading occurs. Therefore,

$$A(i(R_d - R_t) - \delta iR_t) = \delta i(R_f + R_t) + iR_t. \quad \text{IV-5}$$

This reduces to

$$\delta i = \frac{i[R_t(-1 - A) + AR_d]}{R_f + R_t + AR_t}. \quad \text{IV-6}$$




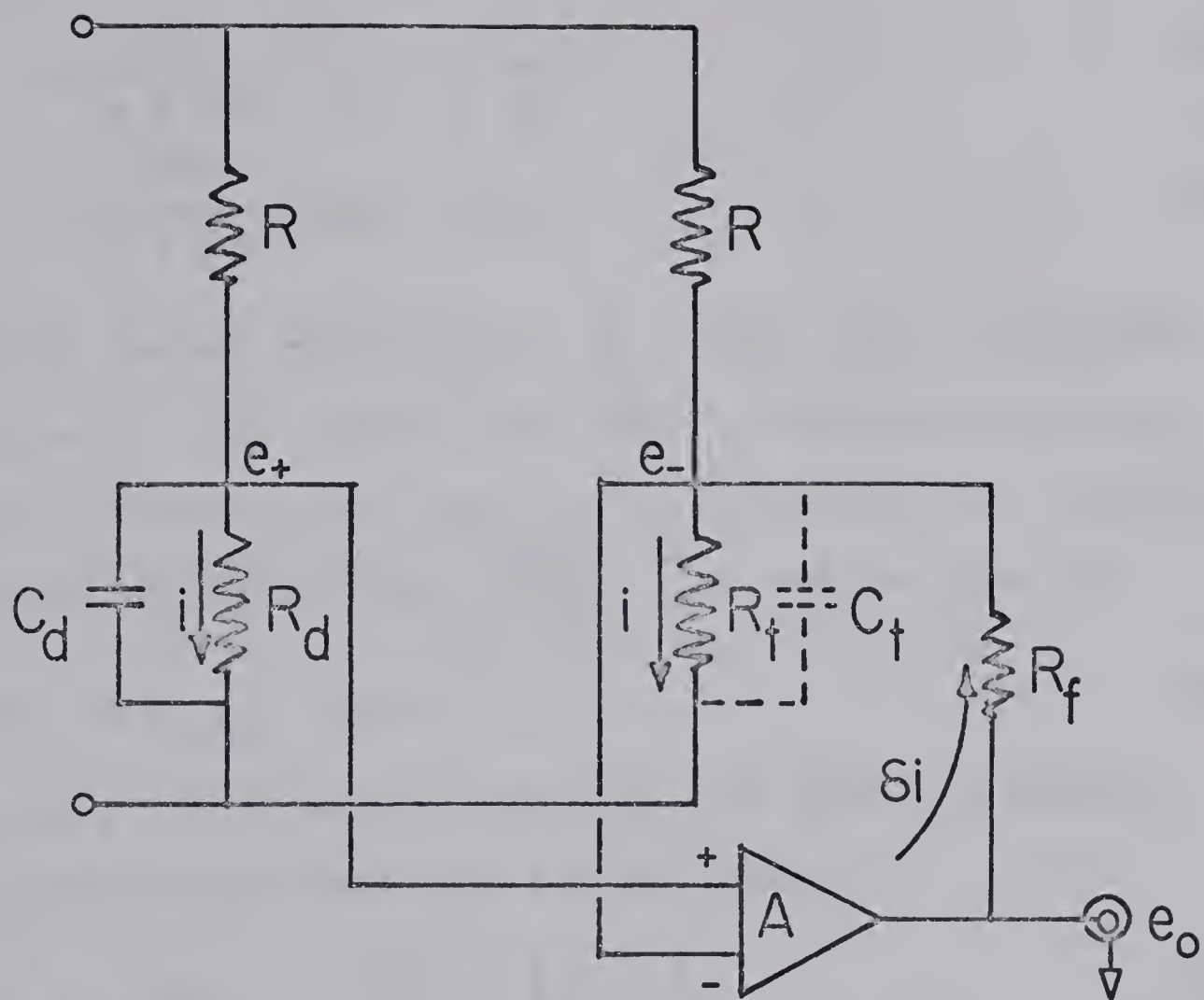


Figure 10

The simplified bridge circuit.







Setting  $\beta$  equal to

$$\beta = \frac{R_t}{R_f + R_t}, \quad \text{IV-7}$$

one has

$$\delta i = \frac{i[\beta(-1 - A) + \beta A R_d / R_t]}{1 + \beta A} \quad \text{IV-8}$$

$$= \frac{i\beta A}{1 + \beta A} \left[ \frac{-1}{A} - 1 + \frac{R_d}{R_t} \right] \quad \text{IV-9}$$

$$\sim \frac{i\beta A}{1 + \beta A} [R_d g_t - 1], \quad \text{IV-10}$$

where the tunnel conductance  $g_t = 1/R_t$  and  $A \sim 50,000$ .

The value of  $\beta A$  varies from  $\sim 250$  to  $\sim 10,000$  with the circuit elements used, and the variation of  $R_t$ . Therefore, to a good approximation  $\frac{\beta A}{1 + \beta A} \sim 1$ , and one then has

$$\delta i \sim i[R_d g_t - 1]. \quad \text{IV-11}$$

Going back to expression IV-4 for the output voltage  $e_o$  and substituting the value for  $\delta i$ , gives

$$e_o = i[R_d g_t - 1][R_f + \frac{1}{g_t}] + \frac{i}{g_t} \quad \text{IV-12}$$

$$= iR_d R_f g_t + i(R_d - R_f). \quad \text{IV-13}$$

Therefore  $e_o$  is linear in the junction conductance  $g_t$ , and the normalized conductance  $\sigma$  is obtained from

$$\sigma = \frac{g_{t_{sn}}}{g_{t_{nn}}}. \quad \text{IV-14}$$

Reactive and resistive balance of the bridge





circuit can be sensitively achieved using this detection system. The lock-in device provides continuous ( $0^\circ - 360^\circ$ ) phase shift between the reference signal and the input signal. The circuit is completely balanced for only two values of the phase setting (angle and supplementary angle). At these settings a large reactive imbalance does not affect the resistive balance and vice versa. Any other phase setting results in a false balance so that a change in either the reactive or resistive value now results in a shift in both balance readings.

#### IV.4 Conductance Calibration

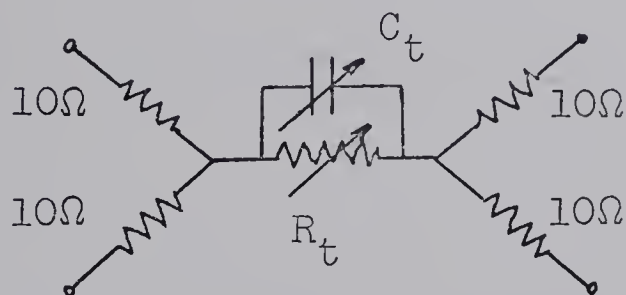
The ac signal voltage across  $R_t$  was usually set at  $\sim 150$   $\mu$ volts peak to peak (pp) or less. This corresponds to  $\sim 50$   $\mu$ volts rms, or less than  $1^\circ\text{K}$  thermal smearing. Modulation levels as low as 50  $\mu$ volts pp were often used.

The conductance was calibrated at a junction bias of 30 millivolts because it was found that in this way the calibration remained the same whether the Pb was normal or superconducting. At lower biases, possible variations in the density of states for the superconducting Pb might affect the calibration and thus invalidate the results.



In calibrating the conductance,  $R_d$  and  $C_d$  were first set to give a complete balance. The junction was then open circuited with the switch (figure 9) in the "zero" position. The signal from  $R_d$  could no longer be equalized and the lock-in output now corresponded to zero conductance. The difference between  $g_t = 0$  and  $g_t = 1$  was then adjusted to give a specific Y deflection on the X-Y recorder. By changing the lock-in and Y-axis sensitivities, fractional percentages of unity conductance could be dialed directly.

Linearity tests on the conductance were carried out with the four terminal network shown below.



Lead resistances of 10 ohms were chosen to approximate actual values.  $R_t$  was varied from  $10\Omega$  -  $5,000\Omega$  with various accompanying values of  $C_t$ . The bridge was found to be linear in conductance to within the ink width of the plotter pen. We estimate that the conductance inaccuracy is less than 0.2% for all of these values. For values of  $R_t$  below about  $100\Omega$  the junction capacitance  $C_t$  began to deviate from  $C_d$  in the reactive balance. This was found to be due to the presence of the lead resistors. However, since the linearity of the conductors was of primary importance, this did not



pose any significant problem.

Using a 100 ohm standard resistance in the place of  $R_t$ , the equivalent circuit noise was measured at less than  $10^{-8}$  volts p.p. on the X-Y recorder, for a circuit time constant of 0.3 seconds. The time constant is related to the bandwidth of the lock-in output by the expression  $B = \frac{1}{2\tau}$ .



## CHAPTER V

## EXPERIMENTAL METHOD

V.1 Specimen Preparation and Mounting Procedure

A tunnel junction consists of a metal-insulator-metal sandwich deposited on a suitable support such as a glass microscope slide. Junction fabrication was begun by thoroughly cleansing a 7/8" x 3/8" piece of glass plate and then flaming it over a bunsen burner until the edges began to soften. Indium metal contacts were then placed on the glass using a soldering iron. Leads were attached to the contacts and then the substrate was placed above a mask in the vacuum deposition bell jar.

Aluminum was used to form the normal metal in this work. This was deposited on the slide first. A vacuum of  $\sim 2 \times 10^{-6}$  mm of Hg was attained before any evaporation was begun.

The insulating layer in the junctions used was always aluminum oxide. This layer was formed by removing the substrate from the vacuum jar after the aluminum evaporation and placing it into an oven heated to  $100^{\circ}\text{C}$  and filled with atmospheric air. An oxidation time of 1 minute usually resulted in forming enough oxide on the aluminum film for junction resistances of between







100 and 300 ohms after the Pb strip was deposited across the oxide.

Junction areas were about 1.5 mm square and their capacitance was normally about 0.024  $\mu$ farads. Two junctions were formed on each substrate so that six wires were required for four terminal measurement of the separate junction conductances. This doubled the chance for a successful high pressure run.

Usually about ten attempts were required before both junctions would be useable on the same substrate.

The specimen resistance and capacitance were measured just after fabrication using a bridge built for this purpose by Rogers (1964). They were then mounted as soon as possible on the termination strip screwed to the bomb cap. Once the junctions were mounted and continuity was checked, the bomb chamber was screwed onto the nut to a tightening torque of about 300 lbs-ft. forming a seal at the lense ring. The experimental chamber inside the bomb could then be evacuated through the high pressure capillary, by attaching a vacuum roughing pump at an outside point. Storage in this vacuum greatly increased the chance of retaining the initial characteristics of the junction while the rest of the steps were being taken to commence a run.

The needle valve and pumping lines were then attach-



ed to the helium reservoir. The thermometer lead connections were then made and tested. The cryostat vacuum can was then soldered into place using Wood's metal alloy. The evacuation of the cryostat was then begun. Once the vacuum reached  $\sim 2 \times 10^{-5}$  mm Hg, the roughing pump was removed from the pressure capillary. The capillary was then connected to the high pressure intensifier section and the whole pressure system, including the working chamber, was flushed with helium gas. Once this was done, the cryostat was cooled to liquid nitrogen temperature. Junctions could be stored at liquid nitrogen temperature for several weeks with constant properties.

## V.2 Description of a Typical Run

After a specimen had been successfully mounted and tested, evacuation of the cryostat was begun and continued until the vacuum was better than  $5 \times 10^{-7}$  mm Hg at liquid nitrogen temperature. Often it was better than  $1 \times 10^{-7}$  mm Hg. This degree of evacuation was essential because once the system was cooled down to working temperatures, the residual gas would constitute a heat leak. This might then result in a temperature gradient across the bomb.

Before commencing the cool-down procedure to liquid



helium temperature, the pressure system was always tested to see if it had any leaks. This test was usually done to pressures of about 55,000 psi. If the electrical lead seal held and none of the cone seals leaked, the final cool-down to liquid helium temperature was begun.

Pressure transmission to the junctions could be checked by monitoring the junction resistance  $R_t$  as a function of pressure. This resistance decreased sensitively as the oxide is compressed, and was effectively used as a means of measuring pressure at the junction. Capillary blockage during pressurization was readily seen since  $R_t$  suddenly remained constant while the outside pressure was still increasing. The changes in the junction resistance were always found to be reversible with pressure change.

### V.3 Low Temperature Pressure Production

The helium cool-down procedure was started by emptying the inner dewar filled with liquid nitrogen and re-installing it over the cryostat. This dewar was then sealed to the recovery system so that the He gas could be collected and re-liquefied.

A larger dewar was then hung around the inner dewar and filled with liquid nitrogen. Liquid helium from a portable storage dewar was then siphoned under a He gas





positive pressure head into the inner dewar. This process was continued until the system was cooled down to about  $30^{\circ} - 35^{\circ}$  Kelvin. At this time the pressure was re-pumped to the desired working value. Heaters on the high pressure capillary were turned on to keep it open. Cool-down and freezing at constant pressure was then commenced by opening the needle valve and sucking helium liquid from below the vacuum can into the pumping can mounted on the pressure bomb.

Constant pressure freezing of 56,000 psi at  $35^{\circ}\text{K}$  resulted in  $\sim 50,000$  psi at  $4.2^{\circ}\text{K}$ . The pressure vs  $R_t$  curve obtained at  $35^{\circ}\text{K}$  served to indicate the final frozen in pressure at the working temperature. The temperature variation of  $R_t$ , for zero pressure, is negligible between these limits so no correction was made for the pressurized run either.

#### V.4 Pressure Dependence of the Barrier

The tunneling transition probability for barrier penetration as used in equation II-27 was assumed to be independent of temperature and energy, for the small energies involved. The probability of barrier penetration takes the form

$$|M|^2 = \exp -2/\hbar \int_{x_2}^{x_1} [2m(\phi(x) - E_x)^{\frac{1}{2}}] dx$$

V-1





where  $\phi(x)$  is the potential barrier height as a function of  $x$ ,  $E_x$  is the  $x$ -component of the electron kinetic energy, and  $m$  is the electron mass.

Assuming that  $|M|^2 \propto \exp(-(\bar{\phi}^{\frac{1}{2}} \cdot (x_1 - x_2)))$  where  $\bar{\phi}$  is an average potential height, and  $x_1 - x_2$  is the barrier thickness, pressurization of the junction should increase  $P$  approximately exponentially as the barrier thickness decreases.

Figures 11 and 12 show resistance vs pressure plots for four different junctions. Figure 13 shows them plotted on a log-linear graph. Notice that the curves have approximately an exponential pressure dependence as one would expect. The lower resistance junctions exhibit a somewhat larger relative change for a given pressure difference. This also conforms to the expectations of an idealized theory.

Deviations from a true exponential behaviour are probably associated with effects at the surfaces separating the oxide from the metals.

In principle, the junction capacitance as a function of pressure should also be obtainable. In practice, these changes were not large enough to provide much pressure sensitivity.

In conclusion, the normal junction conductance



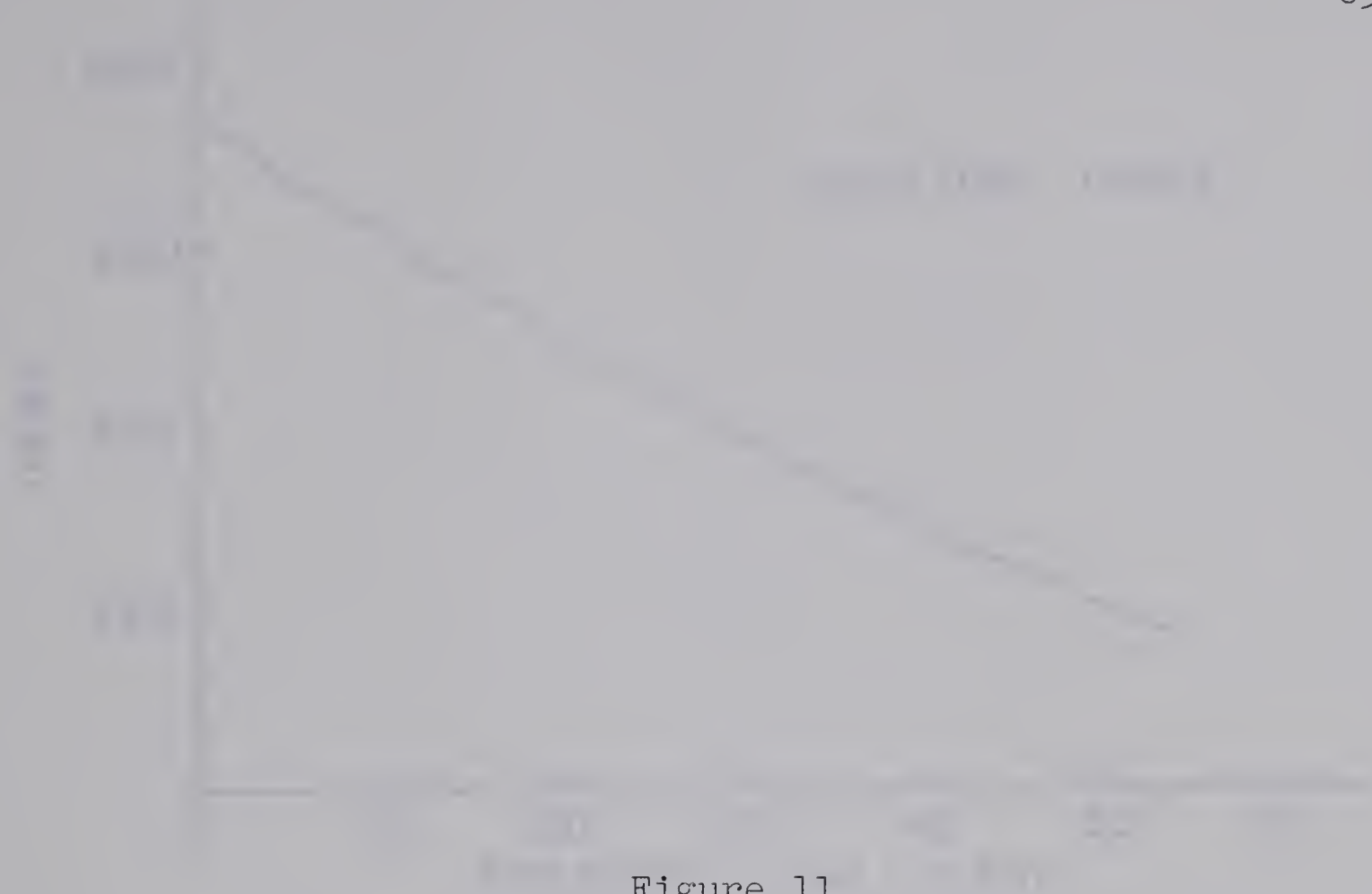


Figure 11

Tunnel resistance vs pressure  
for junctions 1345B and 1345.



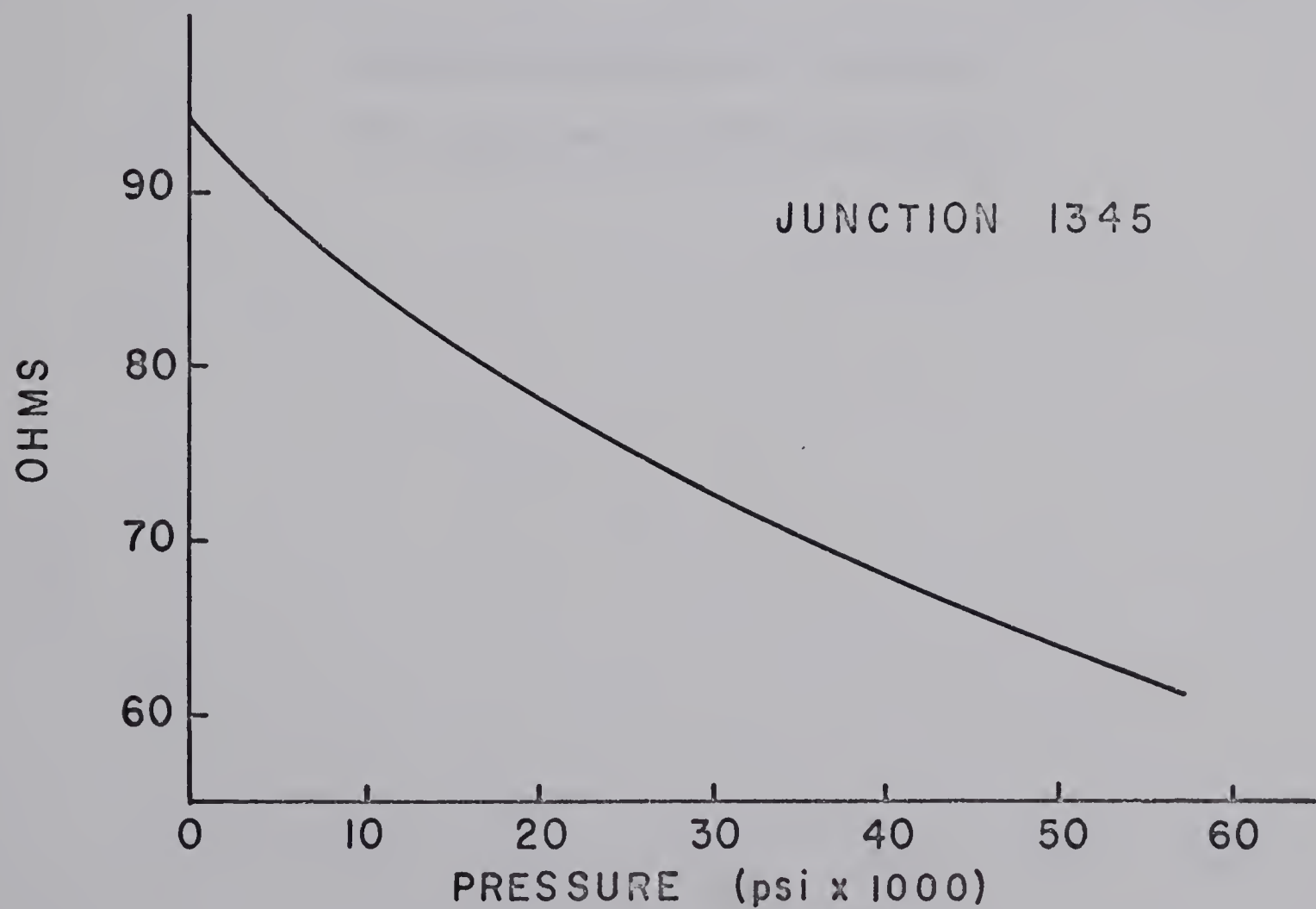
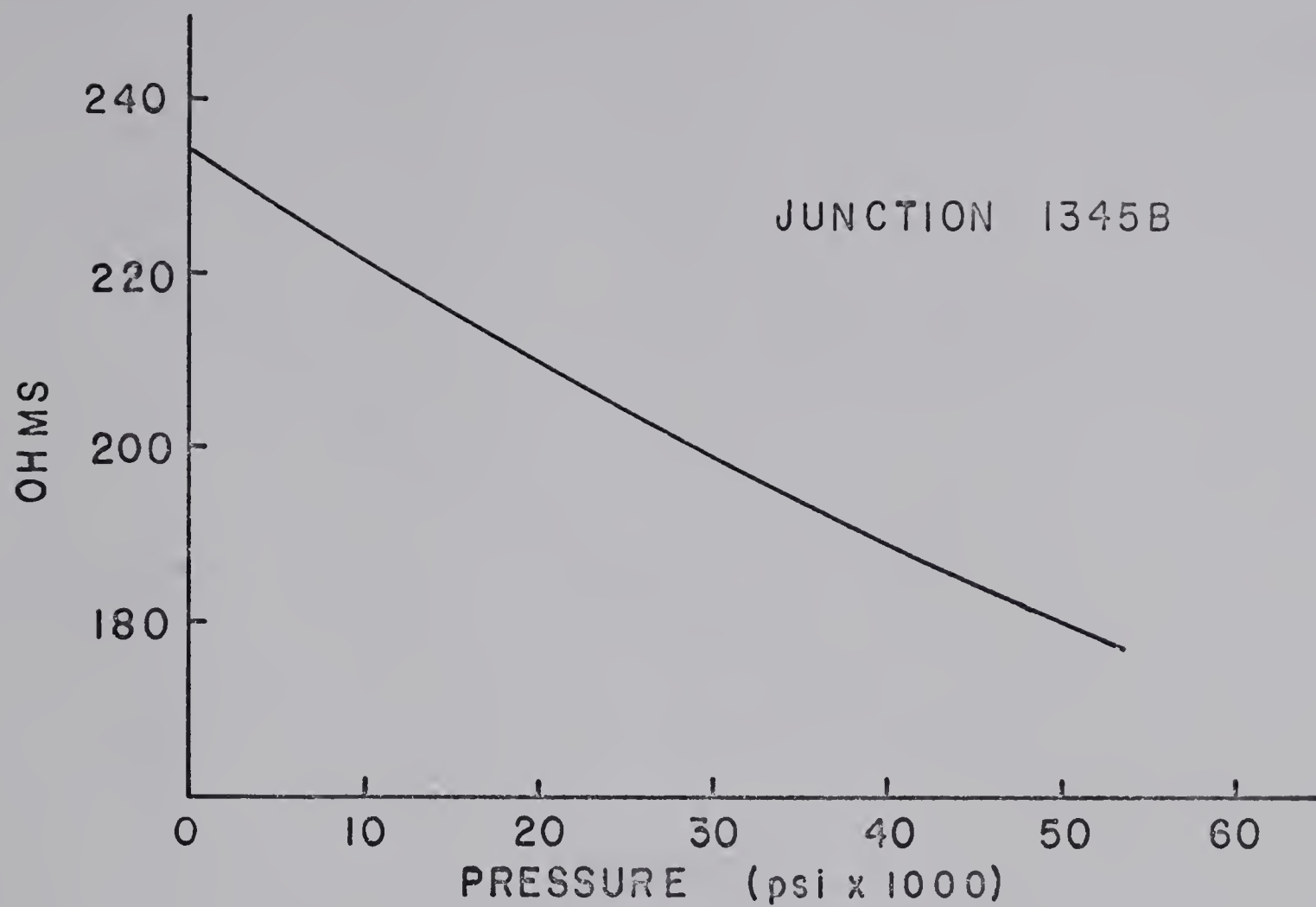




Figure 12

Tunnel resistance vs pressure  
for junctions 1345D and 1345E.





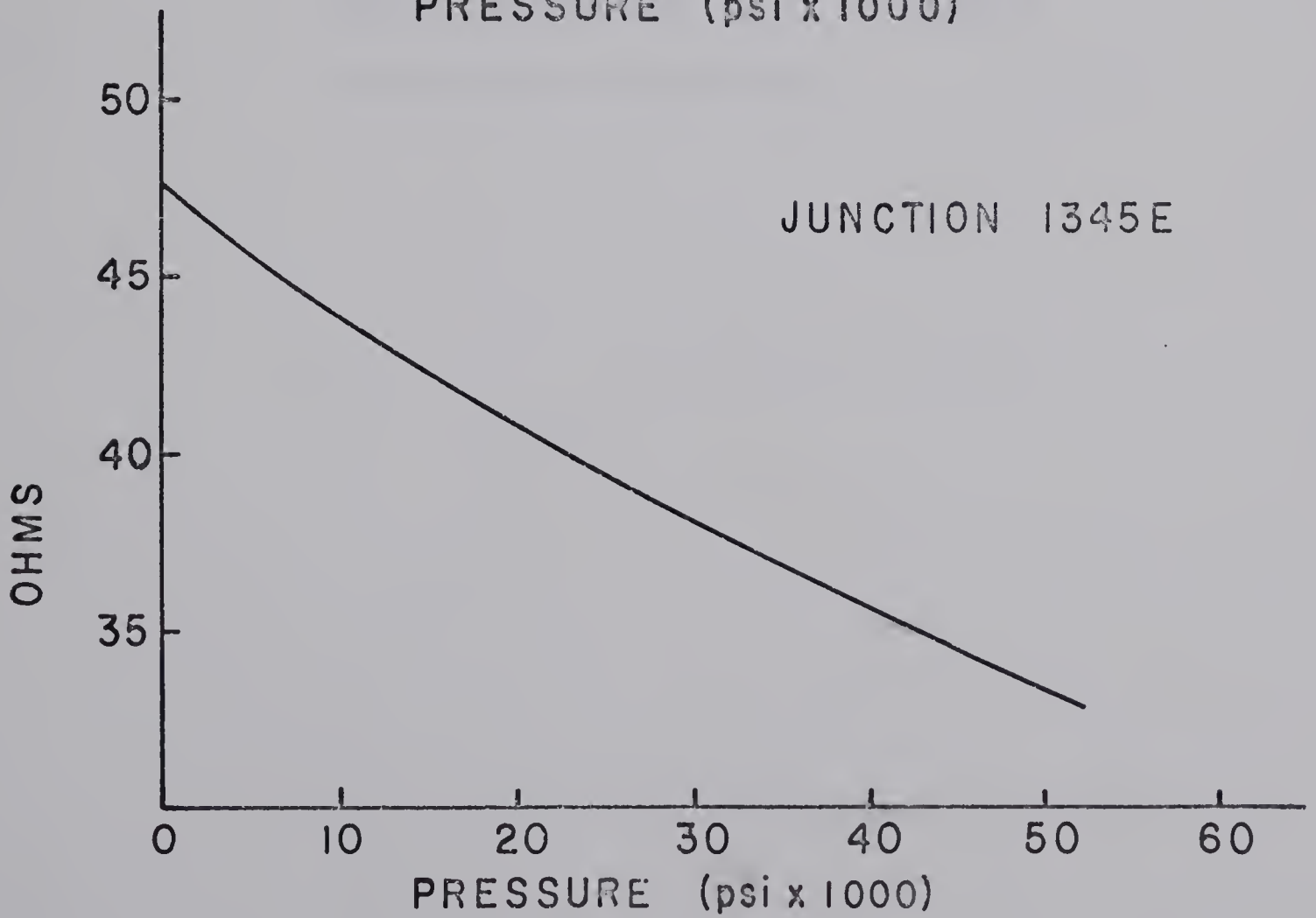
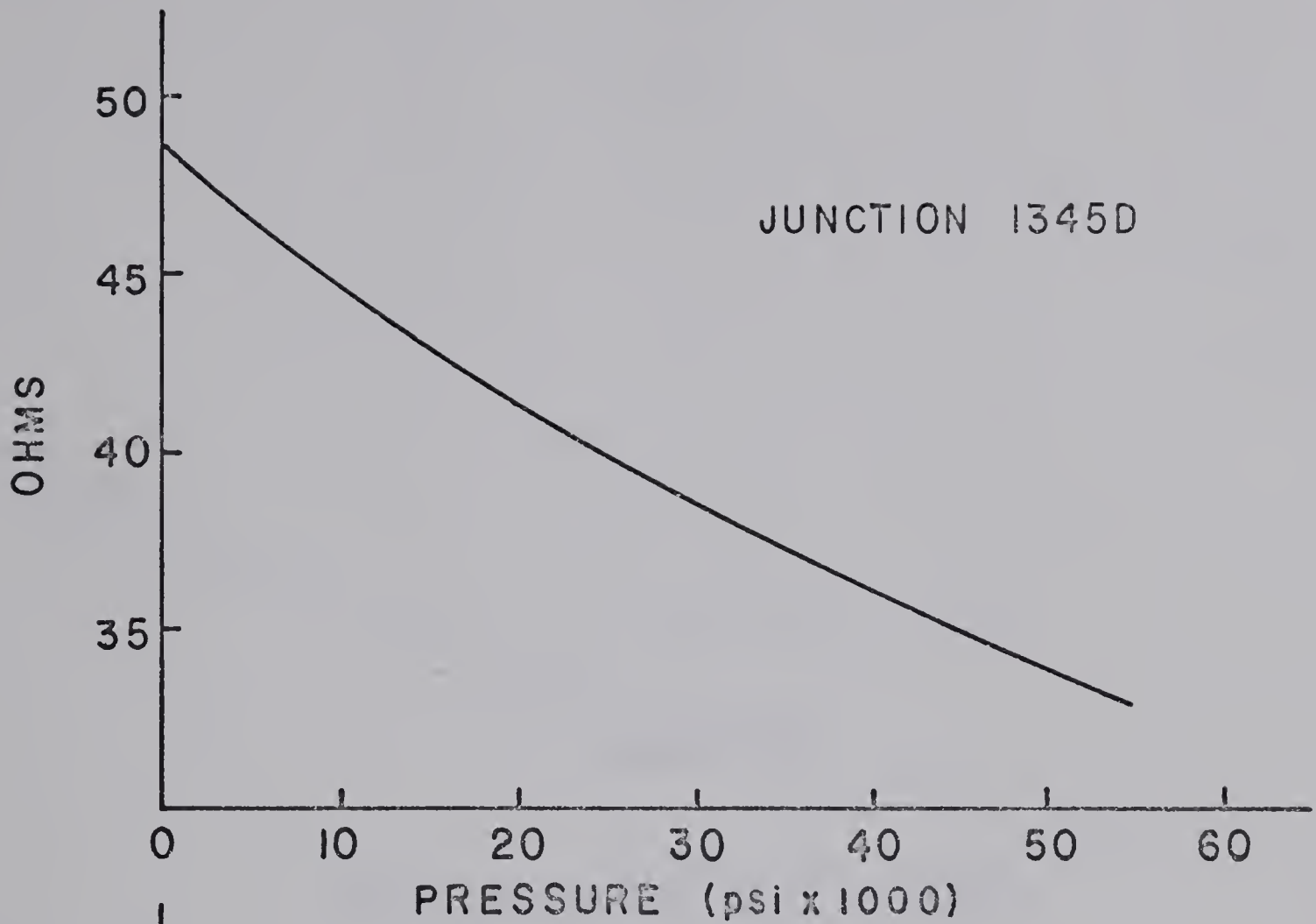




Figure 13

Semi-logarithmic plot of tunnel  
resistance vs pressure.



RESISTANCE

JUNCTION 1345

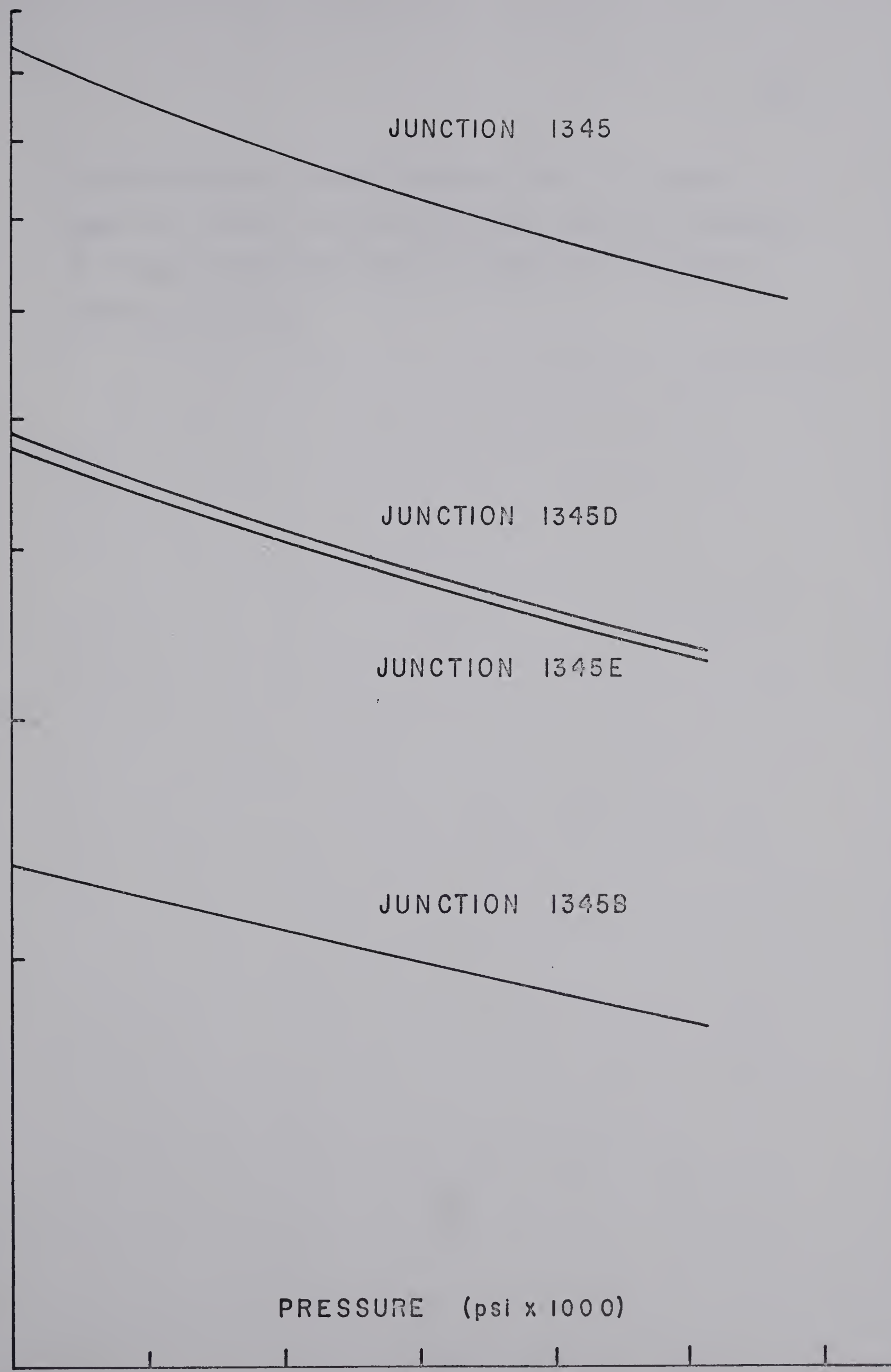
JUNCTION 1345D

JUNCTION 1345E

JUNCTION 1345B

PRESSURE (psi x 1000)

0 10 20 30 40 50 60





is sufficiently pressure sensitive that it can be used as a pressure monitoring device wherever pressures of a few thousand bars must be indirectly measured to moderate accuracy.





## CHAPTER VI

## RESULTS AND DISCUSSIONS

VI.1 The Pressure Dependence of the Transition Temperature

One of the simplest and yet one of the severest tests of the pressure method used in this work concerns the pressure dependence of the critical temperature of Pb. This is, therefore, discussed first.

The Pb transition temperature was obtained for each junction by monitoring the zero bias conductance while the temperature was slowly decreased. At the transition temperature, the energy gap began to develop and this appeared as an abrupt decrease in  $\sigma$ . The transition was well defined in all junctions measured and an average value of four readings constitutes each quoted temperature. While an error estimate of  $\pm 7$  mdeg is placed on the absolute temperature near  $7^{\circ}\text{K}$ , an estimate of  $\pm 4$  mdeg error is placed on the difference  $\Delta T_c$  due to the application of a pressure (measured in bars). Table 1 shows the shift in transition temperature for several junctions.

While the bulk Pb transition temperature is  $7.193 \pm 0.005^{\circ}\text{K}$ , (Franck and Martin, 1961), most of the thin-film zero-pressure Pb transition temperatures were



slightly higher than this value. This effect is associated with thin film geometry, and is present in most superconductors deposited as films.

TABLE 1

JCN	$T_c(P=0)$ °K	$T_c(P)$ °K	$\Delta P$ bar	$\Delta T_c$ °K	$-dT_c/dP$ °K/bar
1345A	6.965	6.885	2378.0	0.080	$3.36 \pm 0.33 \times 10^{-5}$
1345B	7.246	7.158	2551.2	0.088	$3.45 \pm 0.32 \times 10^{-5}$
1246B	7.240	7.197	1309.9	0.053	$4.05 \pm 0.50 \times 10^{-5}$
1345C	7.240	7.110	3447.5	0.119	$3.45 \pm 0.32 \times 10^{-5}$
1246C	7.248	7.140	3172.0	0.108	$3.40 \pm 0.32 \times 10^{-5}$
1345D	7.225	7.125	2757.2	0.100	$3.63 \pm 0.34 \times 10^{-5}$
1246D	7.225	7.120	2757.2	0.105	$3.81 \pm 0.35 \times 10^{-5}$
1345E	7.243	7.142	2730.0	0.101	$3.69 \pm 0.35 \times 10^{-5}$

$$\text{Average} = 3.61 \pm 0.35 \times 10^{-5}$$

A pressure uncertainty of ~6% is included in the error estimate.

Table 2 shows a list of published values of  $dT_c/dP$  and  $\partial H_c/\partial P$  for Pb. All of the values of  $dT_c/dP$  (except the value measured during this work) were obtained from magnetic field measurements on bulk samples. This can be done by utilizing the relation,

$$\frac{dT_c}{dP} = - \frac{(\partial H_c/\partial P)_T}{(\partial H_c/\partial T)_P}, \quad T \rightarrow T_c.$$



The agreement between thin film and bulk values is quite close and generates confidence in the pressure technique. Obviously, if strain effects are present due to differential contraction between the glass substrate and the films, their effects are not large enough to pose a major problem.

TABLE 2

$(\partial H_c / \partial P)_{T_c}$	$(dT_c / dP)_{H=0}$	AUTHORS
(Gauss/bar)	(°K/bar)	
$-9.62 \pm 0.18 \times 10^{-3}$	$-4.04 \pm 0.08 \times 10^{-5}$	R.R. Hake and D.E. Mapother (1956)
	$-3.86 \pm 0.12 \times 10^{-5}$	T.F. Smith and C.W. Chu (1967)
$-9.03 \pm 0.15 \times 10^{-3}$	$-3.79 \pm 0.07 \times 10^{-5}$	M. Garfinkel and D.E. Mapother (1961)
	$-3.60 \pm 0.35 \times 10^{-5}$	This work



## VI.2 Phonon Shifts in Pb Under Pressure

In section II.8 a discussion was given showing how the predominant phonon-peaks are reflected as structure in the density of states ( $\sigma$ ) for strong-coupling Pb. The phonon emission process is the mechanism leading to this structure, and the structure is of such a form that  $\sigma$  passes through an inflection point, while  $d\sigma/dV$  passes through a minimum at the predominant phonon energies. These energies occur near the ends of the transverse and longitudinal phonon branches.

We have measured the shifts in  $\sigma$  and  $d\sigma/dV$  at  $\bar{\omega}_t$  and  $\bar{\omega}_\ell$  for ten junctions subjected to hydrostatic pressure. Figure 14 shows conductance results taken at 1.4°K for a typical junction. Since the X-Y plotter paper is 14" x 17", the plot has been photographically reduced for presentation here. The phonon energies are measured from the gap-edge energy, so the  $P = 0$  and  $P > 0$  traces have been re-drawn onto a single graph with the gap-edge energies set to coincide. Figures 15 and 16 show actual size traces of  $\sigma$  and  $d\sigma/dV$  for the transverse and longitudinal regions respectively. These figures display several results:

- (1) The shift in  $2\Delta_0$  is directly observable at the left in figure 14.
- (2) The shift in  $\bar{\omega}_\ell$  is easily resolved in both  $\sigma$  and  $d\sigma/dV$ .







Figure 14

The normalized conductance  $\sigma$  for junction 1345C at  $P = 0$  bar and  $P = 3172.0$  bar. The gap-edge energies are set to coincide.



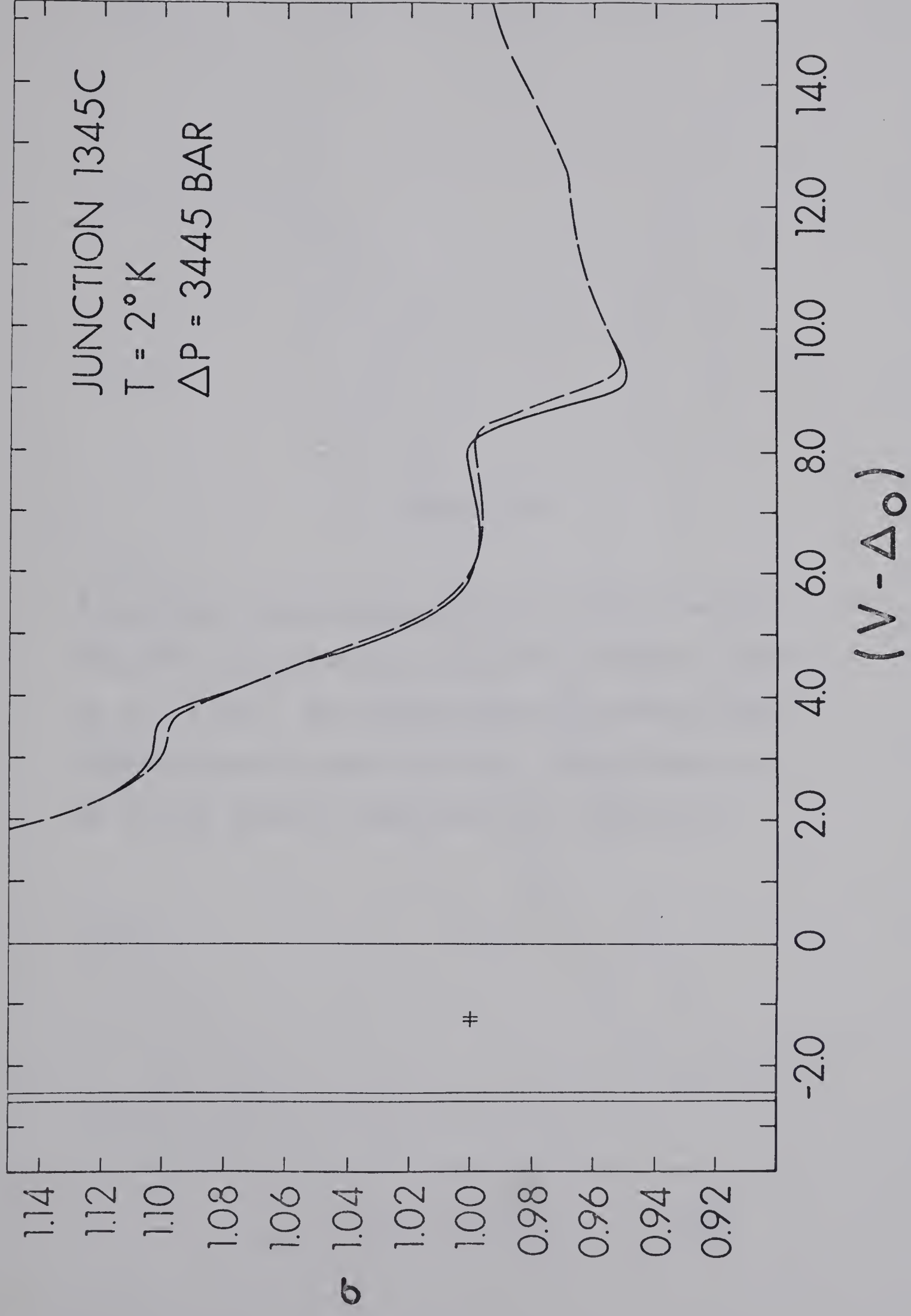




Figure 15

Normalized conductance  $\sigma$  and second derivative  $d^2i/dv^2$  (in arbitrary units) for junction 1345C at  $T = 1.4^\circ\text{K}$ . The energy range near the longitudinal phonon peak is shown. Solid lines are at  $P = 0$ , broken lines are at  $P = 3445$  bar.



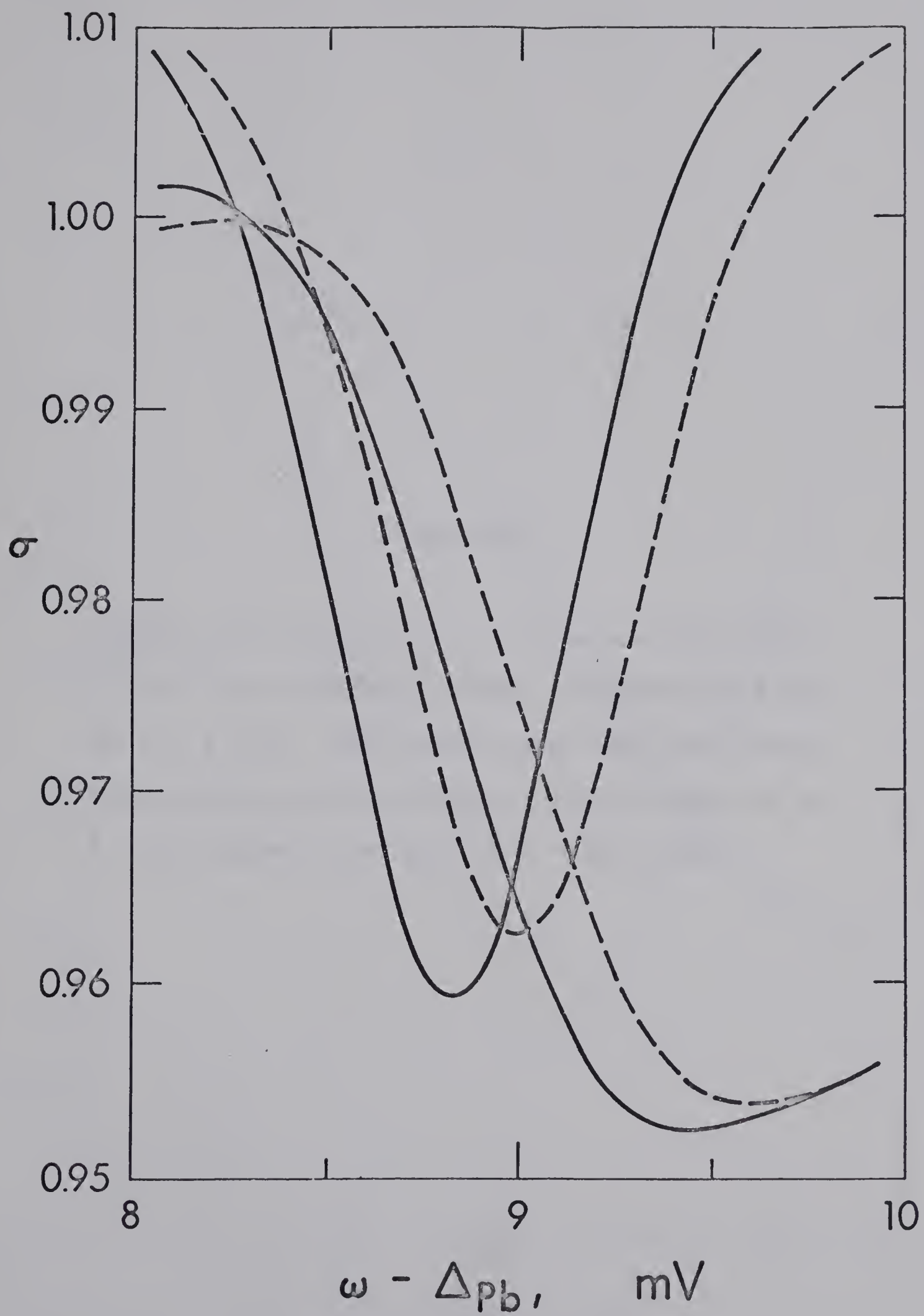


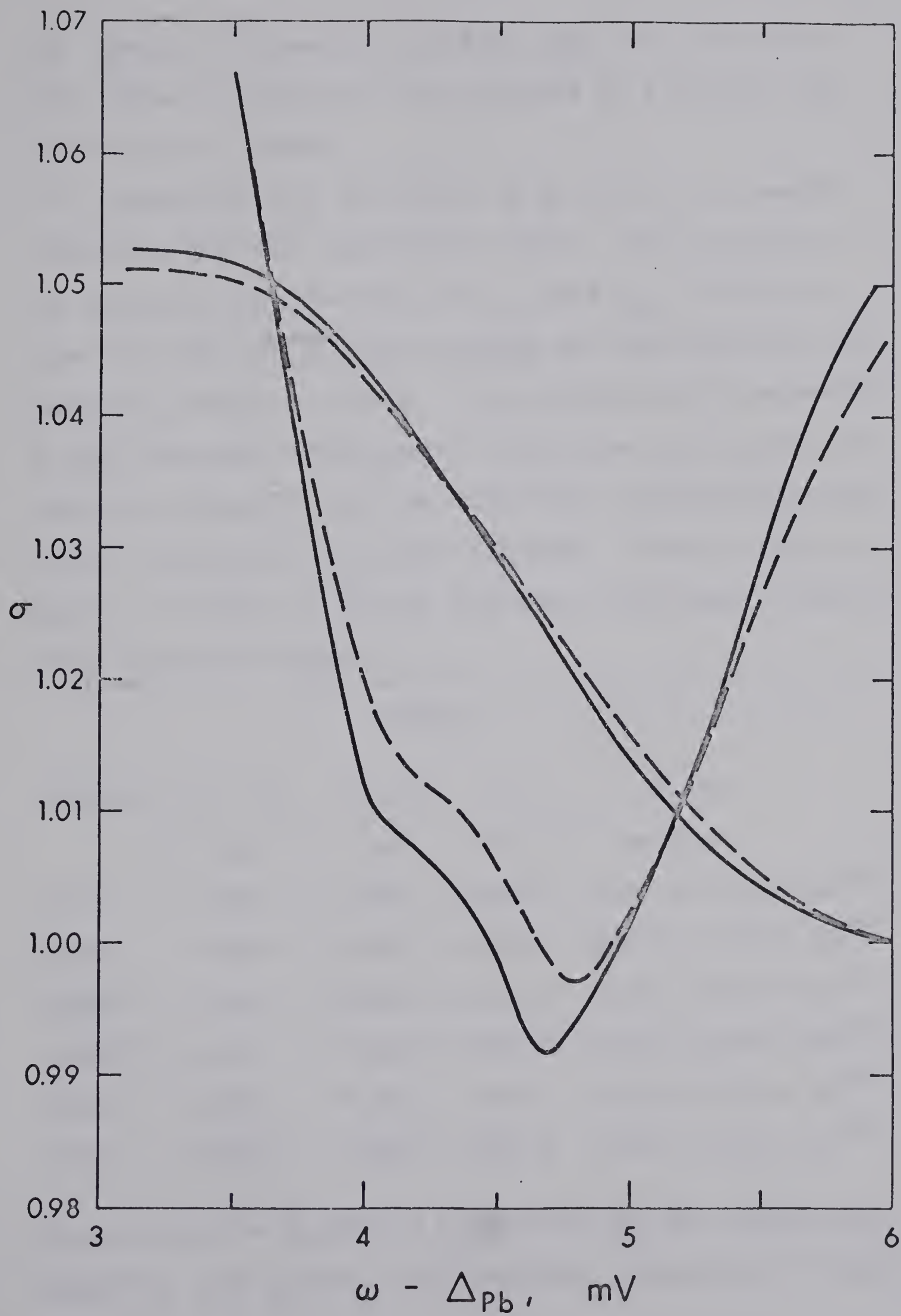




Figure 16

Normalized conductance  $\sigma$  and second derivative  $d^2i/dv^2$  (in arbitrary units) for junction 1345C at  $T = 1.4^\circ\text{K}$ . The energy range near the transverse phonon peak is shown. Solid lines are at  $P = 0$ , broken lines are at  $P = 3445$  bar.







(3) There is a general structure amplitude reduction with pressure associated with changes in  $\alpha^2(\omega)F(\omega)$  and the density of states.

(4) Because of (3), the shift in  $\bar{\omega}_t$  is not as clearly defined as for the longitudinal case. Also, because of the separate contributions of  $\omega_{t_1}$ , and  $\omega_{t_2}$ ,  $d\sigma/dV$  has some structure at  $\bar{\omega}_t$  which renders its use impossible for measuring pressure shifts. A new criterion for measuring  $\bar{\omega}_t$  was therefore established. Its value for a particular curve was obtained from the mid-height (inflection) point in the conductance structure drop-off. Table 3 lists a number of values of  $\delta\bar{\omega}_t/\delta P$  obtained in this way. Table 4 lists values of  $\delta\bar{\omega}_\ell/\delta P$ .

TABLE 3

JUNCTION	$\bar{\omega}_t(P=0)$ meV	$\bar{\omega}_t(P>0)$ meV	$\delta P$ bar	$\delta\bar{\omega}_t/\delta P$ meV/bar
1345A	4.585	4.630	1930.6	$2.33 \pm 1.00 \times 10^{-5}$
1345B	4.580	4.650	2551.2	$2.74 \pm 1.00 \times 10^{-5}$
1345C <sup>1</sup>	4.575	4.642	3447.5	$1.94 \pm 1.00 \times 10^{-5}$
1345C <sup>2</sup>	4.575	4.650	3447.5	$2.18 \pm 0.60 \times 10^{-5}$
1345C <sup>3</sup>	4.585	4.660	3172.0	$2.36 \pm 0.50 \times 10^{-5}$
1345D	4.600	4.675	2757.2	$2.72 \pm 1.00 \times 10^{-5}$

The average for  $\bar{\omega}_t(P=0) = 4.585$  meV, and the average for  $\delta\bar{\omega}_t/\delta P$  is  $2.37 \pm 0.70 \times 10^{-5}$  meV/bar. Therefore we have,



$$\frac{d \ln \bar{\omega}_t}{dP} = 5.17 \pm 1.50 \times 10^{-6} \text{ bar}^{-1}.$$

TABLE 4

JUNCTION	$\bar{\omega}_\ell(P=0)$	$\bar{\omega}_\ell(P>0)$	$\delta P$	$\delta \bar{\omega}_\ell / \delta P$
	meV	meV	bar	meV/bar
1345A	8.710	8.825	1930.6	$5.96 \pm 1.20 \times 10^{-5}$
1345B	8.650	8.810	2551.2	$6.27 \pm 1.20 \times 10^{-5}$
1345C <sup>1</sup>	8.650	8.835	3447.5	$5.37 \pm 0.80 \times 10^{-5}$
1345C <sup>2</sup>	8.675	8.863	3447.5	$5.45 \pm 0.80 \times 10^{-5}$
1345C <sup>3</sup>	8.725	8.930	3172.0	$6.46 \pm 1.00 \times 10^{-5}$
1345D	8.700	8.863	2757.2	$5.91 \pm 1.00 \times 10^{-5}$

$\bar{\omega}_\ell$  average ( $P=0$ ) = 8.685 meV, and the average for  $\delta \bar{\omega}_\ell / \delta P$  is  $5.90 \pm 1.00 \times 10^{-5}$  meV/bar. Thus, in this case we have

$$\frac{d \ln \omega_\ell}{dP} = 6.80 \pm 1.00 \times 10^{-6} \text{ bar}^{-1}.$$

Since the minima in  $d\sigma/dV$  occur at peaks in the phonon spectrum, a shift in  $d\sigma/dV$  as the superconductor is subjected to hydrostatic pressure, gives directly the Gruneisen  $\gamma$  for the predominant modes through the expression

$$\gamma_j = - \frac{d \ln \omega_j}{d \ln V} = \frac{\delta \omega_j / \omega_j}{\delta P} B \quad \text{VI-2}$$

where  $B$  is the bulk modulus, and  $\delta \omega_j$  is the shift in mode  $j$  due to a pressure  $P$ . Using the value of  $B = 4.88 \times 10^5$





bar, due to Waldorf and Alers (1962), gives the Gruneisen values

$$\gamma_{\ell} = (6.80 \pm 1.00)(0.488) = 3.32 \pm 0.49$$

$$\gamma_t = (5.17 \pm 1.50)(0.488) = 2.52 \pm 0.74$$

This result is true for the predominant modes, despite a possible change in the electron-phonon coupling constant (see Appendix A).

It is instructive at this stage to briefly outline the general Gruneisen  $\gamma$  theory in order to facilitate comparison of our results with results obtained by other workers. The Gruneisen rule states that at low temperature, the coefficient of thermal expansion  $\alpha$  is proportional to the constant volume specific heat,  $C_v$ , through the relation,

$$\gamma_G = \frac{V\alpha}{KC_v} \quad \text{VI-3}$$

where  $K$  is the compressibility. This result follows strictly when all  $\gamma_j$  given by

$$\gamma_j = - \frac{d \ln \nu_j}{d \ln V} \quad \text{VI-4}$$

are equal. The subscript  $j$  refers to the  $j^{\text{th}}$  normal mode of vibration, and  $\gamma_G$  is related to these mode gammas

$$\text{by} \quad \gamma_G = \frac{\sum_j \gamma_j C_{vj}}{\sum_j C_{vj}} \quad \text{VI-5}$$



$C_{vj}$  is the Einstein heat capacity of the  $j^{\text{th}}$  mode.

Blackman (1957, 1959) has derived a second form under which VI-3 is also strictly valid. This depends on forming a quantity  $\bar{\gamma}(\nu)$  which is the average of  $\gamma(\nu)$  taken between neighbouring frequency contours. Then,

$$\gamma_G = \frac{\int \bar{\gamma}(\nu) \rho(\nu) C_{\nu} d\nu}{\int \rho(\nu) C_{\nu} d\nu} \quad \text{VI-6}$$

holds strictly when  $\bar{\gamma}(\nu) = \text{constant}$ . Here  $\rho(\nu)$  is the frequency distribution function. Blackman has shown that this is true for two special cases:

- (1) At sufficiently high temperatures, the heat capacity of each mode is constant  $= 3/2 k$ .
- (2) In the region where the  $T^3$  law for  $C_v$  and  $\alpha$  holds sufficiently well,  $\gamma_G$  can be derived from the free energy and takes the form

$$\gamma_G = \frac{\iiint \sum_{j=1}^3 c_j^{-3} \gamma_j^c d\Omega}{\iiint \sum_{j=1}^3 c_j^{-3} d\Omega} \quad \text{VI-7}$$

where

$$\gamma_j^c = 1/3 - V/c_j (dc_j/dV) \quad \text{VI-8}$$

and  $c_j$  is the velocity of a wave in a given direction in one of the three acoustic branches while  $V$  is the volume. For cubic crystals it can be shown that the velocity of the [100] longitudinal plane wave is  $(C_{11}/\rho)^{1/2}$



where  $\rho$  is the density. At the same time, the velocity of the transverse wave is given by  $(C_{44}/\rho)^{\frac{1}{2}}$ . In these expressions,  $C_{11}$  and  $C_{44}$  are lattice constants associated with propagation in the continuum region of the dispersion curve. Thus, using the definition of  $\gamma_j^c$  one has,

$$\gamma_\ell[100] = 1/3 - \frac{d \ln(C_{11}/\rho)^{\frac{1}{2}}}{d \ln V} \quad \text{VI-9}$$

$$= 1/3 - 1/2 \frac{d \ln C_{11}}{d \ln V} + 1/2 \frac{d \ln \rho}{d \ln V} . \quad \text{VI-10}$$

Since  $\frac{d \ln \rho}{d \ln V} = - \frac{d \ln V}{d \ln V} = -1,$

$$\gamma_\ell[100] = - 1/2 \frac{d \ln C_{11}}{d \ln V} - 1/6. \quad \text{VI-11}$$

Similarly,

$$\gamma_t[100] = - 1/2 \frac{d \ln C_{44}}{d \ln V} - 1/6. \quad \text{VI-12}$$

Acoustic measurements yield the velocity, and hence the elastic constants and  $\gamma$  for a given direction of sound propagation in the non-dispersive region. For a general comparison with other fcc metals,  $\gamma$ 's measured by acoustic experiments (i.e. continuum results) are given in Table 5 along with the present result.

There seems to be very little experimental data available on Pb for comparison with this work. Phonon dispersion curves have been measured in Pb at 100°K by





TABLE 5

DIRECTION	$\Theta_D$	$\gamma_\ell$	$\gamma_{t_1}$	$\gamma_{t_2}$	At.No.	AUTHOR
Na [100]	150	1.51	1.06	1.06	11	W.B.Daniels
[110]		1.36	1.06	1.06		(1960)
[111]		1.34	1.06	1.06		
Al [100]	390	2.28	2.80	2.80	13	R.E.Schmunck &
[110]		2.43	2.80	2.36		Charles S.Smith
[111]		2.43	2.53	2.53		(1959)
Cu [100]	315	2.48	1.92	1.92	29	W.B.Daniels &
[110]		2.30	1.92	1.49		Charles S.Smith
[111]		2.19	1.76	1.76		(1958)
Ag [100]	215	2.71	2.38	2.38	47	W.B.Daniels &
[110]		2.69	2.38	1.96		Charles S.Smith
[111]		2.68	2.21	2.21		(1958)
Au [100]	170	2.86	3.38	3.38	79	W.B.Daniels &
[110]		3.00	3.38	2.31		Charles S.Smith
[111]		3.03	2.94	2.94		(1958)
Pb Av.	105	3.32	2.52	2.52	82	This work

Brockhouse et al (1961A) using inelastic neutron scattering. They have also measured the frequency shift due to change in temperature from 100°K to 425°K for a few phonon modes (1961B). More recently, Stedman et al (1967A), again using inelastic neutron scattering, have made measurements at 80°K and 300°K. The total phonon spectrum  $F(\omega)$  vs  $\omega$  requires the summation of the dispersion curves over all





directions and is, therefore, not easily obtainable. At present,  $F(\omega)$  is not known as a function of temperature. However, Stedman et al have succeeded in calculating  $F(\omega)$  vs  $\omega$  for Pb at 80°K (1967B). They used their dispersion results for three measured symmetry directions of the three main branches. Values for intermediate directions were computer interpolated, and therefore the resultant spectrum is obtained without making any assumptions based on models of the lattice. Their phonon spectrum is almost identical to the published results of McMillan and Rowell (figure 2) on  $\alpha^2(\omega)F(\omega)$  vs  $\omega$  obtained by electron tunneling.

Gilat (1965) has also calculated the Pb phonon spectrum from a general Born-Von-Karman model and knowledge of the dispersion curves of Brockhouse et al. His result is expected to be less accurate since it is primarily a mathematical model calculation, and, in fact, it agrees poorly with the above mentioned results.

While the neutron results are interesting in that they show generally good agreement with the tunneling phonon spectrum, no information regarding the Gruneisen  $\gamma$ 's is given, and these are presently under investigation. Lechner and Quittner (1966) have measured pressure-induced phonon frequency shifts for six true phonon modes



in Pb at room temperature, and 3000 atmospheres pressure. They used inelastic neutron scattering for these measurements, and the Gruneisen  $\gamma$ 's for these modes are listed in Table 6.

TABLE 6

DIRECTION	POLARIZATION	$aq/2\pi$	$\gamma_{qj}$
$[\xi\xi\xi]$	T	0.867	$2.66 \pm 0.30$
$[\xi\xi\xi]$	L	0.867	$0.91 \pm 0.43$
$[\xi 00]$	T	1.000	$3.86 \pm 0.78$
$[\xi 00]$	T	0.650	$0.97 \pm 0.62$
$[\xi 00]$	L	1.000	$1.07 \pm 1.39$
$[\xi 00]$	L	0.750	$2.29 \pm 1.31$

Although Townsend (1964) has indicated that Pb crystallites deposit preferentially with their (111) axes aligned perpendicularly to the film surface, the attitude of Rochlin (1967), that tunnel results yield a directionally averaged phonon spectrum, is taken by this author. Therefore shifts in  $\bar{\omega}_t$  and  $\bar{\omega}_\ell$  obtained in this work cannot be directly compared to the neutron diffraction results of Lechner and Quittner.



Payne (1964) was the first to publish results in which the tunneling technique was used to study shifts in phonon modes under an applied stress. He measured shifts in some of the predominant phonon modes in germanium subjected to uniaxial compression, but he notes that considerable care must be taken in accounting for shear induced effects resulting from this form of "pressure" production. This problem is absent when the junctions are pressurized in a solid helium bath.

Hodder and Briscoe (1966) have attempted to measure the shifts in the phonon structure in Pb, by bending junctions of Pb-Pb-oxide-Pb, at liquid helium temperatures. These junctions exhibit structure in the neighbourhood of the transverse phonon peak which can be identified with the Van Hove singularities in the phonon spectrum. The nature of these singularities has been discussed by Van Hove (1953), by Rosenstock (1955), and by Phillips (1956), while their presence in tunneling results has been explained by Rowell, Anderson, and Thomas (1963), and by Scalapino and Anderson (1964). Hodder and Briscoe therefore shift these singularities by bending their junctions. However, since there are several singularities in the energy region of  $\bar{\omega}_t$ , and since they are not completely resolved from each other, it is doubtful if their measured shifts corres-





pond to actual phonon shifts. Also, their results depend crucially on the choice of Poisson's ratio, since some effort was made to calculate shear effects. This can best be illustrated by their calculated value of  $\delta \ln V/\text{unit strain}$ , which varies from 0.229 - 0.519, depending on the assumptions made. On top of these uncertainties is another large contribution due to the extremely small phonon shifts produced. They find, in this way, that  $\delta \ln \bar{\omega}_t/\text{unit strain} \sim 2 \delta \ln \bar{\omega}_\ell/\text{unit strain}$ . This is in disagreement with our results.

The thermal expansion measurements due to White (1962), possibly yield the best comparison for the present results. If one assumes that  $\gamma(\omega_t)$  and  $\gamma(\omega_\ell)$  remain constant over the whole energy range of the two branches, then at low temperature, where the transverse modes are predominantly excited, equation VI-7 becomes

$$\begin{aligned} \gamma_G &= \frac{2/3(\gamma_t/c_t^3) + 1/3(\gamma_\ell/c_\ell^3)}{2/3(1/c_t^3) + 1/3(1/c_\ell^3)} \\ &= \frac{\gamma_t + 1/2(\gamma_\ell)(c_t/c_\ell)^3}{1 + 1/2(c_t/c_\ell)^3} \\ &\sim \gamma_t = 2.52 \pm 0.73. \end{aligned}$$

At high temperature, where all the modes are excited,





one has,

$$\begin{aligned}\gamma_G &= 2/3 \gamma(\omega_t) + 1/3 \gamma(\omega_\ell) \\ &= 2.78 \pm 0.64.\end{aligned}$$

These values compare with  $\gamma_G$  by White of 2.6 and 2.7 respectively (no uncertainty limits are given). While the present results seem to show more variation than the thermal expansion results, the two sets of values probably agree within experimental error.



### VI.3 The Pressure Dependence of the Energy Gap

Energy gap values were obtained as a function of temperature by relating the zero bias conductance to tabulated values of  $\Delta_0$  found in Bermon's (1964) table. His calculations relate the normalized density of states ( $\sigma$ ) to  $\Delta_0$  for a BCS constant gap-parameter theory. Although, strictly speaking, the gap at the gap-edge energy should have been measured, the use of the conductance minimum gives a more consistent method of estimating  $\Delta_0(T)$ , especially when making the pressure comparison. Furthermore, since  $\Delta_1(\omega) \simeq \text{constant}$  and  $\Delta_2(\omega) \simeq 0$  for energies up to the gap-edge energy and a little beyond, one might expect the temperature variation of the gap to follow a BCS behaviour to a good approximation. We therefore assume that shifts in the zero bias gap value are in 1:1 correspondence with shifts at the gap-edge energy.

Figure 17 shows a plot of  $\Delta_0(T)$  vs  $T$  for Junction 1345E. The lower curve was taken for  $P = 39,600$  psi while the upper consists of  $P = 0$  points taken before and after the pressure run. The reproducibility of the  $P = 0$  points rules out permanent sample deformation as a possible origin of the effect. Points below  $4.2^\circ\text{K}$  become increasingly less accurate because  $\sigma_{\text{min}}$  is now close to zero and is only slightly temperature dependent.



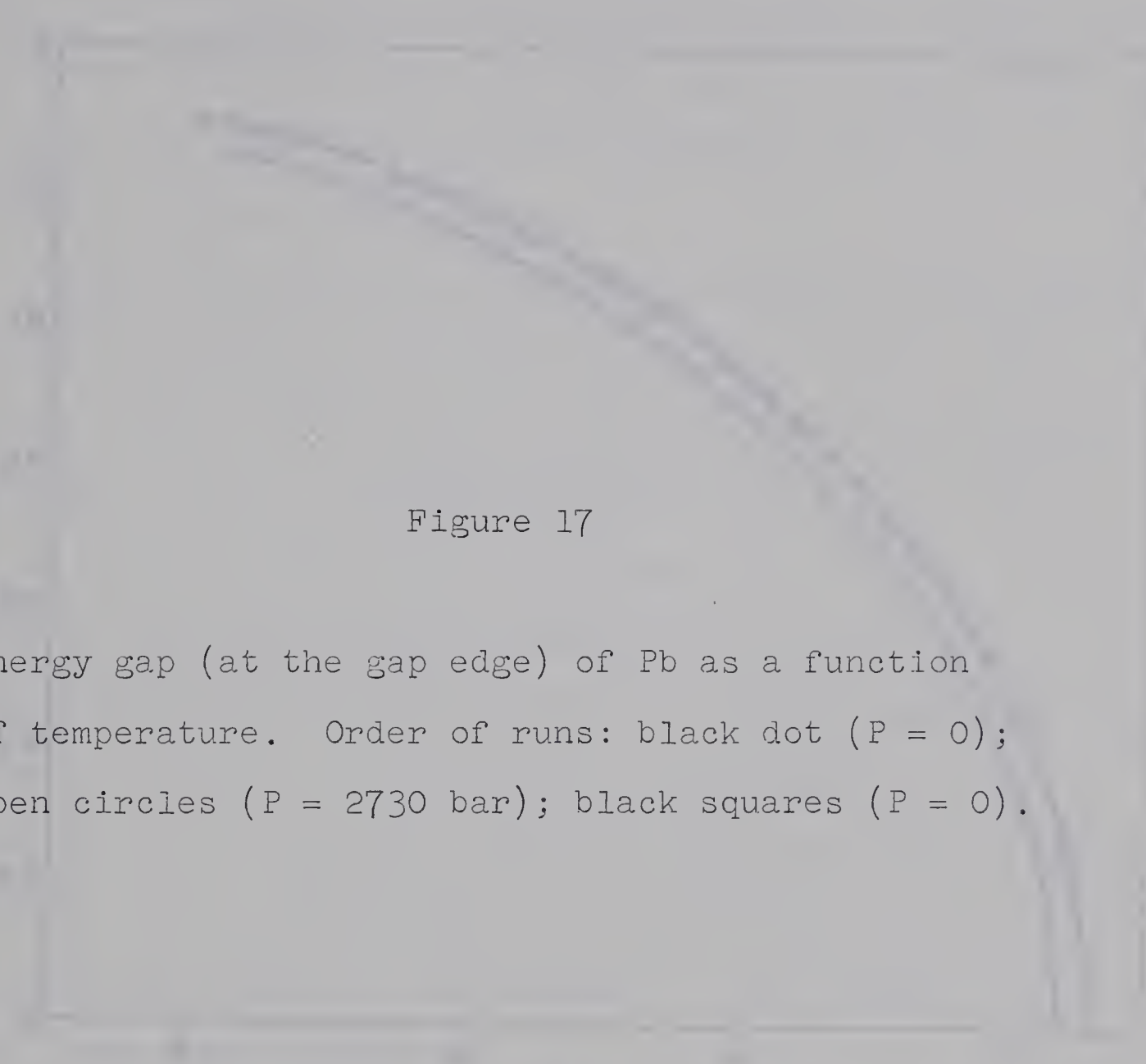


Figure 17

Energy gap (at the gap edge) of Pb as a function of temperature. Order of runs: black dot ( $P = 0$ ); open circles ( $P = 2730$  bar); black squares ( $P = 0$ ).



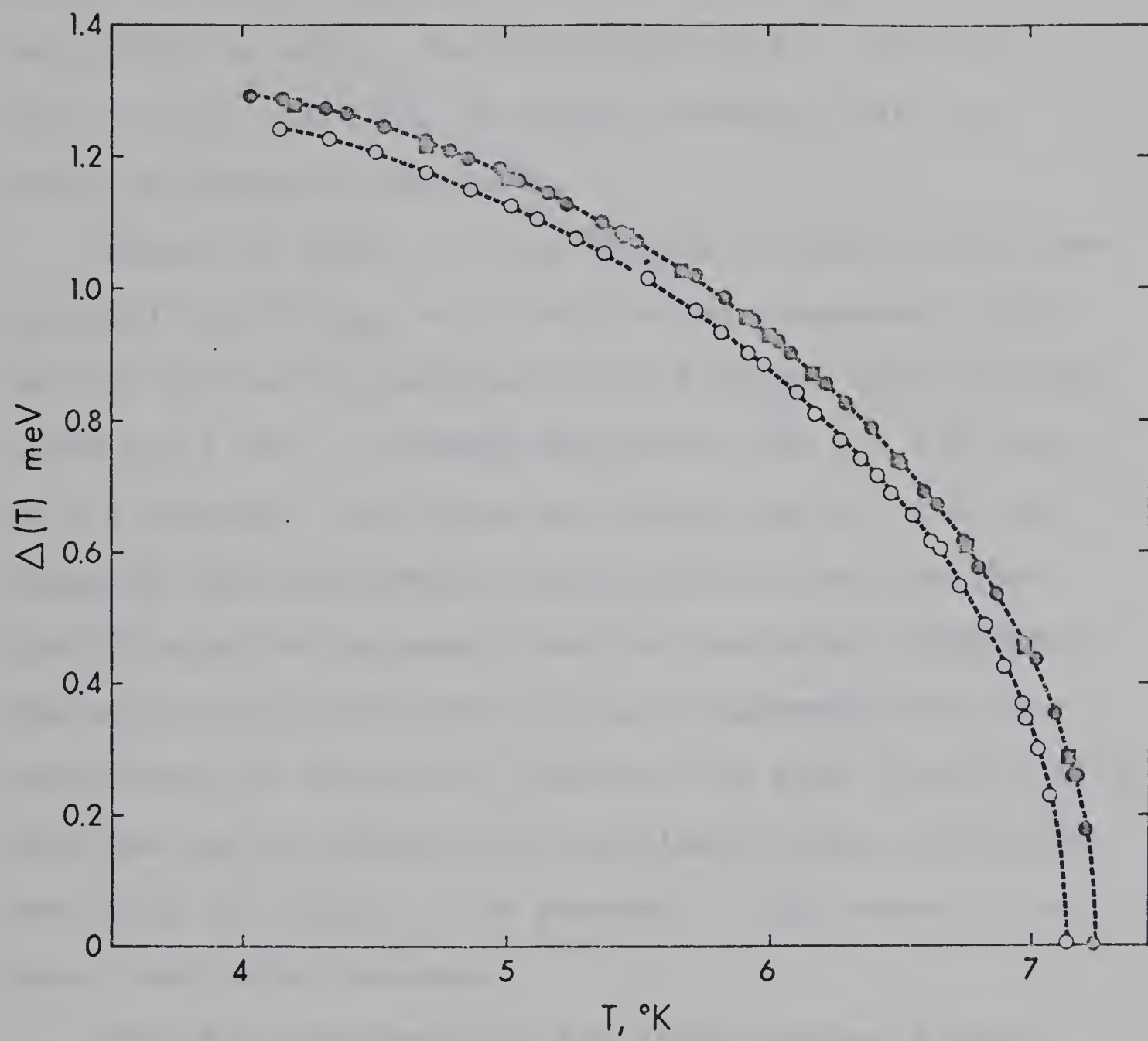






Figure 18 shows a plot of  $(\Delta_o(T)/kT_c)^2$  vs  $t$  for the same junction. The BCS weak-coupling limit prediction, taken from calculations by Muhlschlegel (1959), is plotted as well. The fact that the  $P = 0$  and  $P > 0$  plots do not coincide, is direct evidence that the ratio is pressure dependent.

Figure 19 shows the same points plotted in the form  $(\Delta_o/kT_c)/(\Delta_o/kT_c)_{\text{BCS}}$  vs  $t$  for the two pressures. Both sets of points lie on essentially straight lines through 1.266 and 1.248. Although the points for  $t > 0.8$  seem to lie somewhat lower than the values for  $t < 0.8$ , because of the experimental uncertainty, it was decided that this deviation should not be considered significant. One may conclude from this plot, in agreement with the predictions of Scalapino, Swihart, and Wada (section II.9), that the gap vs temperature relation follows a BCS type variation to "within a few percent". This seems to be true, even under pressure.

From the difference in the least squares fitted horizontal straight lines through the  $P = 0$  and  $P > 0$  plots, one obtains,

$$\delta\left(\frac{2\Delta_o}{kT_c}\right)_{t=\text{const}} = (1.248 - 1.266)(3.528) = -0.0635.$$



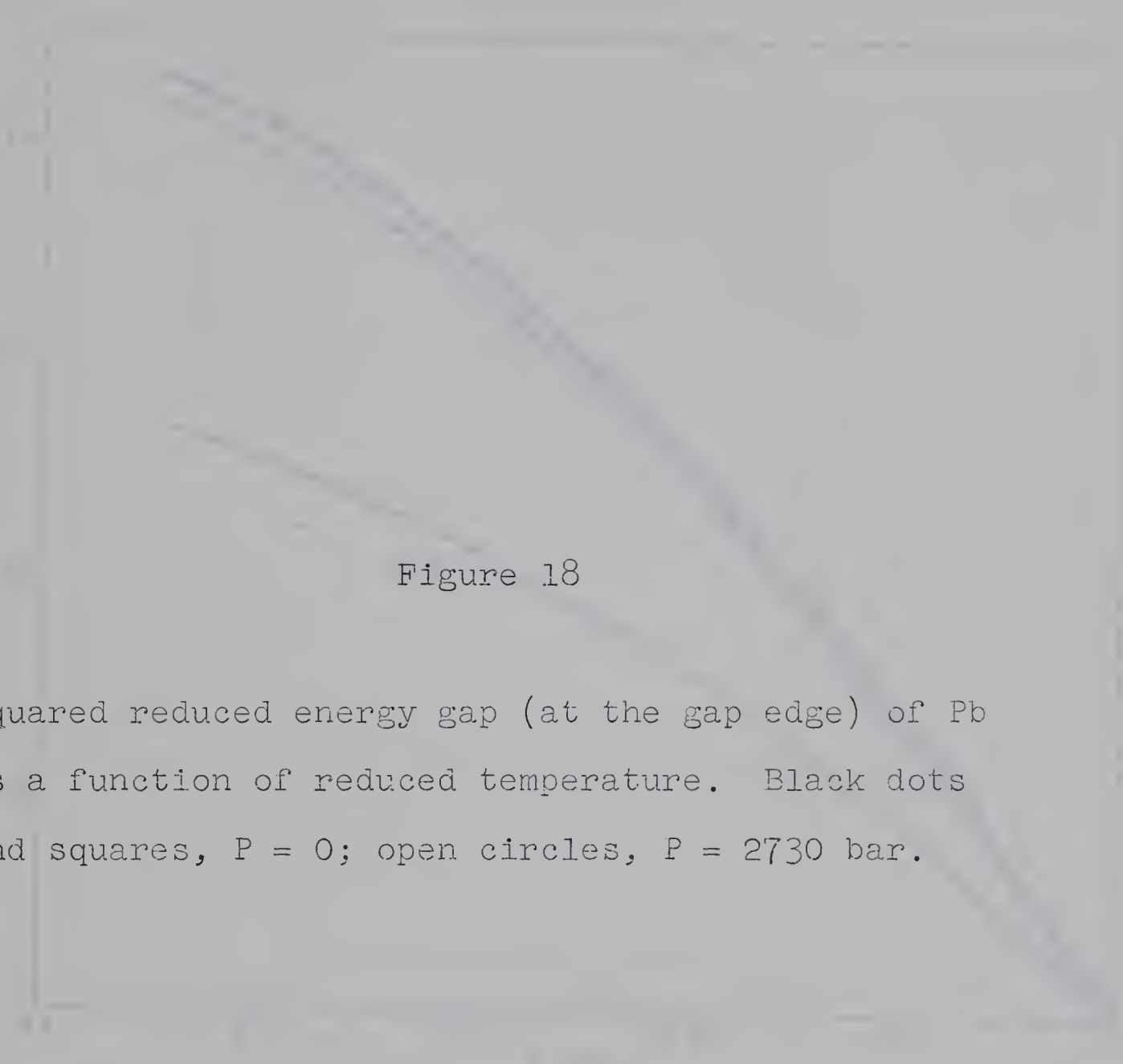


Figure 18

Squared reduced energy gap (at the gap edge) of Pb as a function of reduced temperature. Black dots and squares,  $P = 0$ ; open circles,  $P = 2730$  bar.



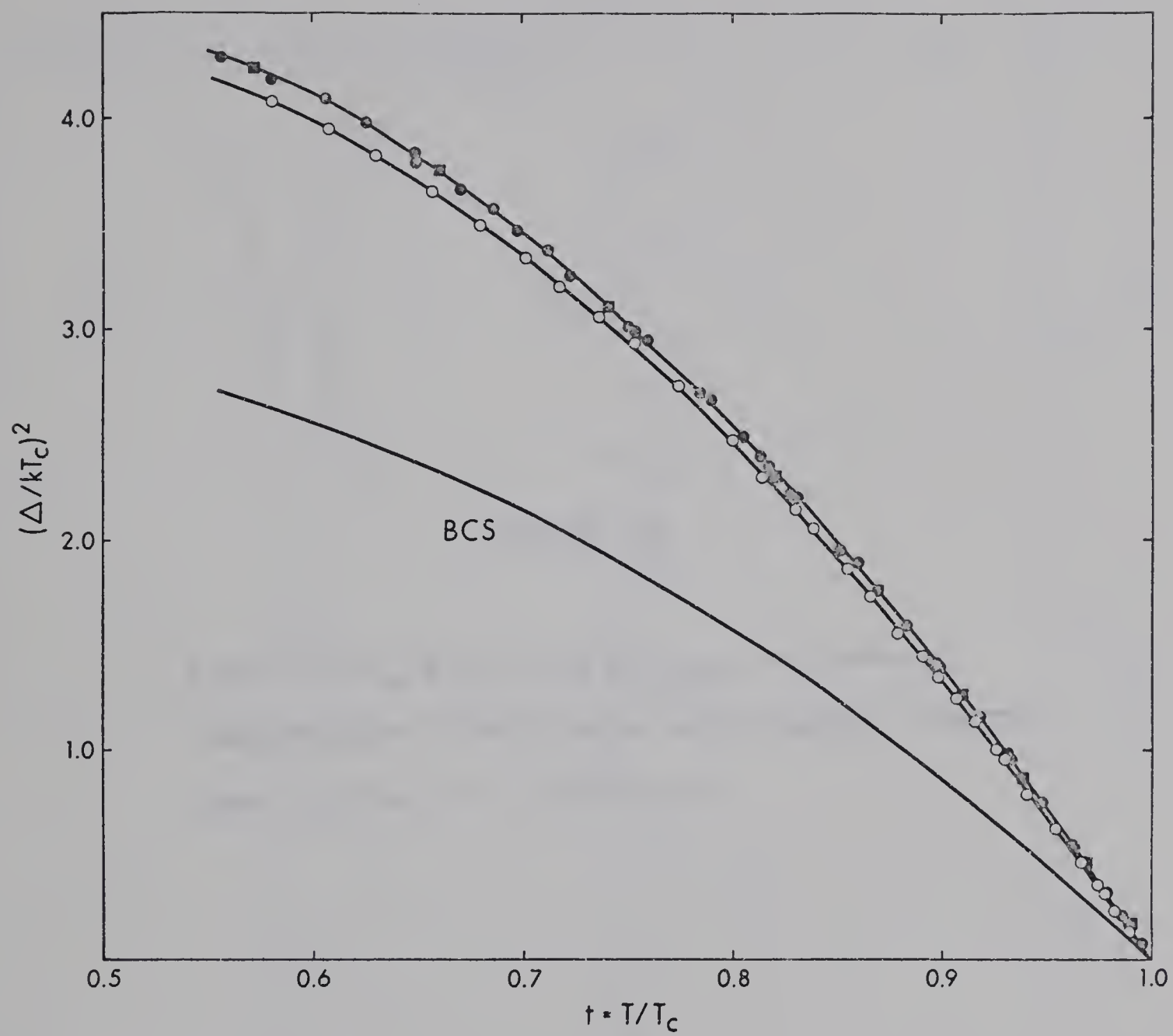


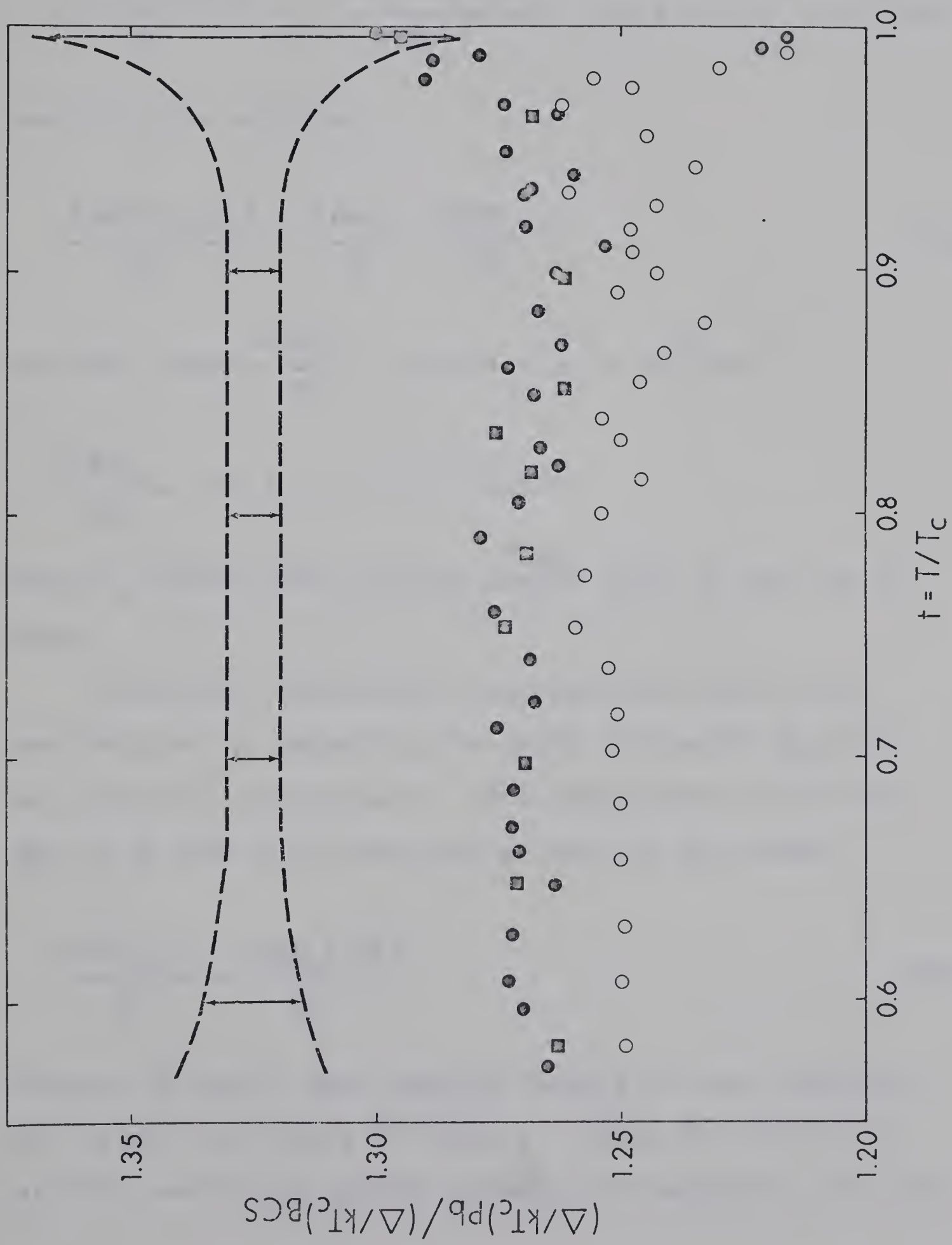


Figure 19

Plot of  $(\Delta_o/kT_c)/(\Delta_o/kT_c)_{\text{BCS}}$  vs reduced temperature; black dots and squares,  $P = 0$ ; open circles,  $P = 2730$  bar.









Thus,

$$\frac{d \ln(2\Delta_o/kT_c)}{dP} = - \frac{0.0635/4.403}{2730.5} = -(5.3 \pm 0.5) \times 10^{-6} \text{bar}^{-1}$$

and from the relation

$$\frac{d \ln(2\Delta_o/kT_c)}{dP} = \frac{d \ln \Delta_o}{dP} - \frac{d \ln T_c}{dP} \quad \text{VI-13}$$

we have, using  $\frac{d \ln T_c}{dP} = -5.06 \pm 0.30 \times 10^{-6} \text{bar}^{-1}$

$$\frac{d \ln \Delta_o}{dP} = -10.3 \pm 1.1 \times 10^{-6} \text{bar}^{-1}.$$

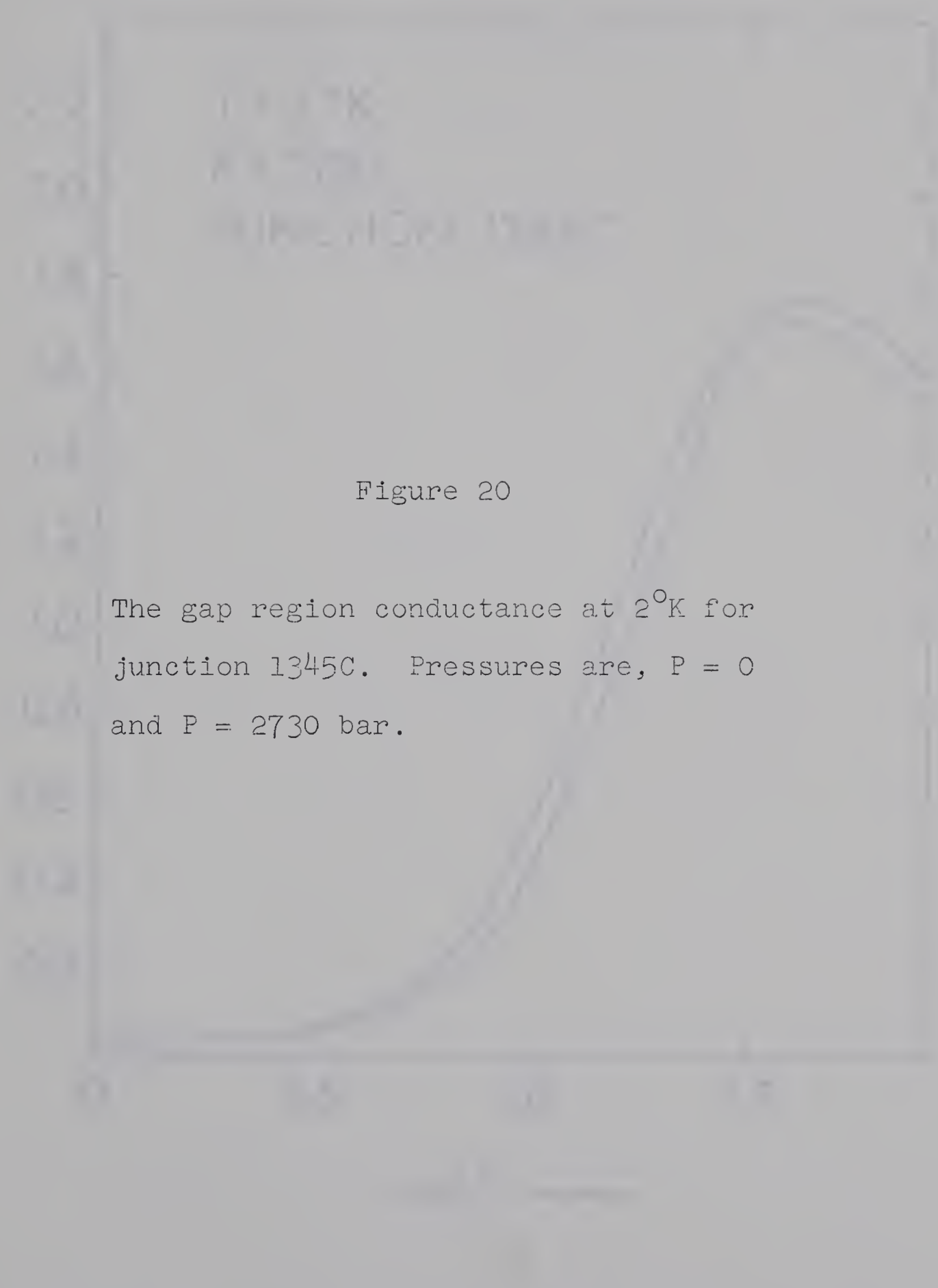
Thus  $\Delta_o$  shifts with pressure almost twice as fast as  $T_c$  does.

Additional information regarding the shift in  $\Delta_o$  was obtained by measuring the shift in the  $2^\circ\text{K}$  gap wall as a function of pressure. At a temperature of  $2^\circ\text{K}$  the gap is 99.28% fully developed so that we may assume

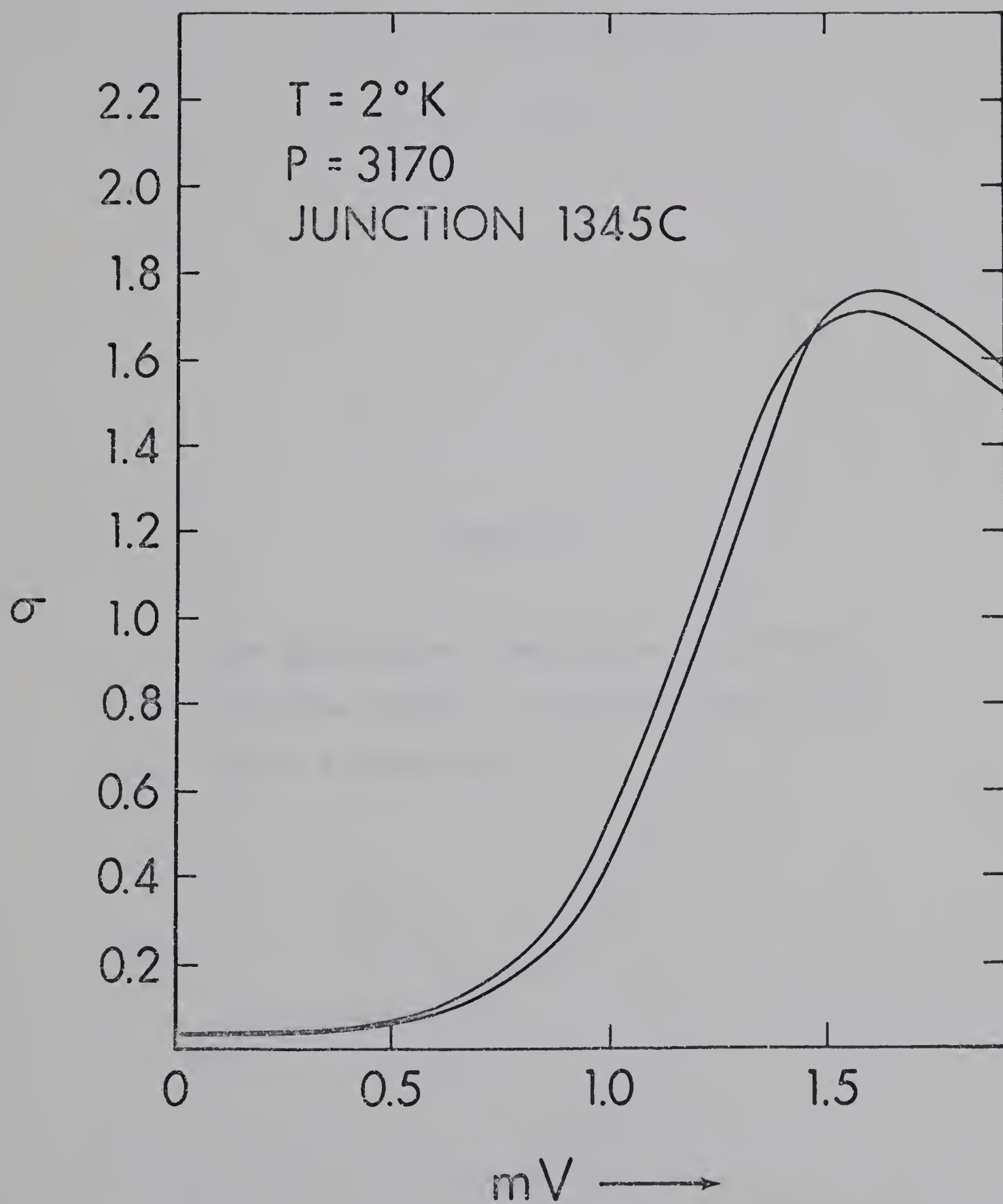
$$\frac{d \ln \Delta_o(0)}{dP} = \frac{d \ln \Delta_o(2^\circ\text{K})}{dP} . \quad \text{VI-14}$$

Figures 20 and 21 show typical results for two junctions. The values are listed in table 7. Since the shift in  $t$  at  $2^\circ\text{K}$  due to the applied pressure is negligible, one can













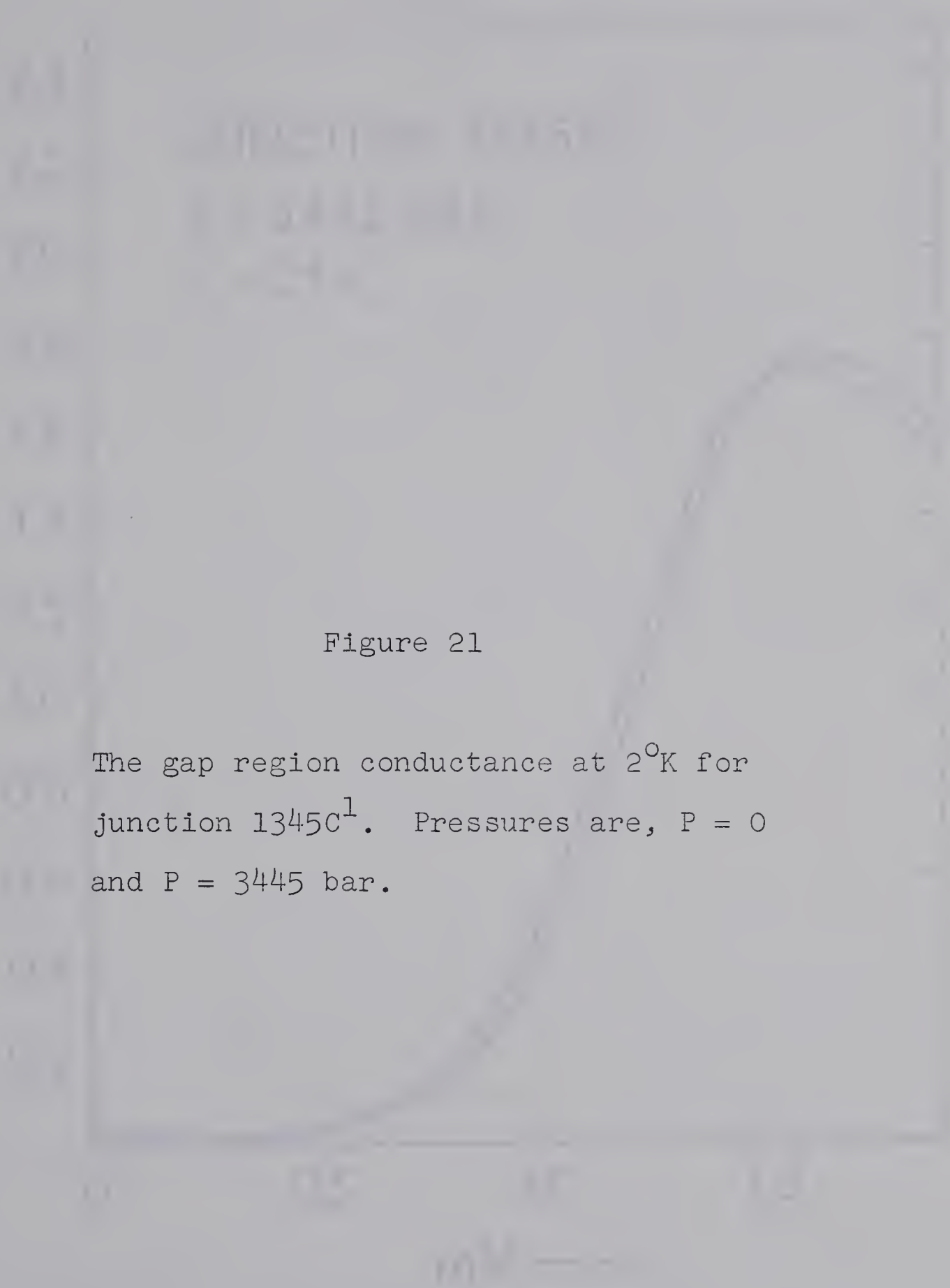


Figure 21

The gap region conductance at  $2^{\circ}\text{K}$  for junction  $1345\text{C}^1$ . Pressures are,  $P = 0$  and  $P = 3445$  bar.



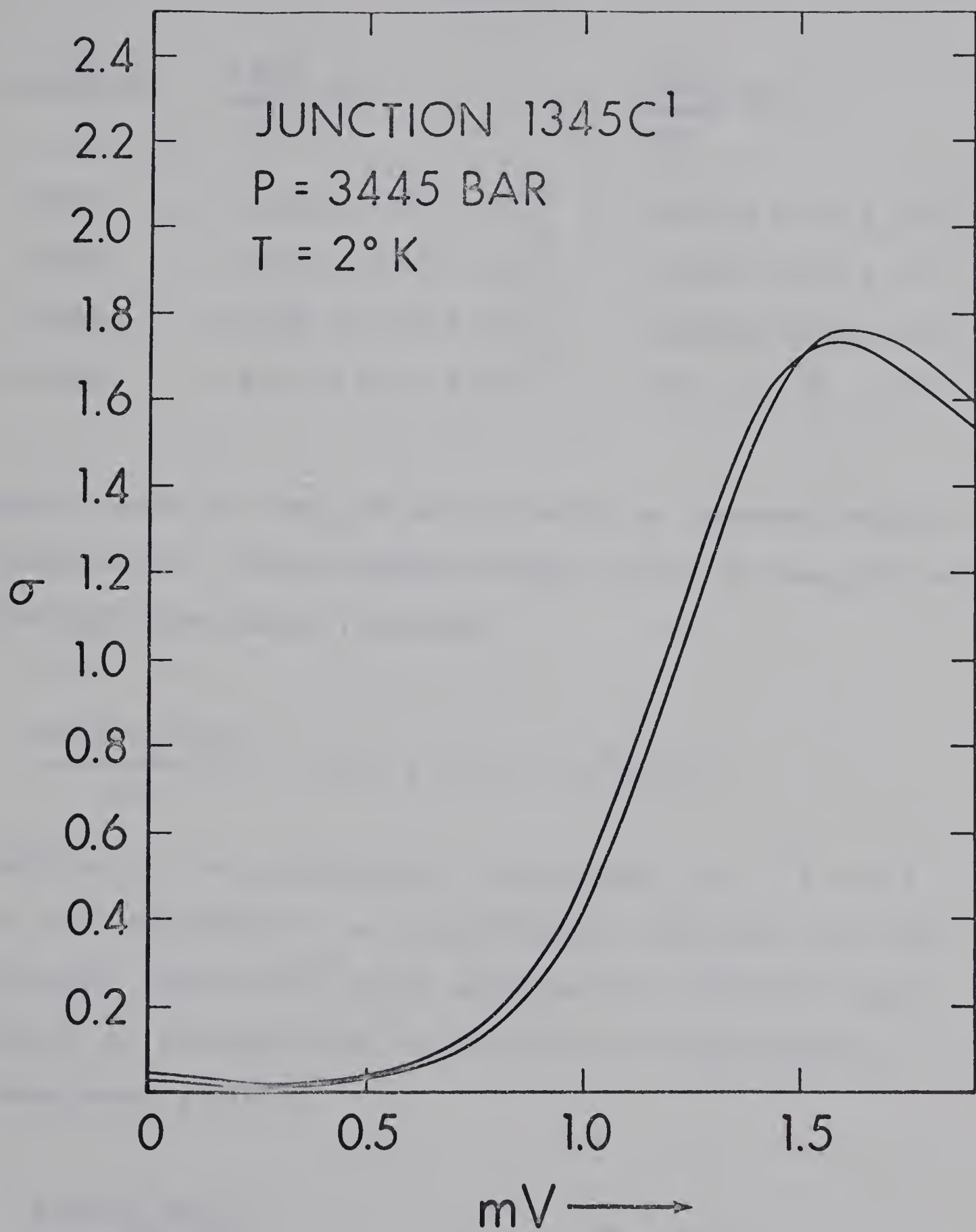




TABLE 7

JUNCTION	$\frac{d \ln \Delta_o}{dP} \text{ bar}^{-1}$	$\frac{d \ln T_c}{dP} \text{ bar}^{-1}$
1345C	$-9.52 \pm 0.80 \times 10^{-6}$	$-4.81 \pm 0.50 \times 10^{-6}$
1345D	$-9.60 \pm 0.80 \times 10^{-6}$	$-4.79 \pm 0.50 \times 10^{-6}$
1345E	$-9.65 \pm 0.80 \times 10^{-6}$	$-5.02 \pm 0.50 \times 10^{-6}$
Average	$-9.6 \pm 0.8 \times 10^{-6}$	$-4.9 \pm 0.5 \times 10^{-6}$

again refer to  $d \ln \Delta_o / dP$  as occurring at constant reduced temperature. Substituting average values of  $d \ln \Delta_o / dP$  and  $d \ln T_c / dP$  from table 7 yields:

$$\frac{d \ln (2\Delta_o / kT_c)}{dP} = -(4.7 \pm 1.3) \times 10^{-6} \text{ bar}^{-1}.$$

Because of the experimental uncertainty, the  $2^\circ\text{K}$  shift is not considered to be significantly different from the extended temperature shift measured for Junction 1345E. Taking an average value to represent the experimental measurements gives,

$$\frac{d \ln (2\Delta_o / kT_c)}{dP} = -(5.0 \pm 0.9) \times 10^{-6} \text{ bar}^{-1}.$$

In the BCS weak-coupling theory both  $T_c$  and  $\Delta_o(0)$  have



the form  $T_c \propto \Delta_0 \propto \Theta_D \exp(-1/N(0)V)$ . Thus pressurizing the system results in identical shifts in both  $T_c$  and  $\Delta_0(0)$  so that the ratio  $2\Delta_0(0)/kT_c$  should remain constant. However, for the strong-coupling ratio measured for Pb, no such simple relation exists between the two parameters. We guess that the pressure dependence of the Pb ratio has its origin in a change in the electron-phonon interaction strength, along with changes in the density of states. McMillan (1968) has published an abstract of a paper to appear in Phys. Rev., in which he finds the coupling constant is strongly frequency dependent, the coupling strength decreasing as the phonon frequencies are increased. Thus by changing  $F(\omega)$  to higher values with pressure, the electron-phonon interaction is somewhat reduced toward a BCS limit as is observed in the  $\text{gap}/T_c$  ratio.

This argument is further substantiated by the work of Zavaritskii (1967). He finds that by depositing the Pb for his Pb-Pb junctions at 1.6°K, a maximum amount of crystalline lattice strain is produced. The associated phonon spectrum exhibits many more low energy modes, and since these modes contribute most in the gap parameter,  $\Delta_0$  is increased. Subsequent annealing of his samples from 100°K to room temperature in stages, increases the definition in  $\alpha^2(\omega)F(\omega)$ , and the spectrum gradually







reverts back to its usual form with an accompanying decrease in the gap-parameter. He does not measure the change in the transition temperature as a function of annealing, so nothing can be said about the  $\text{gap}/T_c$  ratio. However, it appears that the frequency dependent nature of the coupling constant is further borne out.

Although this author feels confident that this explanation of the measured pressure dependence of  $\Delta_o(0)/kT_c$  is correct, two sources of possible anomalous behaviour cannot be completely discounted. These include anisotropy and low temperature strain arguments.

Anisotropy of the energy gap in Pb has been studied by Richards and Tinkham (1960), by Townsend and Sutton (1963), and by Rochlin (1967). Richards and Tinkham performed electromagnetic absorption experiments, while the latter two investigations were carried out with tunnel junctions. In the tunnel junctions, the anisotropy, which leads to two or more gap values, is a function of film thickness and disappears for films less than  $\sim 0.7 \mu$  in thickness. In these thin films, due to the small electron mean free path, the superconductor takes on the behaviour of a "dirty" superconductor and exhibits a single average energy gap, even for high purity samples. (The Pb and Al films used in the present work for junction fabrication, are between  $1,000 \overset{\circ}{\text{A}}$  and  $3,000 \overset{\circ}{\text{A}}$  in thickness, so anisotropy effects should not be too significant.)



Two schools of thought exist concerning the origin of the gap anisotropy. Townsend and Sutton ascribe it to Fermi surface irregularities, while Bennett (1965) and Rochlin (1967) feel it is associated with anisotropy in the phonon spectrum.

Attempts to associate the pressure dependence of  $2\Delta_0(0)/kT_c$  with an increase in gap anisotropy (due to Fermi surface distortion), can be ruled out, in view of the work done on the pressure dependence of the Fermi surface of Pb. Anderson and Gold (1965), and Anderson, O'Sullivan, and Schirber (1967), have carried out de Haas-Van Alphen measurements on Pb subjected to hydrostatic pressure. In the first paper, the Fermi surface is found to scale in all directions under pressure at a rate close to free-electron model predictions. In the second paper, this is somewhat revised in that isotropic scaling still occurs, but now it scales at approximately 2 times free electron predictions. In any event, excessive distortion of the Fermi surface due to pressurizing, seems to be an unlikely explanation of the observed pressure dependence of the ratio  $2\Delta_0(0)/kT_c$ . The association of the result with increased phonon anisotropy under pressure remains as a possible explanation of the effect in terms of gap anisotropy. If an average gap value is measured, with





directional contributions from relations of the form  $2\Delta_{o1}(0) = m_1 kT_{c1}$ ,  $2\Delta_{o2}(0) = m_2 kT_{c2}$ , . . . etc, since only the maximum transition temperature value  $T_{c,max}$  is measured, the result  $d\Delta_{o,Av}(0)/dT_{c,max} \neq \text{constant}$  implies that either the  $m_i$  values are pressure dependent (the explanation favoured by this author) or that some of  $d\Delta_{o1}(0)/dP$ ,  $d\Delta_{o2}(0)/dP$ , . . . are not equal. The only sure test of this would be to pressurize Pb-Pb junctions with detectable gap anisotropy and try to relate  $dT_c/dP$  to the pressure dependence of the largest gap value.

The remaining possibility for explaining the pressure dependence of  $2\Delta_o(0)/kT_c$  is film strain at low temperature. Caswell, Priest, and Eudo (1963), have measured low temperature strain in Pb films and find that the amount depends on the evaporation conditions, the amount of annealing carried out at room temperature, and on film thickness. This therefore parallels (and precedes) the results obtained by Zavaritskii (1967). All of the junctions used in the present work were annealed at room temperature for at least one day, and sometimes for up to three weeks. Since the results are all similar, the annealing time does not seem to effect the pressure dependent result. This is probably due to the fact that differential effects are measured. Also, the annealed condition of a given sample can be considered constant, since no temperature



annealling occurs until the temperature exceeds  $100^{\circ}\text{K}$  (Zavaritskii (1967)). Between the  $P = 0$  and  $P > 0$  runs the temperature never goes above  $\sim 40^{\circ}\text{K}$ .

Wu (1967), Adler, Jackson, and Will (1967), and Claeson (1966, 1967), have changed the electron-phonon coupling strength in Pb by alloying with indium and thallium. Their results have been summarized in Table 8 (taken from Wu).

TABLE 8

Alloy	Electrons per atom	$\Delta_0(0)$	$T_c$		$2\Delta_0(0)/kT_c$	
			Theor.	Exptl.	Theor.	Exptl.
Pb	4	1.38	7.20	7.22	4.45	4.43
$\text{Pb}_{0.80}\text{Tl}_{0.20}$	3.8	1.23	6.96	7.08	4.10	4.04
$\text{Pb}_{0.60}\text{Tl}_{0.40}$	3.6	1.02	6.22	6.16	3.78	3.81
$\text{Pb}_{0.40}\text{Tl}_{0.60}$	3.4	0.68	4.51	4.60	3.51	3.43
Pb	4	1.38	7.20	7.22	4.45	4.43
$\text{Pb}_{0.75}\text{In}_{0.25}$	3.8	1.29	6.92	6.86	4.31	4.36
$\text{Pb}_{0.60}\text{In}_{0.40}$	3.6	1.21	6.68	6.63	4.19	4.22
$\text{Pb}_{0.40}\text{In}_{0.60}$	3.4	1.18	6.65	6.60	4.11	4.16

For the Pb-Tl case, Wu explains the reduction in the ratio  $2\Delta_0(0)/kT_c$  in the following way. As the electron concentration decreases, the effective ionic charge also decreases, as does the Fermi momentum. Hence the momentum





space available for the integral which determines the electron-phonon coupling constant  $\alpha^2(\omega)$  (equation II-38) is also reduced.

For the Pb-In case, although the electron concentration decreases along with the electron-phonon coupling strength, the transverse phonon peak shifts to lower frequencies where it enters the integral for the energy-gap with greater weight. The two effects tend to compensate each other somewhat and the ratio decreases more slowly.

In attempting to explain the pressure dependence of  $2\Delta_0(0)/kT_c$  for pure Pb along these lines, one notes that although the electron concentration per unit volume is slightly increased with pressure, the phonon modes are shifted to higher energies. The latter dependence tends to reduce the coupling-constant through its frequency dependence, and tends to reduce  $\Delta_0(0)$  by decreasing the effective low energy modes entering its calculation. It is of interest to note that although the electron concentration increases under pressure (and the Fermi surface expands), the actual density of states decreases in the region of the Fermi level (Garfinkel and Mapother (1961)), so that it is hard to estimate the concentration effect on the integral of the coupling constant  $\alpha^2(\omega)$ . This effect is discussed in more detail in section VI.5.



#### VI.4 Changes in the Thermodynamic Properties with Pressure

Garfinkel and Mapother (1961) have carried out magnetic field measurements on bulk Pb subjected to hydrostatic pressure. They report the following results:

- (1) The pressure dependence of the zero temperature critical magnetic field is,

$$\frac{d\ln H_0}{dP} = - (9.72 \pm 0.26) \times 10^{-6} \text{ bar}^{-1}.$$

- (2) The pressure dependence of the critical field in the limit as  $T \rightarrow T_c$  is

$$\left(\frac{dH_c}{dP}\right)_{T_c} = - (9.32 \pm 0.30) \times 10^{-3} \text{ gauss/bar}.$$

- (3) They use result (1) in estimating the pressure dependence of the normal metal electronic specific heat which is given by

$$\lim_{T \rightarrow 0^+} \frac{\Delta S}{V} = \gamma^* T = \left(\frac{\gamma}{V}\right) T = -\left(\frac{1}{4\pi}\right) \lim_{T \rightarrow 0^+} H_c \left(\frac{\partial H_c}{\partial T}\right)_P \quad \text{VI-15}$$

where  $V$  is the molar volume, and  $\gamma$  is the coefficient of the normal electronic specific heat per mole. This is done by expanding

$$H_c(P, T) = H_0(P) + A_1(P)T^2 + A_2(P)T^4 \dots, \quad \text{VI-16}$$

neglecting terms in  $T^4$ , and estimating  $A_1(P)$  from the



temperature dependence of  $H_c$ . This gives

$$(1/\gamma^*)(d\gamma^*/dP) = (1/H_o)(dH_o/dP) + (1/A_1)(dA_1/dP). \quad \text{VI-17}$$

They obtain the result

$$\frac{d \ln \gamma^*}{dP} = -(8.20 \pm 1.54) \times 10^{-6} \text{ bar}^{-1}.$$

Since  $\gamma^* = 2/3\pi^2 k^2 N(0)$ , where  $N(0)$  is the renormalized density of states, they obtain,

$$\frac{d \ln N(0)}{dP} = -(8.20 \pm 1.54) \times 10^{-6} \text{ bar}^{-1}.$$

This information along with the present measurements on  $d \ln \Delta_o / dP$ , can be used in estimating the pressure dependence of the condensation energy. As mentioned in section II.10, Wada has shown that in general,

$$\frac{H_o^2}{8\pi} = N(0) I \quad (\text{where } I = \frac{1}{2}\Delta_o^2 \text{ for the BCS theory}). \quad \text{VI-18}$$

Here  $I$  is a function of the renormalization factor and of the complex gap. Introducing the ratio  $I/(\frac{1}{2}\Delta_o^2)$ , and using it as an approximate measure of the coupling strength, one finds that for  $P = 0$  the ratio is 0.83. The pressure dependence of this ratio is given by

$$d \ln (I/\Delta_o^2) / dP = 2(d \ln H_o / dP - d \ln \Delta_o / dP) - d \ln N(0) / dP. \quad \text{VI-19}$$





Substituting the relevant measured results gives

$$d \ln(I/(\frac{1}{2}\Delta_0^2)) = (8.7 \pm 3.4) \times 10^{-6} \text{ bar}^{-1}$$

The indicated error includes the errors for  $d \ln H_0/dP$  and  $d \ln N(0)/dP$  quoted by Garfinkel. One finds therefore, in agreement with the result on the gap- $T_c$  ratio, that increasing the pressure, changes the properties of Pb towards those of a BCS superconductor.

The pressure dependence of the energy gap can be used in estimating the pressure dependence of the jump in electronic specific heat at the zero field s-n transition. As mentioned in section II.10, Wada has used strong-coupling theory in deriving an expression for this jump. At present, we do not have sufficient information available to carry out a comparison with his theory, however, the present work can be compared to strong-coupling model calculations, through the form of the temperature dependence of  $(\Delta_0(T)/kT_c)^2$ .

The BCS assumption of an energy independent gap, leads to the prediction that the electronic specific heat should exhibit a discontinuity at  $T_c$  given by the expression,

$$\frac{\Delta C_{el}}{\gamma T_c} = \frac{3}{2\pi^2} \frac{d(\Delta_0(T)/kT_c)^2}{dt} \quad \text{VI-20}$$

where the limiting slope is to be taken. The BCS weak-coupling limit result for this is 1.43. Figure 18 shows a plot





of  $(\Delta_o(T)/kT_c)^2$  vs  $t$  for Junction 1345E. The limiting slope for the  $P = 0$  curve results in a value of  $\Delta C_{el}/\gamma T_c = 2.22 \pm 0.05$ . The same slope has been measured for four other junctions. One can also estimate values of  $\Delta_1(\omega = 0)$  for  $t = 0.98$  (figure 3) and  $t = 0.96$  from the model calculations of Scalapino, Wada, and Swihart (1965) and Swihart, Scalapino, and Wada (1965). If these values are plotted on the same graph, and the bulk transition temperature is used, the theoretically predicted slope is also 2.2, which indicates excellent agreement between theory and experiment. If, however, one takes the calorimetrically measured jump in the electronic specific heat (Shiffman et al (1963), Decker et al (1958), and Neighbor et al (1967)) and makes use of the low temperature determination of  $\gamma$  (van der Hoeven and Keesom (1965) and N.E. Phillips (1967)), the predicted ratio using equation VI-20 would be  $2.65 \pm 0.06$ .

It is felt that this discrepancy between the present work and the calorimetrically determined value is more apparent than real, since the framework surrounding the development of equation VI-20 does not really apply for strong-coupling Pb. Swihart (1962) interpreted the discrepancy between the BCS value and the calorimetric value of 2.65 as being due to an increase in the gap as one moves away from the gap edge. This is probably the case, and,



moreover, this argument can be used in comparing the present work to the calorimetric result since choice of  $\Delta(\omega = 0)$  in forming the plot of  $(\Delta/kT_c)^2$  vs  $t$  is an approximation to the energy dependence of the gap, while the calorimetric measurement naturally embodies the correct energy dependence of  $\Delta(\omega)$ .

Although Eliashberg (1963) may have been the first to realize the importance of the strong-coupling electron-phonon interaction on this result, Wada was the first to account for it in a proper way. This will undoubtedly be borne out when a direct comparison to his theory can be made.

From the shift in the slope of  $(\Delta/kT_c)^2$  vs  $t$  with pressure (figure 18), it is tempting to speculate that the specific heat jump should decrease as the pressure is increased. This should again be explainable using Wada's theory and the pressure-dependent phonon spectrum for Pb.



### VI.5 Other Shifts in Pb Under Pressure

In equation II-42, the density of states (conductance) was expanded as

$$\sigma = \frac{N_T(\omega)}{N(0)} = 1 + \frac{\Delta_1^2(\omega) - \Delta_2^2(\omega)}{2\omega^2} + \dots \quad \text{VI-21}$$

If an energy region is considered where  $\Delta_2 \sim 0$ , then one gets

$$\left. \frac{d \ln(\sigma - 1)}{dP} \right|_{\omega=\text{const}} = \left. \frac{d \ln \Delta_1^2(\omega)}{dP} \right|_{\omega=\text{const}} \quad \text{VI-22}$$

This condition is satisfied for the gap-edge region of the density of states. Pressure-induced shifts in the conductance at constant energy in the region near the gap edge are listed in Table 9 for 2°K, 4.2°K, and for  $t = T/T_c$  close to 1. Typical 2°K shifts are shown in figures 20 and 21, while figure 23 shows the pressure amplitude shift for  $t = 0.92$  and  $t = 0.95$ .

Structure amplitude reductions were noticed in the region of  $\bar{\omega}_t$  and  $\bar{\omega}_l$  when the junctions were subjected to a pressure. These effects can be seen in figures 14, 15, and 16. The structure is associated with the phonon emission process, and should be sensitive to a reduction in the electron-phonon coupling strength. Defining the structure amplitude as  $S = |\sigma - 1|$ , for both the transverse and longitudinal regions (see figures 15 and 16),





TABLE 9

Temperature Junction $\delta(\sigma - 1)/(\sigma - 1)$			$\delta P$ (bar)	$d \ln(\sigma - 1)/dP$ ( $10^{-5}/\text{bar}$ )
$2^{\circ}\text{K}$	1345C	-0.037/0.765	3172.0	-1.52
$2^{\circ}\text{K}$	1345C <sup>1</sup>	-0.040/0.765	3447.5	-1.52
$4.2^{\circ}\text{K}$	1345B	-0.040/0.700	2551.2	-2.24
$4.2^{\circ}\text{K}$	1345B	-0.020/0.700	1309.9	-2.18
$t = 0.95$	1345A	-0.30/7.200	2378.8	-1.75
$t = 0.92$	1345A	-0.50/11.80	2378.8	-1.78
$t = 0.95$	1246A	-0.20/7.200	2137.3	-1.30
$t = 0.92$	1246A	-0.40/11.80	2137.3	-1.59
				Average = -1.73

one is again tempted to associate this with the pressure dependence of the gap through the relation,

$$\frac{d \ln |\sigma - 1|}{dP} \Big|_{\omega=\text{const}} = \frac{d \ln S}{dP} \Big|_{\omega=\text{const}} = \frac{d \ln \Delta_{\text{Av}}^2}{dP} \Big|_{\omega=\text{const}} \quad \text{VI-23}$$

An average value of  $\Delta^2$  is taken, since there is no way of estimating  $d \ln \Delta_1^2(\omega)/dP$  and  $d \ln \Delta_2^2(\omega)/dP$  separately in this energy region. Several values of pressure induced shifts in S at the longitudinal and transverse phonon energies are listed in Table 10.





TABLE 10

JCN	$\frac{\delta S(\omega_t)}{S(\omega_t)}$	$\frac{\delta S(\omega_\ell)}{S(\omega_\ell)}$	$\delta P$	$\frac{d \ln S(\omega_t)}{dP}$	$\frac{d \ln S(\omega_\ell)}{dP}$
			(bar)	( $10^{-5}/\text{bar}$ )	( $10^{-5}/\text{bar}$ )
1345C	-0.60/10.00	-0.70/10.00	3447.5	-1.72	-2.03
1345D	-0.50/9.90	-0.50/9.60	2757.2	-1.83	-1.88
1345C <sup>1</sup>	-0.60/10.00	-0.60/9.80	3172.0	-1.89	-1.93
Average =				-1.81	-1.95

Taking an average of the structure shifts in Tables 9 and 10 gives as a final average,

$$\frac{d \ln(\sigma - 1)}{dP} = -(1.81 \pm 0.35) \times 10^{-5} \text{ bar}^{-1}. \quad \text{VI-24}$$

Using VI-23, this gives,

$$\frac{d \ln \Delta_{Av}}{dP} = -(9.1 \pm 1.7) \times 10^{-6} \text{ bar}^{-1}.$$

Since the directly measured gap shift was

$$\frac{d \ln \Delta_o}{dP} = -(9.9 \pm 0.8) \times 10^{-6}$$

(see section VI.3), good agreement between the two independent results is obtained.

The pressure dependence of  $\gamma^*$  as obtained by Garfinkel and Mapother (1961) provides information about the magnitude of the pressure derivative of the renormalization



parameter  $Z_n(0)$ . Writing the renormalized density of states as a product of the free electron expectation times  $Z_n(0)$ , one has,

$$\gamma^* = \frac{2\pi^2}{3} k^2 N(0) = \frac{2\pi^2}{3} k^2 N_{f.e.}(0) Z_n(0), \quad \text{VI-25}$$

where  $N(0)$  always refers to the density of states per unit volume. Therefore,

$$\frac{d \ln \gamma^*}{dP} = \frac{d \ln N_{f.e.}(0)}{dP} + \frac{d \ln Z_n(0)}{dP}. \quad \text{VI-26}$$

The free electron model predicts a pressure dependence

$$\frac{d \ln N_{f.e.}(0)}{dP} = + K/3 \quad \text{VI-27}$$

where  $K$  is the compressibility and the density of states per unit volume is used. Anderson and Gold (1965) and Anderson, O'Sullivan, and Schirber (1967) have found that the Fermi surface for Pb scales with pressure at a rate close to the free electron prediction. Therefore, using  $K/3 = 0.68 \times 10^{-6} \text{ bar}^{-1}$  for  $d \ln N_{f.e.}(0)/dP$ , and  $d \ln \gamma^*/dP = -(8.20 \pm 1.53) \times 10^{-6} \text{ bar}^{-1}$ , due to Garfinkel and Mapother (1961), gives

$$\frac{d \ln Z_n(0)}{dP} = -(8.88 \pm 1.53) \times 10^{-6} \text{ bar}^{-1}. \quad \text{VI-28}$$



From McMillan and Rowell (1965) we have,

$$Z_n(0) = \frac{m^*}{m} = 1 + 2 \int_0^\infty \frac{\alpha^2(\omega) F(\omega) d\omega}{\omega} \quad \text{VI-29}$$

$$= 2.33 \pm 0.02.$$

Therefore,

$$\frac{d \ln Z_n(0)}{dP} = \frac{d \ln m^*}{dP}$$

and the effective mass is decreased toward the free-electron value. This is again in keeping with the idea of the strong-coupling superconductor becoming more like a weak-coupling BCS metal.

This information can be used in estimating the magnitude of the pressure derivative of the electron-phonon coupling constant  $\alpha^2(\omega)$ . If one assumes that  $d\alpha^2(\omega)/dP$  is independent of energy, then from VI-29,

$$\frac{dm^*}{m} = 2\alpha^2 d\left(\int_0^\infty \frac{F(\omega) d\omega}{\omega}\right) + 4\alpha d\alpha \int_0^\infty \frac{F(\omega) d\omega}{\omega}. \quad \text{VI-30}$$

Now,

$$d \ln \left( \int_0^\infty \frac{F(\omega) d\omega}{\omega} \right) / dP = d \ln \left( \int_0^{\omega_D} \frac{9N\omega^2 d\omega}{\omega \omega_D^3} \right) / dP \quad \text{VI-31}$$

$$= \frac{-d \ln \omega_D}{dP} \quad \text{VI-32}$$



which can be represented as

$$d \ln \left( \int_0^{\infty} \frac{F(\omega) d\omega}{\omega} \right) / dP = \frac{-d \ln \Theta_D}{dP}, \quad \text{VI-33}$$

where  $3N$  is the number of degrees of freedom, and  $F(\omega)$  is chosen to be a Debye phonon spectrum. We have, therefore,

$$\frac{dm^*}{m} = -2\alpha^2 (d \ln \Theta_D) \int_0^{\infty} \frac{F(\omega) d\omega}{\omega} + 4\alpha d\alpha \int_0^{\infty} \frac{F(\omega) d\omega}{\omega} \quad \text{VI-34}$$

$$= \int_0^{\infty} \frac{F(\omega) d\omega}{\omega} [4\alpha d\alpha - 2\alpha^2 d \ln \Theta_D] \quad \text{VI-35}$$

$$= \left( \frac{m^*}{m} - 1 \right) \frac{1}{2\alpha^2} [4\alpha d\alpha - 2\alpha^2 d \ln \Theta_D] . \quad \text{VI-36}$$

Multiplying by  $m/m^*$  gives

$$d \ln m^* = (1 - m/m^*) [2d \ln \alpha - d \ln \Theta_D] . \quad \text{VI-37}$$

For  $m/m^* = 1/2.33$

$$\frac{d \ln m^*}{dP} = 0.571 \left[ \frac{d \ln \alpha^2}{dP} - \frac{d \ln \Theta_D}{dP} \right] . \quad \text{VI-38}$$

Taking  $d \ln \Theta_D / dP$  as an average between  $d \ln \bar{\omega}_t / dP$  and  $d \ln \bar{\omega}_\ell / dP$  results in

$$d \ln \Theta / dP = (6.0 \pm 1.3) \times 10^{-6} \text{ bar}^{-1} . \quad \text{VI-39}$$





Using the value of  $d \ln Z_n(0)/dP = d \ln m^*/dP$  from equation VI-28, results in

$$\frac{d \ln \alpha^2}{dP} = -(9.6 \pm 2.2) \times 10^{-6} \text{ bar}^{-1}. \quad \text{VI-40}$$

Thus the electron-phonon coupling constant decreases with pressure at the same rate as the effective mass (renormalization factor) does. Interestingly, this is approximately equal to  $d \ln \Delta_o/dP$  and one-half of  $d \ln(\sigma - 1)/dP$ . Therefore one can tentatively assign the pressure dependence of the conductance structure with a squared dependence in the electron-phonon coupling constant. That is,

$$\frac{d \ln(\sigma - 1)}{dP} = \frac{2 d \ln \Delta_{Av}}{dP} = \frac{2 d \ln \alpha^2}{dP} \quad \text{VI-41}$$

or,

$$(\sigma - 1) \propto \Delta_{Av}^2 \propto (\alpha^2)^2. \quad \text{VI-42}$$

Although the estimate for  $d \ln \alpha^2/dP$  is admittedly crude, it seems hard to believe that the interaction strength increases with an increase in pressure, as has been suggested by Garfinkel and Mapother (1961). Using the BCS expression for the condensation energy (a poor assumption for strong-coupling Pb), they predict that the



interaction strength  $V$  should increase with pressure. They then conclude that  $T_c$  decreases with pressure because the change in the density of states over-rides the change in  $V$ . Although a rigorous comparison between  $d\ln\alpha^2/dP$  and  $d\ln V/dP$  cannot be carried out — and indeed is not justified in this case because of the crudeness of both interpretations — it is intuitively more reasonable to assume that the reduction in  $T_c$  (and also in the gap- $T_c$  ratio) is associated with the interaction tending toward a BCS weak-coupling limit.

An article by McMillan (1968), which applies to the results in this section, has recently appeared. Accordingly, this discussion is continued in Appendix B.



## VI.6 The Recombination Effect

The recombination effect as proposed by Scalapino, Swihart, and Wada (1965), was outlined in section II.9. The effect arose theoretically in the finite temperature calculations of  $\Delta_1(\omega)$  and  $\Delta_2(\omega)$  for Pb. In particular, for temperatures close to  $T_c$ , a new negative peak in  $\Delta_2(\omega)$  at energy  $\omega + \Delta_0(T) = \omega_\lambda$  was found, where  $\omega_\lambda$  is the energy of a predominant phonon group. This new peak in  $\Delta_2(\omega)$  was reflected as additional structure in the tunnel density of states, which they then calculated for  $t = 0.92$  and  $t = 0.95$ . The process ostensibly involves combination of an injected electron with a thermally excited quasi-particle such that a phonon is emitted and the pair then becomes a ground state pair. The process is most probable when the phonon energy equals the predominant transverse mode energy  $\omega_t$ .

Khanna and Woods (1966) have investigated this effect in Pb with only limited success. They find experimental tunnel conductance curves which should correspond to lower reduced temperatures from the theoretical picture, and, at the same time, their results do not seem to scale with temperature. Thus, further studies of the effect were undertaken as part of this work.

Since the conductance amplitude is highly temperature sensitive in this temperature region, accurate temperature control and calibration are required. The thermometer





calibration accuracy is estimated at 0.1%, while the conductance circuitry is accurate to 0.2%. This results in an estimate of the uncertainty in the tunnel conductance of approximately  $\pm 0.003$  for the gap-edge region. Figure 22 shows the tunnel conductance (density of states) for four reduced temperatures near  $t = 1$  obtained from junctions 1345 and 1345A. Shown as well, is the conductance predicted by Scalapino et al for  $t = 0.92$  and  $t = 0.95$ . The average magnitude of the conductance is in good agreement with the predictions. However, the fact that the experimental conductance exceeds the calculated value between approximately 1.7 and 3.9 meV is direct evidence that the peak in  $\Delta_2(\omega)$  is smaller than calculated. A reduction of  $\Delta_2(\omega)$  in equation VI-21 would increase  $\sigma$  at the gap edge and would also result in a reduction of the predicted structure at  $V = \omega = \omega_t - \Delta_0(T)$ . The zero-temperature tunneling results on Pb by McMillan and Rowell (1965) shows that the transverse peak is broader than assumed by Scalapino et al in their model calculation, so that use of a more realistic lattice spectrum would lead to a more shallow minimum in  $\Delta_2(\omega)$  and consequently, better agreement with the experimental results.

The interpretation is further complicated by the fact that the phonon emission anomaly near  $\omega_t + \Delta_0(T)$  is not sufficiently separated from the recombination anomaly

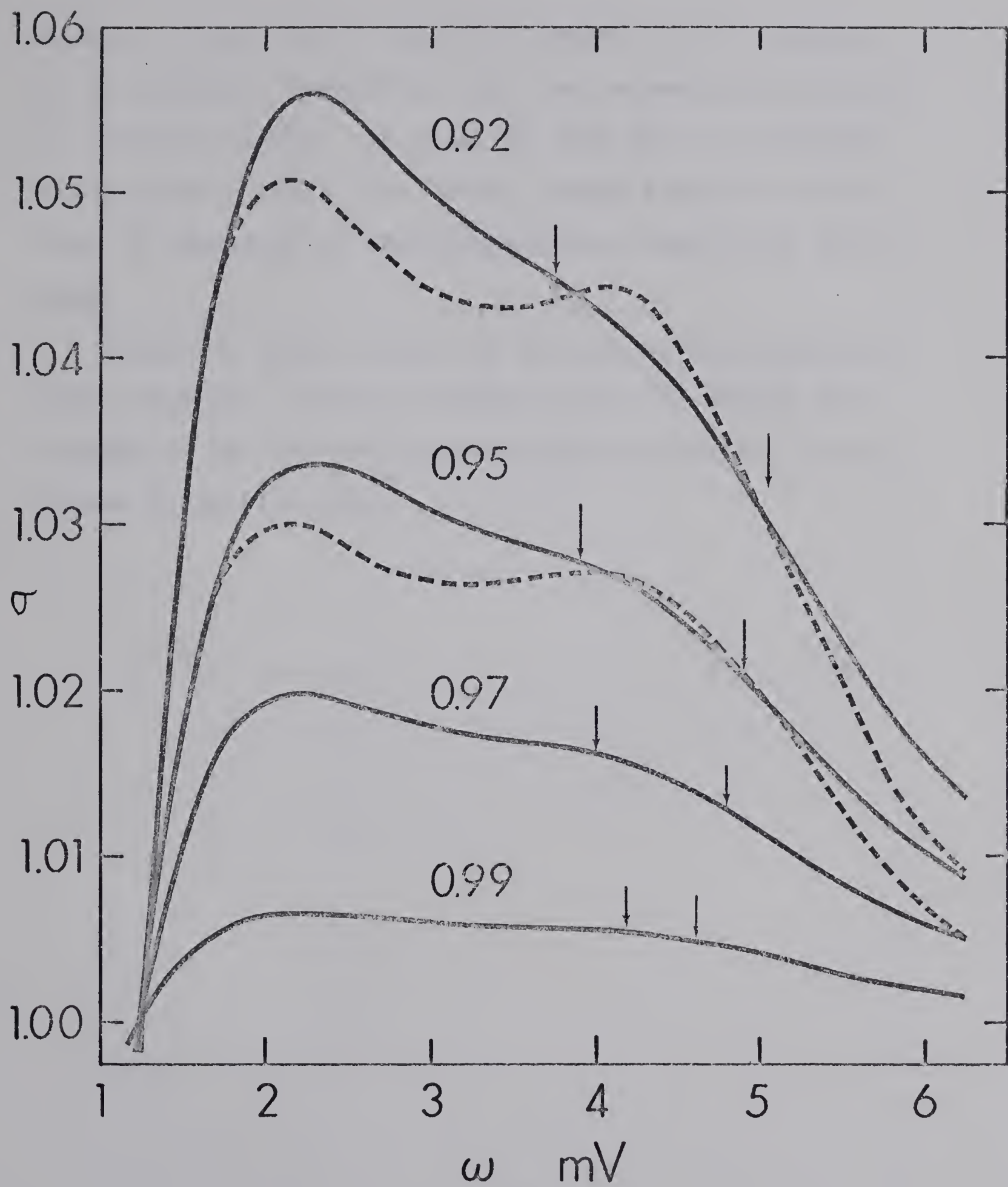




Figure 22

Normalized conductance  $\sigma$  for junctions 1345 and 1345A (full lines); the parameter gives the reduced temperature. The dashed lines are calculated normalized conductance for  $t = 0.92$  and  $0.95$ . The arrows indicate the energies  $\omega_t - \Delta_o(T)$  and  $\omega_t + \Delta_o(T)$ .







near  $\omega_t - \Delta_0(T)$  for  $t$  close to 1 where  $\Delta_0(T)$  is small. It is possible, therefore, that the recombination effect is entirely absent. In order to test for it experimentally, some process with better energy resolution than that of tunneling at this temperature, would have to be used.

Figure 23 shows a shift in the conductance amplitude under pressure. This is thought to be associated with changes in the electron-phonon coupling constant as discussed in section VI.5.



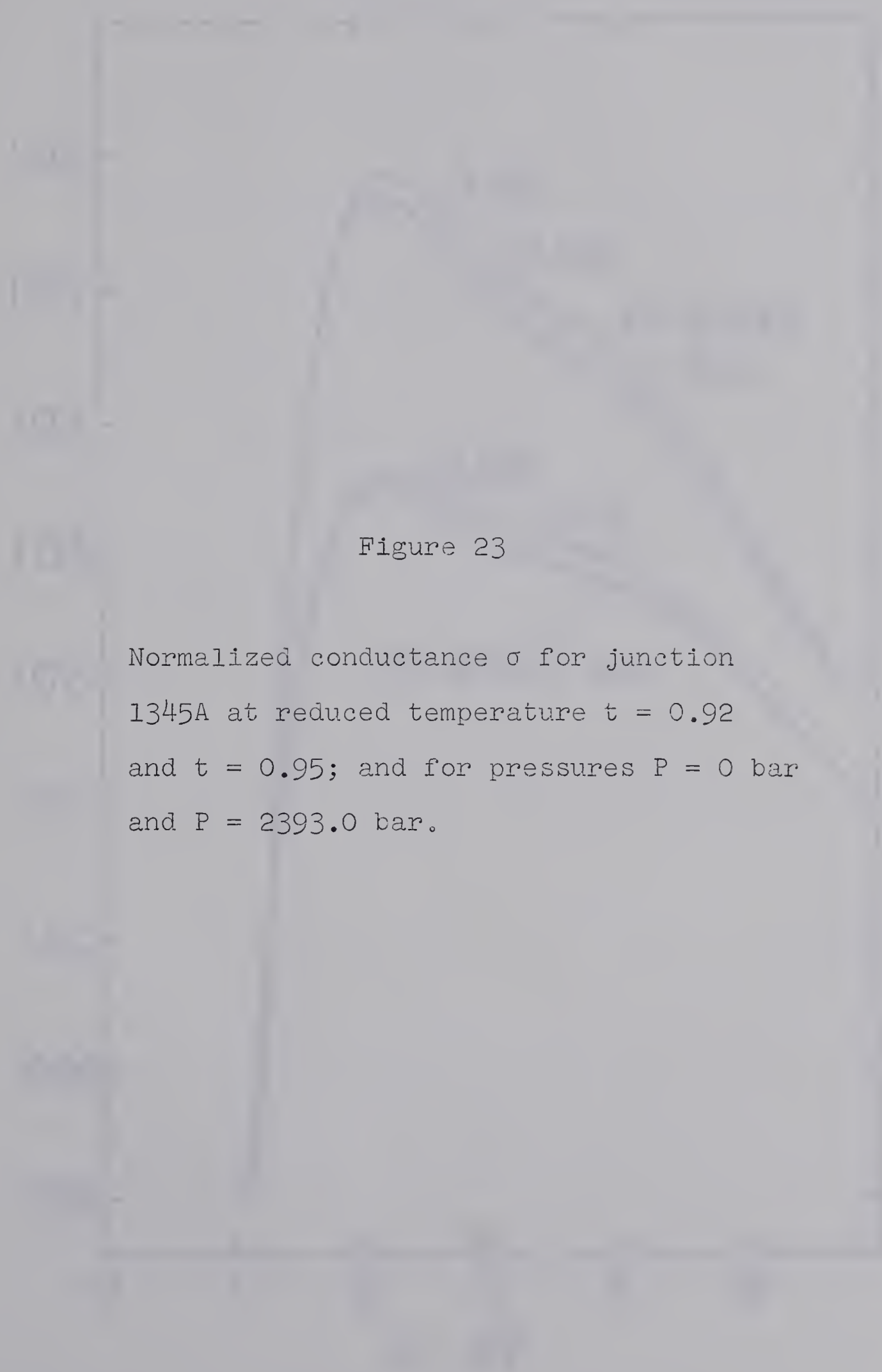
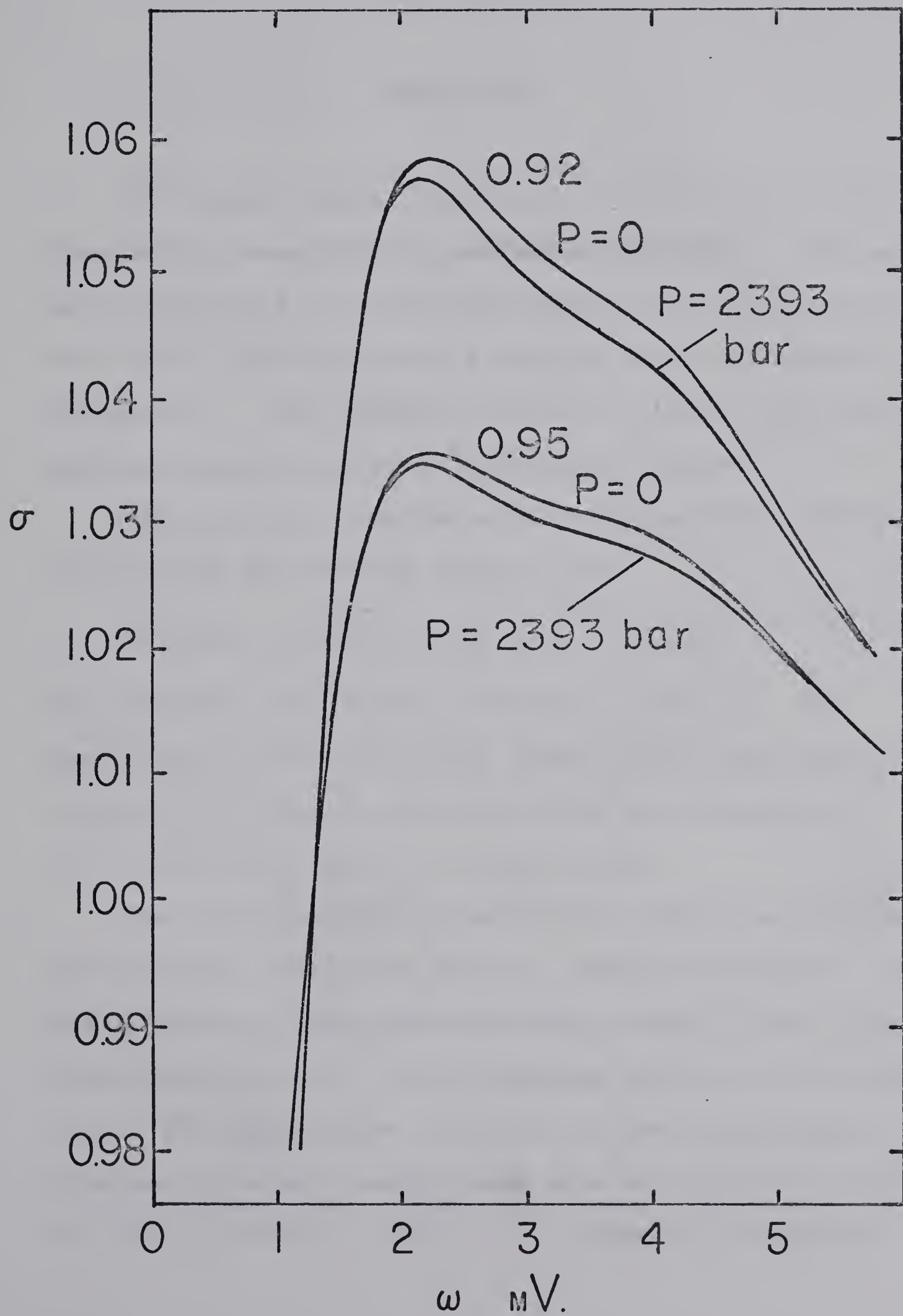


Figure 23

Normalized conductance  $\sigma$  for junction 1345A at reduced temperature  $t = 0.92$  and  $t = 0.95$ ; and for pressures  $P = 0$  bar and  $P = 2393.0$  bar.









## CHAPTER VII

## CONCLUSION

The normal tunnel resistance of Pb-Al junctions was found to be reversibly dependent on pressure. The pressure dependence is associated mainly with compression of the oxide layer and results roughly in an exponential dependence. This suggests the use of tunnel junctions as four terminal pressure monitoring devices.

The pressure dependence of the transition temperature of the Pb film was found to be

$$dT_c/dP = -(3.60 \pm 0.35) \times 10^{-6} \text{ } ^\circ\text{K}/\text{bar},$$

in agreement with values obtained on bulk Pb. The Gruneisen  $\gamma$ 's for the phonon peaks in the high dispersive region of the phonon spectrum in Pb were measured at  $\gamma_t = 2.52 \pm 0.74$  and  $\gamma_\ell = 3.32 \pm 0.49$ .

The zero-pressure recombination effect as proposed by Scalapino, Wada, and Swihart (1965) was tested. Results indicate that the effect may be due to the rather idealized choice of the Pb spectrum used in the calculation. The temperature variation of the energy-gap as obtained from zero conductance data was found to follow the BCS relation to within a few percent, in agreement



with the theoretical predictions of Scalapino et al.

The shift in the gap parameter  $\Delta_0$  with hydrostatic pressure was measured for the first time. The average value obtained was

$$d\ln\Delta_0/dP = -(9.9 \pm 1.0) \times 10^{-6} \text{ bar}^{-1}.$$

This leads to a pressure dependence in  $2\Delta_0/kT_c$  given by,

$$\frac{d\ln(2\Delta_0/kT_c)}{dP} \Big|_{t=\text{const.}} = -(5.3 \pm 0.9) \times 10^{-6} \text{ bar}^{-1}.$$

The pressure dependence is thought to be associated with a change in the electron-phonon coupling constant, such that the superconductor tends toward a weak-coupling BCS behaviour under pressure. Further evidence to this effect is provided by the fact that, under pressure, the condensation energy tends toward a BCS prediction.

The conclusion by McMillan (1968) that the parameter  $\lambda$  defined by

$$\lambda = 2 \int_0^\infty \frac{\alpha^2(\omega) F(\omega) d\omega}{\omega},$$

is dependent on frequency in the manner,

$$\lambda \propto \frac{1}{\langle \omega^2 \rangle}$$

has been verified. Within this approximation and using



$$\frac{d \ln Z(0)}{dP} = \frac{d \ln(1 + \lambda)}{dP},$$

$$\frac{d \ln Z(0)}{dP} = -(6.70 \pm 1.35) \times 10^{-6} \text{ bar}^{-1}.$$

This is in good agreement with the value

$$\begin{aligned} \frac{d \ln Z(0)}{dP} &= \frac{d \ln \gamma^*}{dP} - \frac{d \ln N_{f.e.}(0)}{dP} \\ &= -(8.88 \pm 1.53) \times 10^{-6} \text{ bar}^{-1}, \end{aligned}$$

obtained using

$$\frac{d \ln \gamma^*}{dP} = -(8.20 \pm 1.53) \times 10^{-6} \text{ bar}^{-1}$$

due to Garfinkel and Mapother (1961), and  $d \ln N_{f.e.}(0)/dP$  per unit volume given by  $K/3$ .





## APPENDIX A

Pressure Shifts in  $F(\omega)$ 

Consider first an energy-independent Gruneisen  $\gamma$  and a constant electron-phonon coupling constant  $\alpha^2$ , in the region of  $\omega_t$  and  $\omega_\ell$

$$\gamma = - \frac{d \ln \omega}{d \ln V} \quad \text{A-1}$$

Under pressure  $P$  each frequency changes such that

$$\omega_f = \omega_i + \Delta\omega_i$$

where  $\omega_f$  and  $\omega_i$  are final and initial frequencies.

Writing  $\omega_f = \lambda \omega_i$ , and remembering that the compressibility is given by

$$K = - \frac{1}{V} \left( \frac{dV}{dP} \right)_T$$

we have,

$$\gamma = - \frac{\Delta\omega/\omega}{\Delta V/V} \frac{P}{P} \quad \text{A-2}$$

so that,

$$\Delta\omega = KP\gamma\omega \quad \text{A-3}$$

$$\text{and,} \quad \lambda = 1 + KP\gamma \quad \text{A-4}$$

Writing the shifted frequency spectrum as

$$F(\omega) = AF_o(\omega/\lambda) \quad \text{A-5}$$

and remembering that the total number of degrees of



freedom is  $3N$ ,

$$\int_0^{\infty} F_0(\omega) d\omega = 3N = \int_0^{\infty} F(\omega) d\omega. \quad A-6$$

We have also

$$\int_0^{\infty} A F_0(\omega/\lambda) d\omega = \int_0^{\infty} F_0(\omega) d\omega, \quad A-7$$

and

$$\int_0^{\infty} A \lambda F_0(\omega/\lambda) \frac{d\omega}{\lambda} = \int_0^{\infty} F_0(\omega) d\omega, \quad A-8$$

$$\text{so} \quad A = \frac{1}{\lambda}, \quad \text{whence} \quad F(\omega) = \frac{1}{\lambda} F_0(\omega/\lambda). \quad A-9$$

Differentiating,

$$\frac{dF(\omega)}{d\omega} = \frac{1}{\lambda^2} \frac{dF_0(\omega/\lambda)}{d\omega}. \quad A-10$$

If  $\omega_m$  is the location of a maximum in  $F_0(\omega)$  such that  $F'_0(\omega) = 0$ , then  $\omega = \lambda\omega_m$  is the location of a maximum in  $F(\omega)$ .

Therefore the shift in the maximum gives  $\lambda$  from which one gets

$$\gamma = \frac{\lambda - 1}{KP}. \quad A-11$$

We now consider the case of an energy-dependent  $\gamma$ . If we assume the coupling constant is slowly and smoothly varying with pressure near  $\omega_t$  and  $\omega_\ell$ , but is essentially independent of energy in either the



transverse or longitudinal branches, we introduce a pressure dependent term so that

$$F(\omega) = A(P) F_0(\omega/\lambda(\omega)). \quad A-12$$

Differentiating with respect to energy,

$$F'(\omega) = A(P) F'_0(\omega/\lambda(\omega)) \left( \frac{1}{\lambda} - \frac{\omega}{\lambda^2} \frac{d\lambda(\omega)}{d\omega} \right). \quad A-13$$

Again for a maximum in  $F_0(\omega/\lambda(\omega))$  such that  $F'_0(\omega/\lambda(\omega))$  equals zero, a maximum will occur in  $F(\omega)$  such that

$$\omega = \lambda(\omega)\omega_m, \text{ and } \gamma(\omega) = \frac{\lambda(\omega)}{KP} - 1. \quad A-14$$

Note, however, that when  $\lambda(\omega) = \omega\lambda'(\omega)$  that  $F'(\omega) = 0$  as well. These new extrema in  $F(\omega)$  are associated with extrema in  $d\lambda(\omega)/d\omega$ . These will probably be of the same relative importance as the energy dependence of shifts in the electron-phonon coupling constant with pressure which we ignored in our original assumptions. It is safe to assume that the conductance structure shifts associated with these secondary effects, will be much smaller in amplitude than the structure changes in the predominant  $\omega_t$  and  $\omega_\ell$  modes. If this is the case, then we will not detect them anyway.



## APPENDIX B

A Recent Article on Strong-Coupling Theory

Since the completion of this thesis, a publication by W.L. McMillan (1968) has appeared, regarding, among other things, the frequency dependence of the electron-phonon coupling constant. In the paper McMillan uses existing strong-coupling theory along with experimental results to consolidate the known information about both elemental and alloy type superconductors.

He defines a dimensionless "electron-phonon coupling constant" as

$$\lambda = 2 \int_0^{\omega_0} \alpha^2(\omega_q) F(\omega_q) \frac{d\omega_q}{\omega_q} \quad \text{B-1}$$

and from equation VI-24, it can be seen that

$$Z_n(0) = \frac{m^*}{m} = 1 + \lambda, \quad \text{B-2}$$

so that  $\lambda = 1.33$  for Pb.

Although most of the paper is concerned with bcc transition metals, some of his findings are applicable to Pb. In terms of  $\lambda$  defined above, he obtains an expression for the electronic heat capacity coefficient,  $\gamma$ , given by

$$\gamma^* = \frac{\gamma}{v} = \frac{2\pi^2}{3} k^2 N_{bs}(0) (1 + \lambda). \quad \text{B-3}$$





Here  $N_{bs}(0)$  is the "band structure density of states" per unit volume (containing the Coulomb interaction between electrons) and  $1 + \lambda$  is an enhancement factor due to the electron phonon interaction. Clearly, the band structure density of states in B-3 is to replace the free electron density of states in VI-35 and  $1 + \lambda$  takes the place of  $Z_n(0)$ . Provided the band structure density of states has approximately the same pressure dependence as the free electron density of states, equation VI-28 should still hold.

McMillan finds that the frequency dependence of  $\lambda$  for metals such as Al, In, and Pb is empirically given by,

$$\lambda \sim \frac{\text{Constant}}{M\langle\omega^2\rangle} \sim \frac{K}{\langle\omega^2\rangle} \quad \text{B-4}$$

where  $M$  is the mass and  $K$  is a constant. Using B-2 and B-4 one has,

$$\frac{d \ln Z_n(0)}{dP} = \frac{d \ln m^*}{dP} = \frac{d \ln(1 + \lambda)}{dP} = \frac{d \ln(1 + \frac{K}{\langle\omega^2\rangle})}{dP} \quad \text{B-5}$$

where (from equation VI-28),

$$\frac{d \ln m^*}{dP} = -(8.88 \pm 1.53) \times 10^{-6} \text{ bar}^{-1}.$$

The pressure shifts of  $\bar{\omega}_t$  and  $\bar{\omega}_\ell$  can be used in estimating



$$\frac{d \ln(1 + \frac{K}{\langle \omega^2 \rangle})}{dP} .$$

From Tables 3 and 4 one has the following values

$$\bar{\omega}_t(P=0) = 4.585 \text{ meV}$$

$$\bar{\omega}_\ell(P=0) = 8.865 \text{ meV}$$

and from the average values of  $\delta \bar{\omega}_\lambda / \delta P$ ,

$$\delta \bar{\omega}_t = 0.075 \quad \text{for } \delta P = 3172.0 \text{ bar}$$

$$\delta \bar{\omega}_\ell = 0.163 \quad \text{for } \delta P = 2757.2 \text{ bar.}$$

Since  $1 + \lambda = 1 + k/\langle \omega^2 \rangle \sim 2.33$  (McMillan and Rowell (1965))

$$\delta(1 + K/\bar{\omega}_t^2)/\delta P = \frac{2.2873 - 2.3300}{3172.0} \text{ bar}^{-1}$$

$$\frac{d \ln(1 + \frac{K}{\langle \omega_t^2 \rangle})}{dP} = \frac{1}{2.33} \frac{\delta(1 + \frac{K}{\langle \omega_t^2 \rangle})}{\delta P} = -5.78 \times 10^{-6} \text{ bar}^{-1}.$$

Similarly

$$\delta(1 + K_2/\bar{\omega}_\ell^2)/\delta P = \frac{2.281 - 2.330}{2757.2} \text{ bar}^{-1}$$

and

$$\frac{d \ln(1 + \frac{K_2}{\bar{\omega}_\ell^2})}{dP} = -7.63 \times 10^{-6} \text{ bar}^{-1}.$$

B-6

Taking an average of the two gives



$$\frac{d \ln(1 + \lambda)}{dP} = \frac{d \ln(1 + \frac{K_2}{\omega_l^2})}{dP} = -(6.70 \pm 1.35) \times 10^{-6} \text{ bar}^{-1}.$$

B-7

where the error is estimated at about 20%.

The agreement with the independently measured value of  $d \ln m^*/dP$  by Garfinkel (VI-28) is good considering the assumptions made, and thus the prediction of an inverse squared frequency dependence for  $\lambda$  is borne out. One can also relate the pressure dependence of  $\lambda$  to the pressure dependence of  $\alpha^2(\omega)$  as shown below. By definition

$$\lambda = 2 \int_0^{\omega_0} \frac{\alpha^2(\omega) F(\omega) d\omega}{\omega}$$

where  $\omega_0$  is the phonon end point energy.

If we assume  $\alpha^2(\omega)$  is independent of energy, then

$$\frac{d\lambda}{dP} = 2 \frac{d}{dP} \left( \int_0^{\omega_0} \frac{\alpha^2(\omega) F(\omega) d\omega}{\omega} \right). \quad \text{B-8}$$

Using the development of equations VI-30 to VI-36 and the assumption of a Debye phonon spectrum,  $\lambda$  replaces  $m^*/m - 1$  and one has

$$\frac{d\lambda}{dP} = \left( \frac{m^*}{m} - 1 \right) \left[ \frac{d \ln \alpha^2}{dP} - \frac{d \ln \Theta_D}{dP} \right]. \quad \text{B-9}$$

Again assuming the renormalization parameter can be written as

$$Z_n(0) = \frac{m^*}{m} = 1 + \lambda,$$



$$\lambda = \frac{m^*}{m} - 1 \quad \text{B-10}$$

and

$$\frac{d \ln \lambda}{dP} = \left[ \frac{d \ln \alpha^2}{dP} - \frac{d \ln \Theta_D}{dP} \right] . \quad \text{B-11}$$

Substituting from VI-39 and VI-40 gives

$$\begin{aligned} \frac{d \ln \lambda}{dP} &= [-(9.6 \pm 2.2) - (6.0 \pm 1.3)] \times 10^{-6} \text{ bar}^{-1} \\ &= -(15.6 \pm 3.5) \times 10^{-6} \text{ bar}^{-1}. \end{aligned} \quad \text{B-12}$$

But from B-4,

$$\begin{aligned} \frac{d \ln \lambda}{dP} &\approx - \frac{2 d \ln \Theta_D}{dP} \\ &\approx -(12.0 \pm 2.3) \times 10^{-6} \text{ bar}^{-1}. \end{aligned} \quad \text{B-13}$$

Thus we again have consistency between the various results.





## BIBLIOGRAPHY

- Adler, J. G., Jackson, J. E., and Will, T. A., (1967) Physics Letters 24A, 407.
- Anderson, J. R., and Gold, A. V., (1965) Phys. Rev. 139, 1459.
- Anderson, J. R., O'Sullivan, W. J., and Schirber, J. E., (1967) Phys. Rev. 153, 721.
- Bardeen, J., (1961) Phys. Rev. Letters 6, 57.
- Bardeen, J., Cooper, L. N., and Schrieffer, J. R., (1957) Phys. Rev. 108, 1175.
- Bardeen, J., and Pines, D., (1955) Phys. Rev. 99, 1140.
- Bennett, A. J., (1965) Phys. Rev. 140, A1902.
- Bermon, S., (1964) University of Illinois Technical Report No.1, Grant No. NSF-GP 1100 (unpublished)
- Blackman, M., (1957) Proc. Phys. Soc. B70, 827.
- Blackman, M., (1959) Proc. Phys. Soc. 74, 17.
- Bogolyubov, N. N., (1958) Soviet Physics JETP 34, 41.
- Brandt, N. B., and Ginzburg, N. I., (1965) Soviet Physics USPEKHI 8, 202.
- Brockhouse, B. N., Arase, T., Caglioti, G., Sakamoto, M., Sinclair, R. N., and Woods, A. D. B., (1961A) Inelastic Scattering of Neutrons in Solids and Liquids (International Atomic Energy Agency, Vienna) p 113.
- Brockhouse, B. N., Arase, T., Caglioti, G., Sakamoto, M., Sinclair, R. N., and Woods, A. D. B., (1961B) Inelastic Scattering of Neutrons in Solids and Liquids (International Atomic Energy Agency, Vienna) p 531.
- Caswell, H. L., Priest, J. R., and Budo, Y., (1963) Journal of Applied Physics 34, 3261.
- Claeson, T., (1966) Phys. Rev. 147, 340; (1967) Solid State Commun. 5, 119.



- Clement, J. R., and Quinnett, E. H., (1952) Phys. Rev. 85, 502.
- Cohen, M. H., Falicov, L. M., and Phillips, J. C., (1962) Phys. Rev. Letters 8, 316.
- Cooper, L. N., (1956) Phys. Rev. 104, 1189.
- Daniels, W. B., (1960) Phys. Rev. 119, 1246.
- Daniels, W. B., and Smith, Charles, S., (1958) Phys. Rev. 111, 713.
- Decker, D. L., Mapother, D. E., and Shaw, R. W., (1958) Phys. Rev. 112, 1888.
- Dugdale, J. S., and Simon, E. F., (1953) Proc. Roy. Soc. A218, 291.
- Dugdale, J. S., (1965) Physics of High Pressure and the Condensed Phase, ed Itterbeek, North Holland p 386.
- Eliashberg, G. M., (1960) Soviet Physics JETP 11, 696.
- Eliashberg, G. M., (1962) Soviet Physics JETP 16, 780.
- Franck, J. P., and Keeler, W. J., (1967) Phys. Letters 25A, 624.
- Franck, J. P., and Keeler, W. J., (1967) Phys. Rev. 163, 373.
- Franck, J. P., and Keeler, W. J., (1968) Phys. Rev. Letters 20, 379.
- Franck, J. P., and Martin, D. L., (1961) Can. Journ. of Phys. 39, 1320.
- Frohlich, H., (1950) Phys. Rev. 79, 845; (1950) Proc. Phys. Soc. A63, 778.
- Frohlich, H., (1952) Proc. Roy. Soc.(London) A215, 291.
- Garfinkel, M., and Mapother, D. E., (1961) Phys. Rev. 122, 459.
- Gilat, G., (1965) Solid State Commun. 3, 101.
- Goree, W. S., McDowell, B., and Scott, T. A., (1965) Rev. Sci. Instr. p 99.



- Gorter, C. J., and Casimir, H. B. G., (1934) Phys. Z. 35, 963; Z. Techn. Phys. 15, 539.
- Gruneisen, E., (1926) Geiger-Scheel Handbuch der Physik 10, 1.
- Hake, R. R., and Mapother, D. E., (1956) J. Phys. Chem. Solids 1, 199.
- Hodder, R. E., and Briscoe, C. V., (1966) Ph.D. Thesis University of North Carolina, Chappel Hill.
- Keesom, P. H., and van der Hoeven, Jr. B. J. C., (1963) Phys. Letters 3, 360.
- Khanna, S. M., and Woods, S. B., (1966) Phys. Letters 20, 335.
- Lechner, R., and Quittner, G., (1966) Phys. Rev. Letters 17, 1259.
- Levy, M., and Olsen, J. L., (1965) Physics of High Pressure and the Condensed Phase, ed A. Van Itterbeek, North Holland Publ. p 525.
- London, H., and London, F., (1935) Proc. Roy. Soc.(London) A149, 71; (1934) Physica 2, 341.
- Maxwell, E., (1950) Phys. Rev. 78, 477.
- McMillan, W. L., (1968) (to be published). Has now appeared in (1968) Phys. Rev. 167, 331.
- McMillan, W. L., and Rowell, J. M., (1965) Phys. Rev. Letters 14, 108.
- Meissener, W., and Ochsenfeld, R., (1933) Naturwissenschaften 21, 787.
- Mills, R. L., and Grilly, E. R., (1955) Phys. Rev. 99, 480.
- Muhlschlegel, B., (1959) Z. Physik 155, 313.
- Neighbor, J. E., Cochran, J. F., and Shiffman, C. A., (1967) Phys. Rev. 155, 384.
- Olsen, J. L., and Rohrer, H., (1960) Helv. Phys. Acta 33, 695.
- Onnes, H. K., (1911) Commun. Phy. Lab. Univ. Leiden No.119B.





- Payne, R. T., (1964) Phys. Rev. Letters 13, 53.
- Phillips, J. C., (1956) Phys. Rev. 104, 1263.
- Phillips, N. E., (1967) Physica Fennica 1, 69.
- Reynolds, C. A., Serin, B., and Nesbitt, L. B., (1951) Phys. Rev. 84, 691.
- Richards, P. L., and Tinkham, M., (1960) Phys. Rev. 119, 575.
- Rickayzen, G., (1965) "Theory of Superconductivity" Interscience Monographs.
- Rochlin, G. L., (1967) Phys. Rev. 153, 513.
- Rogers, J. S., (1964) Phonon Effects on Electron Tunneling into Superconductors, Ph.D. Thesis (unpublished) Appendix II, University of Alberta, Edmonton.
- Rosenstock, H. B., (1955) Phys. Rev. 97, 290.
- Rowell, J. M., Anderson, P. W., and Thomas, D. E., (1963) Phys. Rev. Letters 10, 334.
- Rowell, J. M., and Kopf, L., (1965) Phys. Rev. 137, A907.
- Scalapino, D. J., and Anderson, P. W., (1964) Phys. Rev. 133, A921.
- Scalapino, D. J., Schrieffer, J. R., and Wilkins, J. W., (1966) Phys. Rev. 148, 263.
- Scalapino, D. J., Wada, Y., and Swihart, J. C., (1965) Phys. Rev. Letters 14, 102.
- Schmunck, R. E., and Smith, Charles S., (1959) J. Phys. Chem. Solids 9, 100.
- Schrieffer, J. R., (1964) Revs. of Modern Phys. 36, 200.
- Schrieffer, J. R., (1964) "Theory of Superconductivity" Benjamin Publishing Co.
- Schrieffer, J. R., Scalapino, D. J., and Wilkins, J. W., (1963) Phys. Rev. Letters 10, 336.
- Sharma, S. M., (1965) Master's Thesis University of Alberta, Edmonton.





- Shapiro, S., Smith, P. H., Nicol, J., Miles, J. L., and Strong, P. F., (1962) IBM Journal of Research and Devel. 6, 34.
- Shiffman, C. A., Cochran, J. F., and Garber, M., (1963) J. Phys. Chem. Solids 24, 1369.
- Smith, T. F., and Chu, C. W., (1967) Phys. Rev. 159, 353.
- Stedman, R., Almqvist, L., Nilsson, G., and Raunio, G., (1967A) Phys. Rev. 162, 545.
- Stedman, R., Almqvist, L., and Nilsson, G., (1967B) Phys. Rev. 162, 549.
- Swihart, J. C., (1962) IBM Journal of Research and Devel. 6, 14.
- Swihart, J. C., Scalapino, D. J., and Wada, Y., (1965) Phys. Rev. Letters 14, 106.
- Swihart, J. C., Scalapino, D. J., and Wada, Y., (1965) Low Temp. Physics LT-9 Part (A) p 607.
- Swenson, C. A., (1960) Solid State Physics volume 11 p 109.
- Thouless, D. J., (1960) Phys. Rev. 117, 1256.
- Townsend, P., (1964) Revs. of Modern Phys. 36, 207.
- Townsend, P., and Sutton, J., (1963) Phys. Rev. Letters 11, 154.
- van der Hoeven, Jr., B. J. C., and Keesom, P. H., (1965) Phys. Rev. 137, A103.
- Van Hove, L., (1953) Phys. Rev. 89, 1189.
- Wada, Y., (1964) Revs. of Modern Phys. 36, 253.
- Wada, Y., (1964B) Phys. Rev. 135, A1481.
- Waldorf, D. L., and Alers, G. A., (1962) J. Applied Phys. 33, 3266.
- White, G. K., (1962) Philosophical Magazine 7, 271.
- Wu, T. M., (1967) Phys. Rev. Letters 19, 508.
- Zavaritskii, N. V., (1967) Soviet Physics JETP Letters 6, 155.





**B29887**